NANOPOROUS MATERIALS FOR CARBON DIOXIDE SEPARATION AND STORAGE

A Dissertation

by

VICTOR VARELA GUERRERO

Submitted to the Office of Graduate Studies of
Texas A&M University
in partial fulfillment of the requirements for the degree of

DOCTOR OF PHILOSOPHY

May 2011

Major Subject: Materials Science and Engineering

Nanoporous Materials for Carbon Dioxide Separation and Storage

NANOPOROUS MATERIALS FOR CARBON DIOXIDE SEPARATION AND STORAGE

A Dissertation

by

VICTOR VARELA GUERRERO

Submitted to the Office of Graduate Studies of
Texas A&M University
in partial fulfillment of the requirements for the degree of

DOCTOR OF PHILOSOPHY

Approved by:

Chair of Committee,	Hae-Kown Jeong
Committee Members,	Daniel F. Shantz
	Mahboobul Mannan
	Victor Ugaz
Intercollegiate Faculty Chair,	Ibrahim Karaman

May 2011

Major Subject: Materials Science and Engineering

ABSTRACT

Nanoporous Materials for Carbon Dioxide Separation

and Storage. (May 2011)

Victor Varela Guerrero, B.A., Universidad Autonoma del Estado de Mexico;

M.S., Iberoamerican University

Chair of Advisory Committee: Dr. Hae-Kwon Jeong

Global climate change is one of the most challenging problems that human beings are facing. The large anthropogenic emission of CO_2 in the atmosphere is one of the major causes for the climate change. Coal-fired power plants are the single-largest anthropogenic emission sources globally, accounting for approximately one third of the total CO_2 emissions. It is therefore necessary to reduce CO_2 emission from coal-fired power plants.

Current technologies for the post-combustion CO_2 capture from flue gas streams can be broadly classified into the three categories: absorption, adsorption, and membrane processes. Despite challenges, CO2 capture by adsorption using solid sorbents and membranes offers opportunities for energy-efficient capture and storage of CO2.

Nanoporous materials have attracted tremendous interest in research and development due to their potential in conventional applications such as catalysis, ion-exchange, and gas separation as well as in advanced applications such as sensors, delivery, and micro-devices.

In the first part of this dissertation, we will study the synthesis of membranes using an emerging class of nanoporous materials, metal-organic frameworks (MOFs) for carbon dioxide (CO_2) separations. Due to the unique chemistry of MOFs which is very different from that of zeolites, the techniques developed for the synthesis of zeolite membranes cannot be used directly. In order to overcome this challenge, a couple of novel techniques were developed: 1) "thermal seeding" for the secondary growth and 2) "surface modification" for the in situ growth. Membranes of HKUST-1 and ZIF-8, two of the most important MOFs, were prepared on porous α-alumina supports using thermal seeding and the surface modification techniques, respectively.

The second part of this dissertation demonstrates a simple and commercially viable application of nanoporous materials (zeolite 5A and amine-functionalized mesoporus silica), storing CO_2 as a micro-fire extinguishers in polymers. Materialist is observed that by dispersing these highly CO_2-philic nanoporous materials in polymer matrices, the propagation of flame was greatly retarded and extinguished. This flame retarding behavior is attributed to the fact that CO_2 released from the sorbents (zeolite 5A and mesoporous silica), blocks the flow of oxygen, therefore causing the fire to be effectively extinguished. Our results suggest that the binding strength of CO_2 on sorbents play an important role. If the binding strength of CO_2 is too low, CO_2 releases too early, thereby ineffective in retarding the flame.

To the love of my life for all her support
To my future children
And, finally, to God

ACKNOWLEDGEMENTS

I would like to thank my committee chair, Dr. Hae-Kwon Jeong, for his guidance and support throughout the course of this research. Without his guidance and constant help this dissertation would not have been possible. I would like to thank my committee members, Dr. Daniel F. Shantz, Dr. Sam Mannan and Dr. Victor Ugaz, for their guidance and support throughout the course of this research.

Thanks should also be given to my friends and colleagues and the department faculty and staff for making my time at Texas A&M University a great experience. I also want to extend my gratitude to CONACYT for their financial support. I also thank my colleagues, Yeonshick, Inho, and Colin, in the Jeong group. I would like to say thanks to Jonathan Lunn and Seung in Shantz's group for their help, advice and collaborations.

Finally, I give thanks to my mother, Maria Enriqueta, and my father, Victor, for their encouragement and to my sisters, Anabel and Patricia, and my brother, Jorge, for their help and support.

TABLE OF CONTENTS

CHAPTER Page

CHAPTER Page

CHAPTER Page

LIST OF FIGURES

FIGURE Page

FIGURE Page

FIGURE Page

FIGURE Page

LIST OF TABLES

CHAPTER I

INTRODUCTION

1.1 Motivation and objectives

Global climate change is one of the most challenging problems that human beings are facing.[1] The large anthropogenic emission of CO_2 in the atmosphere is one of the major causes for the climate change.[2] The atmospheric CO_2 concentration has risen by nearly 35% (383 ppm) since the time of the industrial revolution.[3] Coal-fired power plants are the single-largest anthropogenic emission sources globally, accounting for approximately one third of the total CO_2 emissions. It is therefore necessary to reduce CO_2 emission from coal-fired power plants. Though more integrated oxy-combustion and pre-combustion capture technologies are promising, post-combustion capture is very important mainly due to the fact that it can be retrofitted to the existing plants.[4]

Current technologies for the post-combustion CO_2 capture from flue gas streams can be broadly classified into the three categories: absorption, adsorption, and membrane processes. All of these technologies have been extensively studied with the amine-based absorption process as the current benchmark. Despite aggressive R&D efforts by DOE/NETL for more than a decade, presently, no single technology has been demonstrated to be capable of meeting the requirements set by the DOE/NETL: 90 % CO_2 capture at less than a 35 % increase in the cost of electricity (COE).[5, 6]

This dissertation follows the style of *Nano Letters*.

In almost all absorption and adsorption (chemical) processes, the capture and separation steps consist of the formation of CO_2-based molecular complexes via chemical interactions and subsequent regeneration of CO_2 through significant increases in temperature. This regeneration process by thermal energy accounts for the majority of the parasitic power requirement for CO_2 capture.[7] This is primarily due to the fact that it is both thermodynamically and kinetically energy inefficient to heat large volumes of liquid or solid sorbents and subsequently to cool these materials to prepare for the next sorption cycle: 1) unnecessary heating and cooling of inert materials such as water or oxide solids (though to less extent with solid sorbents) and 2) limited heat transfer rates due to large thermal mass and low thermal conductivity of inert materials, thereby requiring complicated thermal contact schemes. Therefore, there is a critical need to develop transformative CO_2 capture materials and processes that can drastically lower the operation cost of CO_2 capture by addressing the regeneration cost. In this regard, CO_2 capture by physical sorbents (i.e., nonreactive) and membranes can be promising energy-efficient alternatives to the current amine-based absorption systems if the following challenges can be addressed. Physical sorbents extensively studied include zeolites, metal-organic frameworks, and activated carbons.

CO_2 capture by physical sorbents such as carbonaceous materials (such as activated carbon and charcoal) and crystalline materials such as zeolites and more recently metal-organic frameworks is much more energy-efficient as compared to that by chemical sorbents. This is due to the absence of the formation of new chemical bonds between the sorbate and sorbent, thereby requiring significantly less energy for regeneration.[8]

On the other hands, membrane-based CO_2 separation is one of the most energy-efficient ways to capture CO_2.[7] Since membrane separation is pressure-driven, membranes are best suited for separating CO_2 in high partial pressure such as coal gasification. Low partial pressure of CO_2 (~ 0.1 – 0.3 atm) in a flue gas stream poises significant challenge to membrane-based post-combustion CO_2 capture. However, traditional polymer membranes suffer from low CO_2/N_2 selectivity (less than 100). For the membrane-based separation to be viable, the CO_2/N_2 selectivity has to be in the range of 200.[9] Despite the potential of molecular sieve membranes, conventional molecular sieves (i.e., zeolites) are limited for their use for CO_2/N_2 separation due to the similarity of the kinetic diameters of CO_2 (3.3 Å) and N_2 (3.64 Å). Therefore, it is highly desirable to develop advanced molecular sieve membranes with high CO_2/N_2 selectivity.

Two main objectives of the current studies are: 1) to develop metal-organic framework membranes for energy efficient CO_2 separations and 2) to develop nanoporous materials adsorbing with CO_2 as novel micro-fire extinguishers for environmentally friendly flame retardant applications.

1.2 Nanoporous materials

Nanostructured materials could be defined as those materials whose structural elements clusters, crystallite or molecules have dimensions in the 1 to 100 nm range. Nanoporous materials are nanostructured materials that possess pores in the scale of nanometers, showing unique surface and physicochemical properties that underline their

important uses catalysis,[10] molecular biology,[11, 12] medical applications[13-15] and recently in environmental application like CO_2 capture and separation.[16-18]

IUPAC classifies porous materials according to their pores sizes.[19, 20] Microporous materials possess pores with diameters less than 2 nm. Mesoporous and macroporous materials possess pores of diameters between 2 and 50 nm and larger than 50 nm respectively. Throughout this dissertation, microporous and mesoporous materials are also called nanoporous materials.

Nanoporous materials can be inorganic, organic, and inorganic-organic hybrid materials. Inorganic nonporous materials include zeolites (aluminosilicates)[21] and their derivatives (such as $AlPO_4$)[10, 31], carbon,[22] and silica (mesoporous silica)[23, 24] Examples of pure organic nanoporous materials are amorphous porous polymers[25] and covalent organic frameworks (COFs).[26] Organic-inorganic hybrid materials include organic-functionalized ordered mesoporous silica[27] and metal-organic frameworks (MOFs).[28, 29]

In this work, we focus on three important nanoporous materials: 1) zeolites, 2) ordered mesoporous silicas (OMS) and 3) metal-organic frameworks (MOFs). Brief introductions to these materials are given in the following sections.

1.2.1 Zeolites (aluminosilicates)

One of the most important nanoporous materials is inorganic zeolites. In 1756, A.F. Cronstedt, a Swedish mineralogist, observed that when heated, silicate minerals fused readily in a blowpipe flame with marked intumescence.[30] This result led him to call minerals that behaved in this manner zeolites, which derived from the Greek words

"zeo" (to boil) and "lithos" (stone). Zeolites are hydrated, inorganic crystalline solids with a very regular pore size and structure with pores in the scale of subnanometers.

1.2.1.1 History and structure of zeolites

Zeolites are aluminosilicate framework structures made from corner sharing SiO_4 and AlO_4 tetrahedra. Since aluminosilicates have negatively charged frameworks (one charge per framework Al^{3+}), charge-balancing extraframework positive ions are required. Typical cations in natural zeolites are Na^+, K^+, Ca^{2+}, and Ba^{2+}. In addition to natural zeolites, there are both synthetic analogues of natural zeolites and synthetic zeolites with no natural counterparts. The first synthesis of a zeolite that did not have a natural counterpart was accomplished by Barrer et al.[31] using so called hydrothermal synthesis. Later, Flanigen et al.[32] synthesized the first synthetic zeolites containing aluminum-rich or low silicon to aluminum ratio. Aluminum-rich zeolites can contain aluminum concentrations equivalent to silicon.

The next advance in zeolite synthesis was again due to Barrer.[33] In 1961, Barrer and Denny reported a zeolite synthesized using alkylammonium cations which is an intermediate-silica analogue of zeolite A. They noted that the addition of alkylammonium ions to sodium aluminosilicate gel increased the framework Si/Al ratio. This effect has been observed for zeolites that contains sodalite cages, e.g., zeolites A (see Figure 1.1), X, Y (FAU), and sodalite (SOD). The zeolite sodalite is comprised entirely of sodalite cages (see Figure 1.1).

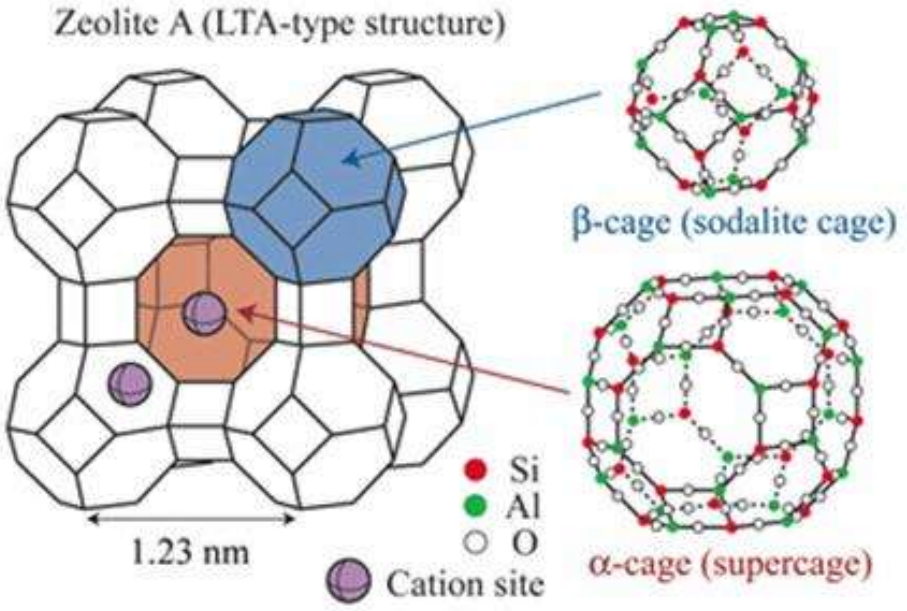

Figure 1.1 Zeolite 5A with SOD cage showing two cage and extra-framework cations[34]

For the sodalite structure, there are six T atoms per sodalite cage and tree anionic charges per cage when Si/Al=1 (one per Al^{3+}). Thus, three extraframework sodium ions per cage are necessary to balance the framework charge, which make these zeolites very hydrophilic.

1.2.1.2 Properties of zeolites

Two of the most important parameters of zeolites are the size of the pores and the presence of extra-framework cations.

The pore size of zeolites is determined by the number of oxygen atoms forming the pore aperture. By changing the number of oxygen in the zeolite framework, the pore size and shape can be controlled. The range of pore size in zeolites is normally between 0.3 ~1.0 nm which can discriminate gas molecules with a resolution of 1~2 Å. Due to the presence of the framework aluminums, zeolites exhibit a negatively charged framework, which is counter-balance by positive cations resulting in a strong electrostatic field on the internal surface. These cations can be exchanged to fine-tune the pore size and/or the adsorption characteristic. For instance, the sodium form of zeolite A has a pore opening of approximately 4 Å (called zeolite 4A). If the sodium ion is exchanged with a larger potassium ion, the pore opening is reduced to approximately 3 Å (Zeolite 3A). When exchanged with calcium, one calcium ion replaces two sodium ions, thereby increasing the pore opening to approximately 5 Å (Zeolite 5A) (see Figure 1.2).

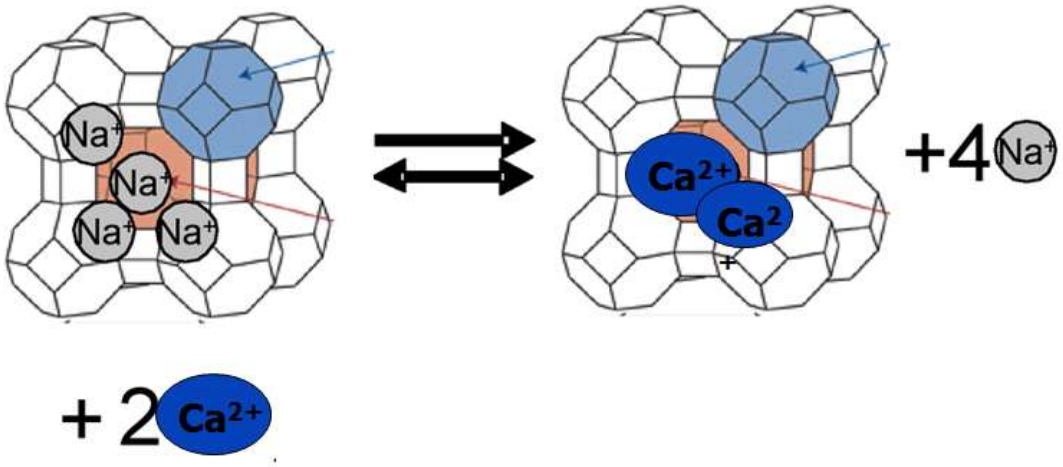

Figure 1.2 Ion exchange sodium by calcium (Zeolite 5A)[34]

1.2.1.3. Synthesis of zeolites

Zeolites are typically synthesized using so called hydrothermal synthesis method. The precursor solutions or gels are prepared by mixing "reactive" forms of silica (sodium silicate, colloidal silica, fumed silica, amorphous silica) and alumina (sodium aluminate, aluminum hydroxide, aluminum sulfate) in the presence of alkali-metal hydroxides in water. Aluminum-rich zeolites (i.e., hydrophilic zeolites due to the large amount of extra-framework cations) such as zeolites A (LTA) and X (FAU) can be crystallized at temperatures below ~ 100 ^{o}C with pH typically greater than 12. In general, the higher the synthesis temperature, the lower water content and the lower the intracrystalline void volumes in zeolites. The aluminum-rich zeolites are at the high end of the porosity scale for zeolites. Flanigen in her synthesis suggests two roles of the alkali-metal cations in the synthesis of zeolites: For aluminum-rich zeolites, the followings are generally observed: 1) the greater the concentration of alkali-metal cations, the smaller the Si/Al ratio (lower limit is 1) tends to be, 2) the framework Si/Al ratio increases to greater than 1 if the gel Si/Al ratio is less than 1, and 3) the framework Si/Al ratio can be lower than that of the gel Si/Al ratio leaving a siliceous solution.

The synthesis of high-silica zeolites (for example, ZSM series) typically requires the addition of organic molecules into the reaction mixture though there is an exception that ZSM-5 can be synthesized without the use of organic reagents in a very narrow range of Na^{+} and aluminum concentrations.[35] The reaction temperatures are normally higher (100-200 ^{o}C) than those for aluminum-rich zeolites. The organic species (often called as

"structure directing agents") direct the zeolite structures as well as balance the framework charge.

In general, zeolites are thermodynamically metastable phases. Due to Ostwalsd's ripening, the first phase produced can be consumed and replaced by a thermodynamically more stable second phase and so on until the most stable phase is formed, e.g., quartz with SiO_2. It should, however, be noted that the formation of zeolites cannot be rationalized on a thermodynamic basis alone and kinetics must be considered as well.

Also zeolite syntheses can be performed under high pH conditions. Normally, is used to solubilize silicate and aluminate species. Flanigen and Patton[36] used F^- instead of OH^- to synthesize zeolites at neutral or acidic conditions. Structures such as MFI, FER, MTT, MTN, and TON have been crystallized using the F^- synthesis method.

1.2.1.4. Applications of zeolites

One of the most important applications of zeolites are in the field of adsorption. This is primarily due to the facts that 1) they are molecular sieves, 2) they contain large void fractions (zeolites A and X have almost a 50% void fraction), and 3) they are hydrophilic.[37]

Natural gas is dried by contact with zeolites since they adsorb water. This application and several others are generally classified as purification operations and rely on surface selectivity for polar or polarizable molecules such as water, CO_2 and sulfur containing molecules.[30, 37] Bulk separations can also be accomplished with zeolites. For example,

zeolite A is used to separate linear from branched hydrocarbons since only the linear ones can be adsorbed. Zeolite A is also used as support in detergent, the sodium ion exchanges for other hard-water ions, e.g., Ca^{2+}. Zeolites are also useful as catalyst and catalyst supports. If the balancing cation in the zeolite is H+, then the framework is a solid acid that can reveal shape-selective properties due to confinement of the acidic proton within the zeolite pore architecture. Zeolites A and X were ion exchanged with calcium salts (creates acid sites by hydrolysis of the water of hydration around the calcium ions located within the zeolite, e.g., $Ca\ (H_2O)_x^{2+} \rightarrow Ca\ (H_2O)_{x-1}\ (OH)^+ + H^+$) and were contacted with primary and secondary alcohols in the vapor phase.[37]

1.2.2 Ordered mesoporous silica (OMS)

Ordered mesoporous silicas (OMS) are mesoporous materials with a very narrow pore size distribution prepared by hydrolysis and condensation of inorganic precursor (the sol-gel process) in the presence of surfactants micelles (templates) represented a significant breakthrough in porous materials synthesis. Many OMS materials are silica base, often using tetraethyl orthosilicates (TEOS, $Si(OC_2H_5)_4$) as the hydrolysable silica source, and long chain ammonium salts, amines or triblock copolymers as template agents. The development of porous materials is currently an area of extensive research, particularly with regard to potential applications in areas including adsorption and catalysis. The first OMS materials were reported by the Mobil Corporation in the early 1990's and are commonly referred to as M41s (though not all of these materials are in fact ordered). [38]

The most studied material in this family is MCM-41. It is synthesized under basic conditions using surfactants as the structure directing agent, typically cetyltrimethylammonium bromide (CTAB). MCM-41 has a hexagonal pore arrangement; other M41S material is MCM-48[39] (cubic, *Ia3d*) (see Figure 1.3a). Other important family of OMS materials is SBA (Santa Barbara), developed in the mid-late 1990's by Stucky et al.[40, 41] at the University of California at Santa Barbara. These materials can have different pore arrangement like hexagonal or cubic (see Figure 1.3b). The one of the most popular material in this family is SBA-15 that has hexagonal pore arrangement and 7-8 nm of pore size. SBA-15 is made under acid conditions using a triblock copolymer (Pluronic 123) as a structure-directing agent during the hydrolysis and condensation of TEOS of tetraethyl orthosilicates.

1.2.2.1. Organic groups tethered to OMS

The term hybrid material is used to describe many different systems spanning a wide range of different materials, such as crystalline highly ordered coordination polymers, amorphous sol-gel compounds, materials with and without interactions between inorganic and organic units. One definition of a hybrid material is that it is a material that includes two moieties blended on the molecular scale. Commonly, one of these compounds is inorganic and the other is organic in nature. The most obvious advantage of inorganic-organic hybrids is that they can favorably combine the often dissimilar properties of organic and inorganic components in one material.

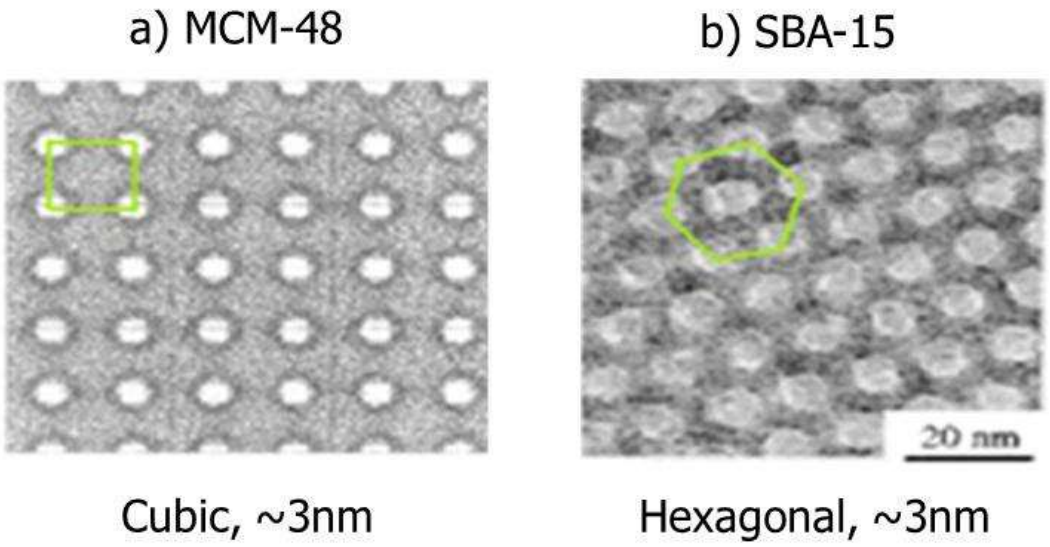

Figure 1.3 Transmission electron micrographs of a) MCM-48[42] and b) SBA-15[43]

Because of the many possible combinations of components, this field is very active; it provides the opportunity to invent an almost unlimited set of new materials with a large spectrum of controllable properties.

Now in this work we will discuss about the chemical functionalization of the inorganic framework of mesoporous materials (OMS). It is a promising approach to develop specific pore surface properties such as hydrophobicity, polarity, catalytic, optical and electronic properties.[44-53] Numerous studies have been performed on modifications of MCM-41[54-56] and SBA-15[48, 57] to increase the potential applicability of these materials. The integration of organic functional groups into inorganic frameworks has led to organic-inorganic hybrid materials with well-defined pore structures and functionality. These materials combine the structural characteristics of ordered mesoporous silica with the chemical functionality of organic groups. This is particularly useful in the context of adsorption[23, 48, 58, 59] and catalysis[60, 61].

1.2.2.2. Synthesis of organic groups tethered to OMS

The synthesis of organic-inorganic materials based on organosilica building blocks is feasible via three pathways: 1) post synthetic functionalization (grafting), 2) Co-condensation of silica and organosilica precursors and 3) direct condensation of bis-silanes. These three pathways result in ordered mesoporous organosilica materials, though with different properties (see Figure 1.4).[27]

Co-condensation method[62] is an one-pot synthesis approach, in which e.g. tretraalkoxysilanes ($Si(OR)_4$ (tetraethoxysilane, TEOS or tetramethoxysilane, TMOS)

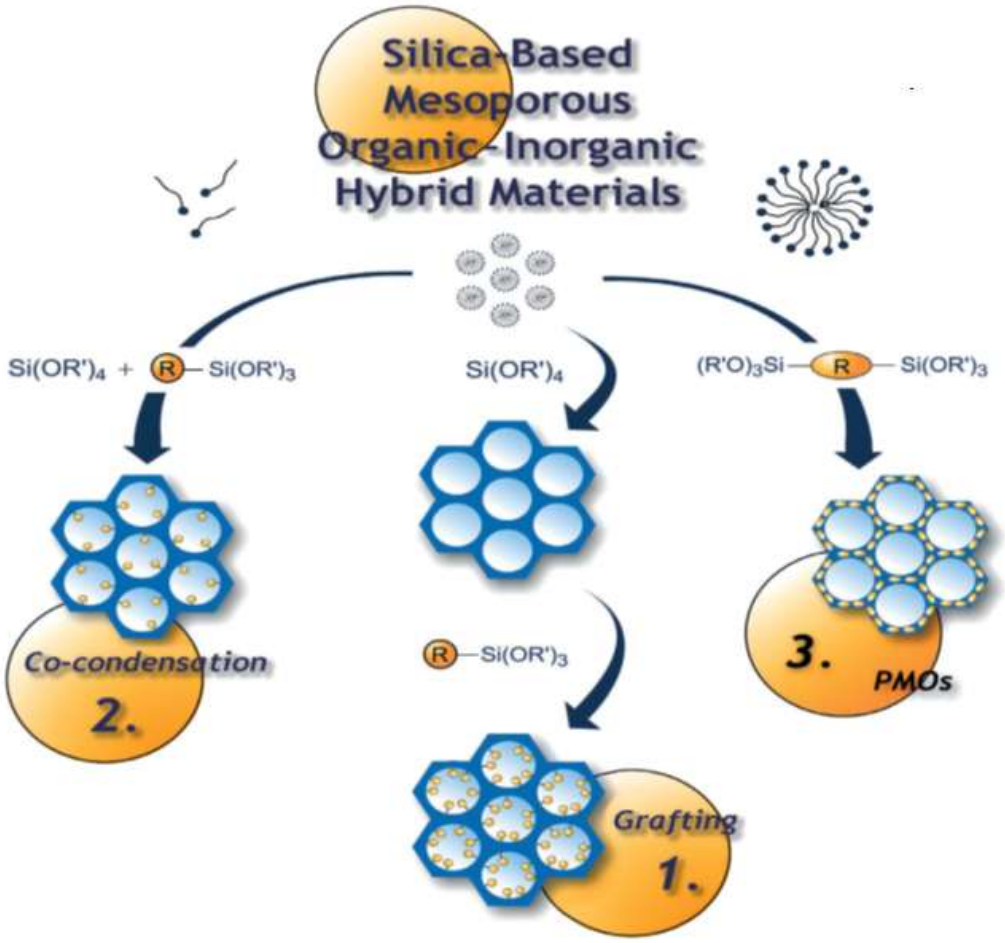

Figure 1.4 Figure extract form Hoffman et al. shows the three different pathways for the synthesis of mesoporous hybrid materials based on organosilica units[27]

are condensed to form an inorganic network in the presence of organically-subsitituted trialkoxysilanes ($R\text{-}Si(OR)_3$. With respect to the formation of porous network, several things must be considered: (1) compared to the post synthesis modification, pore blocking is no problem during co-condensation, since the organic moieties are part of the inorganic network structure; (2) in addition, a better distribution of the organic groups within the matrix is achieved. However, the co-condensation approach also has some disadvantages.

First, network formation can be disturbed to a high degree, e.g. for silica-based M41S materials, the degree of periodicity is strongly influenced by the amount of organosilanes- the higher this amount, typically the lower is the resulting degree of periodicity. Second, high loading with organic groups is in general rather limited: only few examples are known in which the network is built to 100% from an organically substituted precursor. Another inherent problem of this approach is the different condensation kinetics of the precursors.

Homo-condensation is very often favored over co-condensation which not only limits the degree of loading, but also influences the reaction time and the distribution of the organic groups in the network. One more methodological disadvantage, which has to be considered in the synthesis of template materials such as zeolites or M41S and SBA types of materials, is that the removal of the templating agent must be performed very carefully. High temperature-treatments, which are often used, would lead to the simultaneous destruction of the organic function, thus often extraction processes have to be applied.

In the post synthetic functionalization (grafting)[63] method, the organic species can either attach to the porous network by simple adsorption of non-reactive (with respect to the pore wall surface) compound from the gas or liquid phase (noncovalent interactions) or though covalent attachment. The advantage of the organic moenty adsorption approach lies in the ease of processing: however the loading might be a problem since many species tend to agglomerate at the pore entrance resulting in low loadings. Other advantage, it's that the porous network typically retains its structural features.[27]

Incorporation of the desired functionality is also possible by covalent bond formation between the organic moiety and the pore wall. In this case, reactive organic molecules are added to the preformed solid via the gas or liquid phase. The third advantage of this method is that different organo-silanes can selectively be grafted at the pore openings, leading to complete closure of the pores and sealing the air within, potential leading to low-k materials. The difficulties that are encountered are the same as for non covalent anchoring, such as pore blocking, low loading etc. A preferential reaction at the pore entrances hinders the diffusion of the reactive molecules into the pore interior, which might result in a very inhomogeneous distribution of the functional moieties and low loading.

1.2.2.3. Application of organic groups tethered to OMS

Organic-functionalized OMS materials containing organic groups have been used in multiple applications like capture of metals[64], catalysis[55, 60, 65, 66], electronics[67] and CO_2 capture[59, 68-70]. Especially in the capture of CO_2, amine-OMS materials (see Figure 1.5)

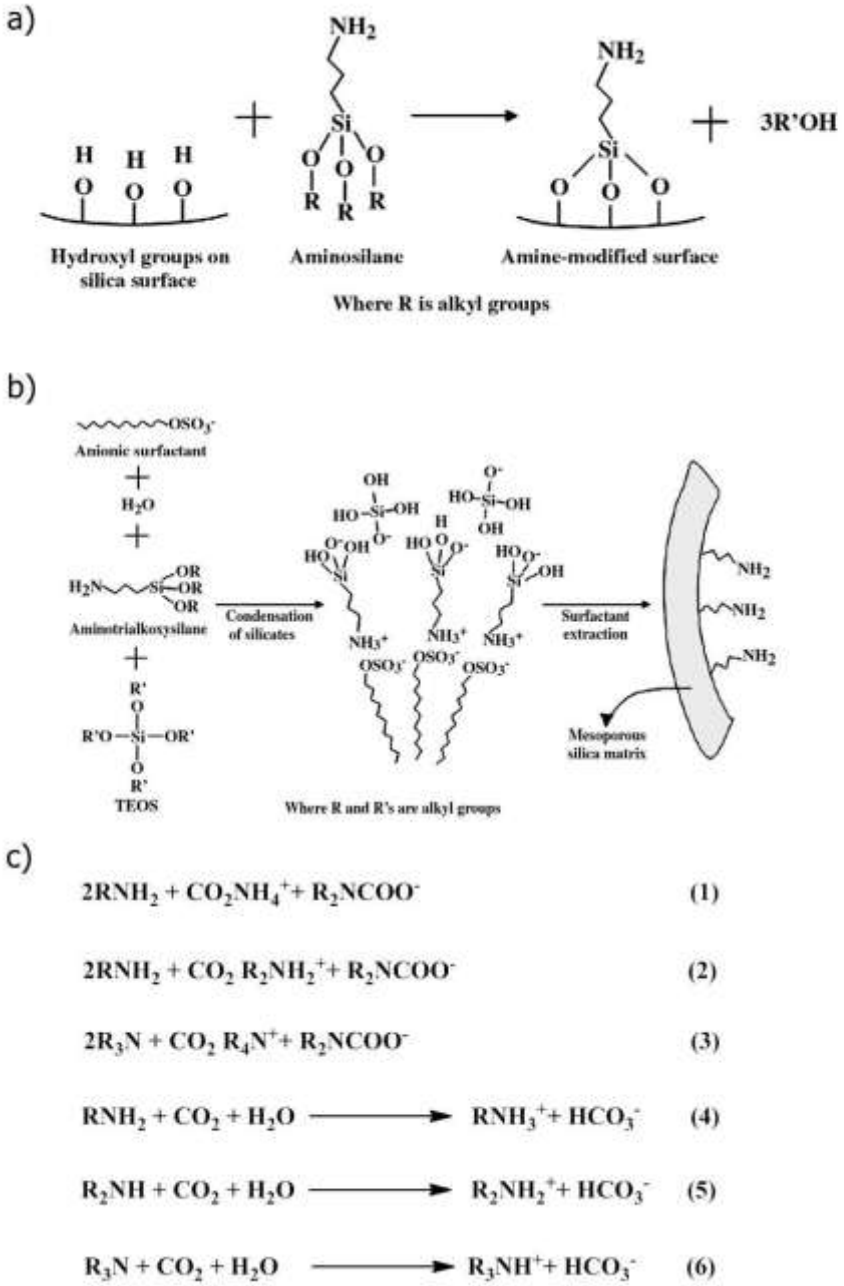

Figure 1.5 Illustration of: a) grafting method for the amine functionalization of OMS materials, b) co-condensation method for the amine functionalization of OMS materials and c) mechanism of reaction between amines and carbon dioxide[23]

have been attracted a lot of attention due to actually there is just one technology to capture CO_2 in the coal power plants, using liquid amines.[71-73] The amine-OMS materials offer the possibility to re-generated and reused[74] several times, reducing the cost of operation of coal power plants.[59, 75] However amine-OMS materials containing CO_2 could have other practical applications that we will explain in the proposal of this work.

1.2.3. Metal organic frameworks (MOFs)

Metal-organic frameworks (MOFs) are a relatively new class of microporous materials comprised of transition metals and transition metal oxides connected by organic linkage to create one, two and three-dimensional microporous structures (see Figure 1.6).[29]

The metallic nodes and organic linker, provide MOFs with unique and interesting properties. Bonds formed at the metal sites give these crystalline materials their mechanical strength and the organic linkers between metal sites allow easy chemical modification (see Figure 1.6).[76] While hundreds of zeolites have been developed for several decades, MOFs have shown numerous numbers of different structures due to their unlimited choice of nodes and spacers.

MOFs have drawn tremendous interest due to their potential applications in gas-storage,[77, 78, 79] gas separation, [80, 81, 82] gas sensing, [83] and catalysis. [84, 85 ,86]

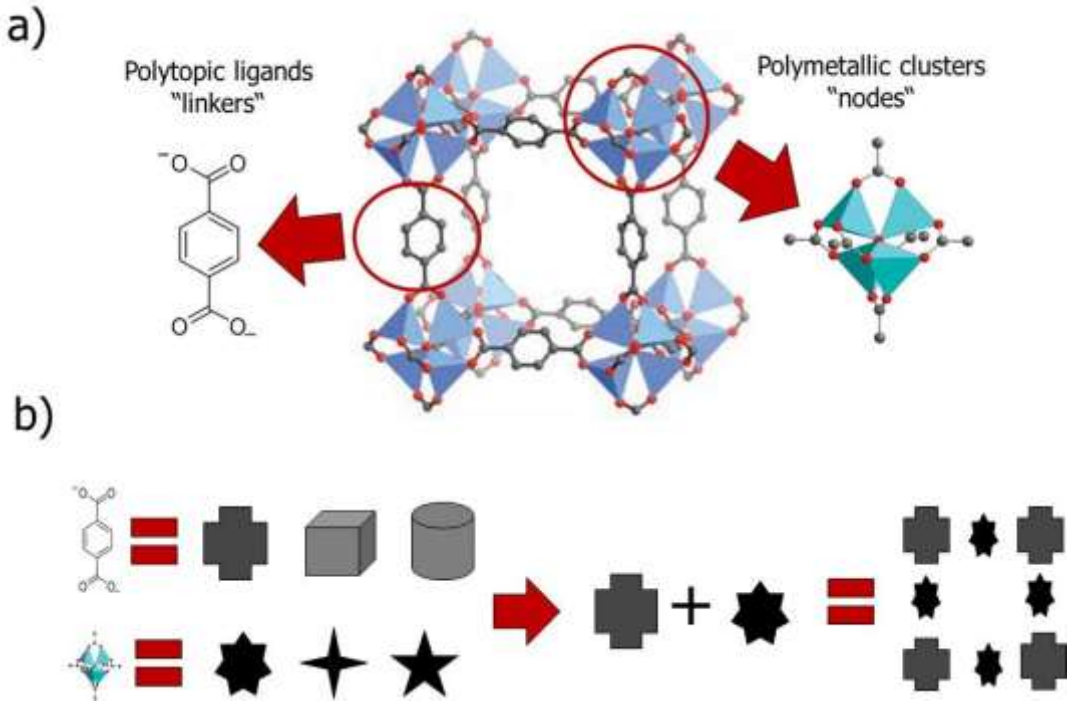

Figure 1.6 Illustration of: a) the metallic nodes and organic linker in the IRMOF-1 structure.[87] b) multiple possible combinations between metallic nodes and organic linkers for the synthesis of MOFs

There are several prominent MOFs leading this research area such as IRMOFs, MILS, HKUST-1, ZIFs and MAMS series showing excellent ability of gas adsorption or gas separation with high porosity and functionality.

1.2.3.1 Chemistry of MOFs

In order to categorize MOF structures using nodes and spacers as zeolite did. Yaghi and co-workers summarized the geometries of 131 Secondary Building Units (SBUs) [88] (see Figure 1.7). Yaghi and co-workers insisted in BSUs and their role for the formation of MOFs. But Ramanan. et al.[89] proposed a different intuitive and rational mechanism of MOFs using point zero charge molecules (PZC) as a "true building blocks".

According to their proposal, a soluble metal complex is immediately formed, when a metal salt is dissolved in solvent and then this complex organizes with organic group. It is important that how metal complex can organize with organic groups in the solvent.

In order to understand the transformation of molecules into the solid, hydrolysis and condensation are needed.

1.2.3.2 Prototypical of MOFs

Since O'Keeffe et al.[90] has used the term MOFs (Metal-Organic Frameworks), it has been distinguished from the term Coordination Polymers (CPs) which contain weaker bonds resulting in lower stability when they are dried.

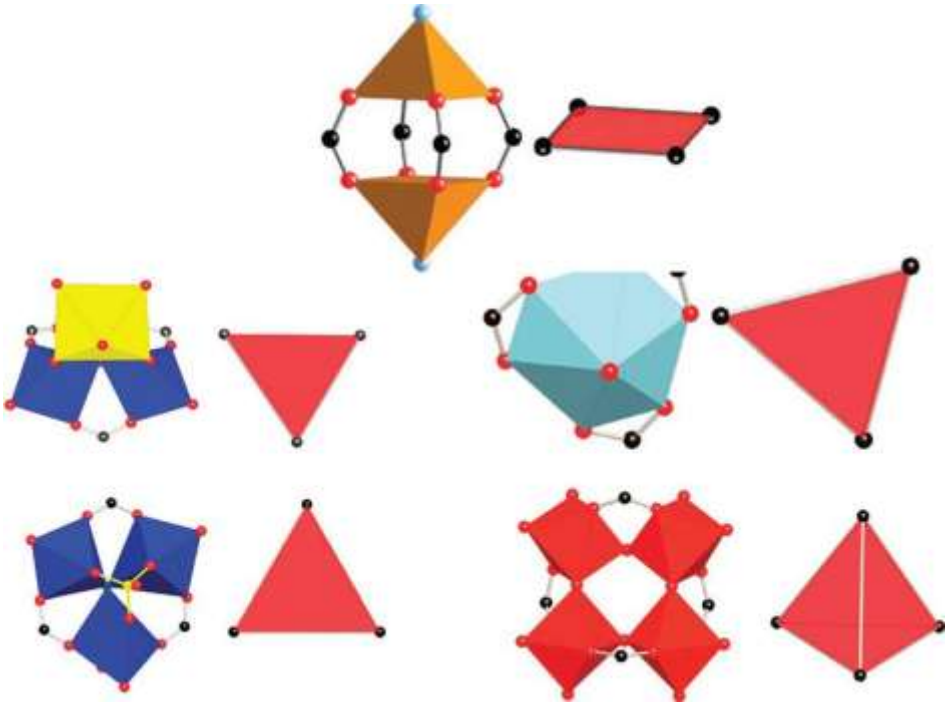

Figure 1.7 Illustration of various SBUs[88]

O'Keefe want MOFs to be considered as more stable hybrid frameworks built by strong directional covalent bonds between metal atoms and organic linkers resulting in 2-D or 3D porous frameworks which has been considered impossible for a long time[91] until Yaghi et al.[28, 77] reported for first time the Zn based MOFs series, (MOF-2, 2-D and MOF-4, 3-D). MOF-2 showed the ability to absorb gases with microporosity and high surface area. It consisted of Zn atoms and benzendicarboxylate in a periodic square array.[52]

According to Yaghi's reticular concept, isoreticular series of MOFs (IRMOFs) were designed by the same topology.[92] The same inorganic cluster and different dicarboxylate-type organic linkers could produce a variety of MOFs with "designed mater (see Figure 1.6b). The importance of this concept is the following. The crystalline materials can be synthesized by predetermined functionality and cavity size. Internal void space increases while organic linkers extends including special case of several cantenated forms (IFMOF-9, -11, -13 and -15).[79] Many applications of IRMOFs have been reported so far, for example, specific gas adsorptions, such as hydrogen and methane. IRMOF-1, known as MOF-5 is one of famous MOF among this series having high hydrogen capacity. [93]

Although IRMOFs have a permanent porosity with rigid structure after removal of solvent and structural diversity, they are less stable under moisture than other MOFs synthesized later such as MILs, HKUST-1, ZIFs and MAMs (see Figure 1.8). In 1998 Ferey et al.[94] have created an open-framework, MIL-1 (MIL, Material Institut Lavoisier), a number of MILs were reported . The most interesting material is MIL-101

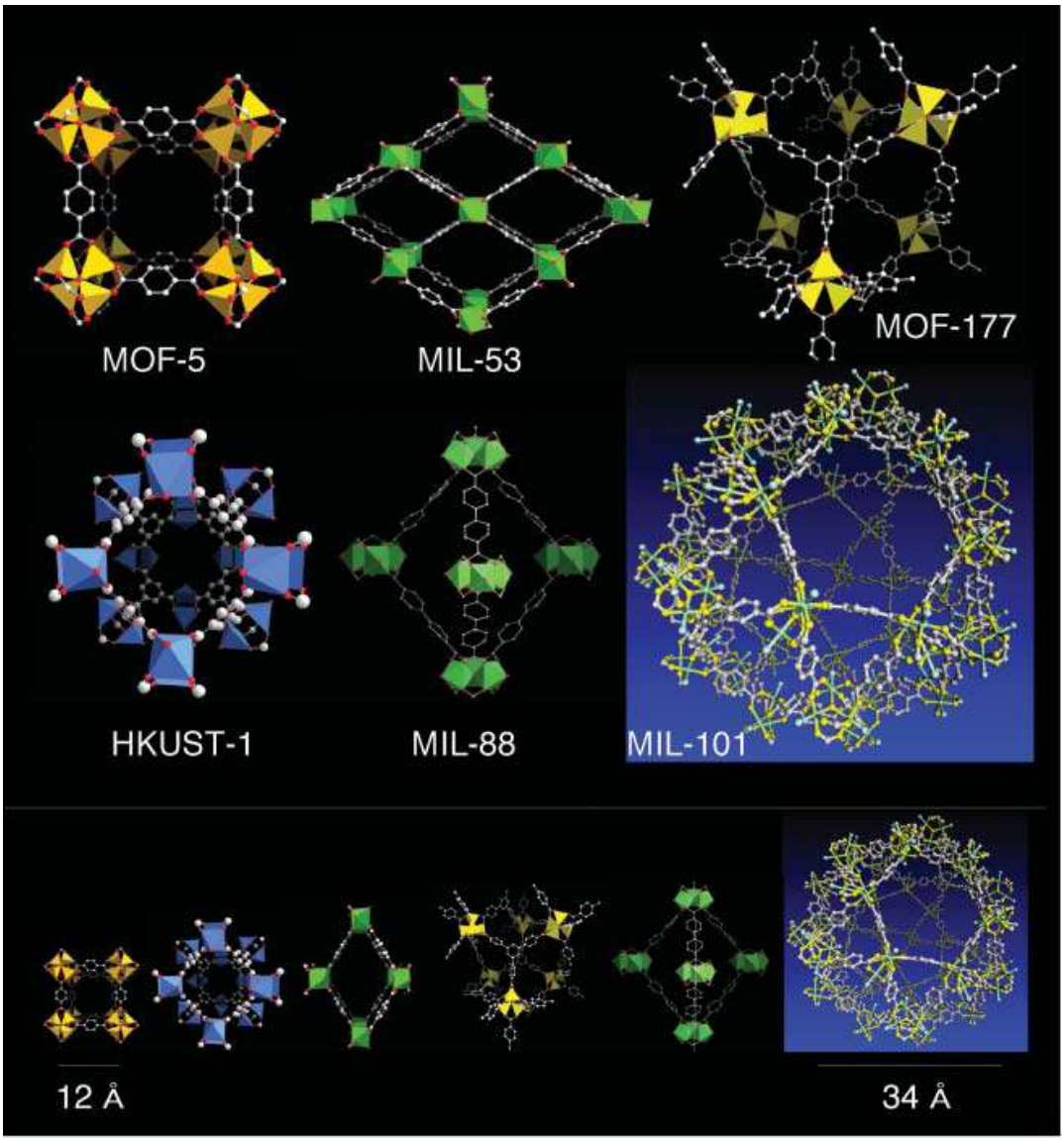

Figure 1.8 The currently most cited MOFs[95]

(reported in 2005), a highly porous chromium terephthalate, having a giant cell volume (~702000 Å^3), large surface area (~5900 m^2/g) and extra-large pore sizes (~30 to 34 Å).[96] The stability of MIL-101 under atmosphere and various organic solvents over several months, as well as the high adsorption capacity make MIL-101 an attractive candidate for the gas adsorption and separation. Other example of this family of materials is MIL-53 which after remove the solvent from the tunnels, it can readsorb big amount of water in his tunnels (V= 1486 Å^3). The breathing effect of MILs as well as high adsorption capacity lead MILs as a curious material in various research fields.

Other important MOF material is HKUST-1, originally reported by Chui et al.[97] consist of $Cu_2(H_2O)_2$ dimer units linked by benzene-1,2,3-tricarboxylate groups, forming a 3D open framework. HKUST-1 (see Figure 1.8) contains intersecting three dimensional channels of ~9 Å in diameter surrounded by tetrahedral side pockets of ~5 Å in diameter. The channels and the side pockets are interconnected via triangular windows of 3.5 Å. Owing to their microporous structure and robustness (thermal stability until 250 ^{o}C) as well as open coordination sites, HKUST-1 has been widely studied experimentally,[98, 99] and computationally[100, 101] for gas purification and separation.

Another exciting class of MOFs is so-called mesh-adjustable molecular sieves (MAMSs).[102-104] MAMSs are comprised of layers, each of which consists of tri-layer structure sandwiching the hydrophilic sub-layer with two hydrophobic sub-layers.

Lastly there has been a tremendous interest in zeolitic imidazolate frameworks (ZIFs) due to their unique thermal and chemical stability compared to other MOFs. This unusual stability of ZIFs is attributed to the strong metal-N bonds.[105-107] ZIFs shows zeolitic topologies due to the bond angle of metal-imidazolate-metal similar to the Si-O-Si bond angle in zeolites. Detailed information on ZIFs is given in the section below.

1.2.3.3. Zeolitic imidazole frameworks (ZIFs)

ZIFs are a subfamily of MOFs constructed by linking four-coordinated transition metals (M) through imidazolate (Im) units to yield extended frameworks based on tetrahedral topologies.[106] The fact that the M-m-M angle is similar to the Si-O-Si angle (~145^{o}) preferred in zeolites has led to the synthesis of a large numbers of ZIFs with zeolite-type tetrahedral topologies (see Figure 1.9).[108]

ZIFs exhibit permanent porosity and high thermal and chemical stability, for example ZIF-8 can be boiled in water, alkaline solutions and refluxing with organic solvents without loss of crystallinity and porosity. Additionally, ZIFs with structures formed from robust links, their frameworks display high thermal stability (Up to 500^{o} C).[106] For this reason in recent years ZIFs have been attracted a lot of attention in carbon dioxide capture,[107-110] hydrogen and methane adsorption.[111,112]. Due to ZIF's properties and potential applications, in the last years over 90 new ZIFs structures have been reported (ZIF-68, -69, -70, -78, -79, -81,-82, -95 and -100). Currently, ZIFs are the best porous material for the selective capture of CO2; furthermore, they show exceptional high capacity for CO_2 among adsorbents operating by physisorption.

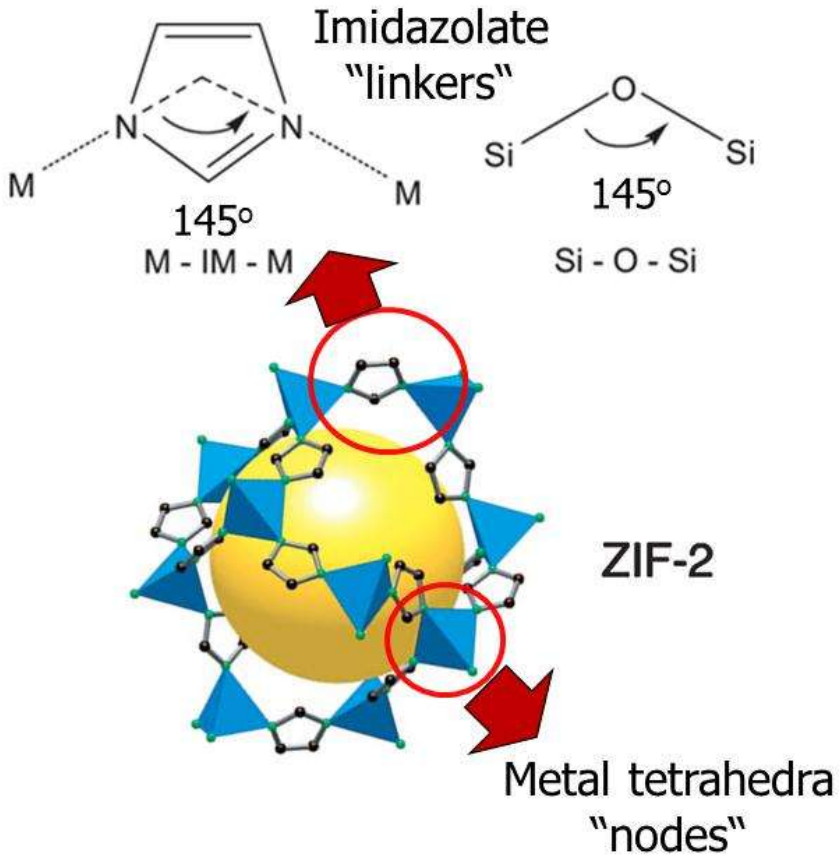

Figure 1.9 Illustration of the bond angles between ZIFs and zeolites. The metal tetrahedral "nodes" with imidazolate linkers are circled[106]

For example, Phan et al.[108] demonstrated that 1 L of ZIF-69 can store 82.6 L of CO_2 at 273 K. Indeed ZIF-69, the best-performing ZIF, displays a superior ability to store CO_2 in comparison to the industrially used adsorbent BPL carbon (see Figure 1.10).[107]

1.2.3.4 Applications of MOFs and ZIFs

MOFs including ZIFs display rich structural diversity, tunable pore size and chemical functionality through unique combined metal and organic structures. Due to these unique structural features of MOFs, MOFs offers new opportunities in gas adsorption and separation. Apart from MOF materials as powders, MOF membranes are of particular interest for advanced applications such as membrane base separations due to their exceptionally higher adsorption ability and porous properties.[113] The relatively high chemical stability of ZIFs compared with other MOFs makes them excellent candidates for more practical applications. Furthermore, ZIFs have been shown to have a high affinity for CO_2 adsorption at low pressures (at 298 K and 1 atm, MOF-777 has a maximum uptake or 7.7 L/L CO2 while ZIF-69 has capacity of 82.6 L/L).[114]

1.3 Organization of dissertation

The dissertation consists of two main topics. Chapters II-V concern the synthesis of metal-organic framework membranes and their applications in gas separations. Chapters VI-VIII deal with the novel application of nanoporous materials containing CO_2 as environmentally friendly flame retardants.

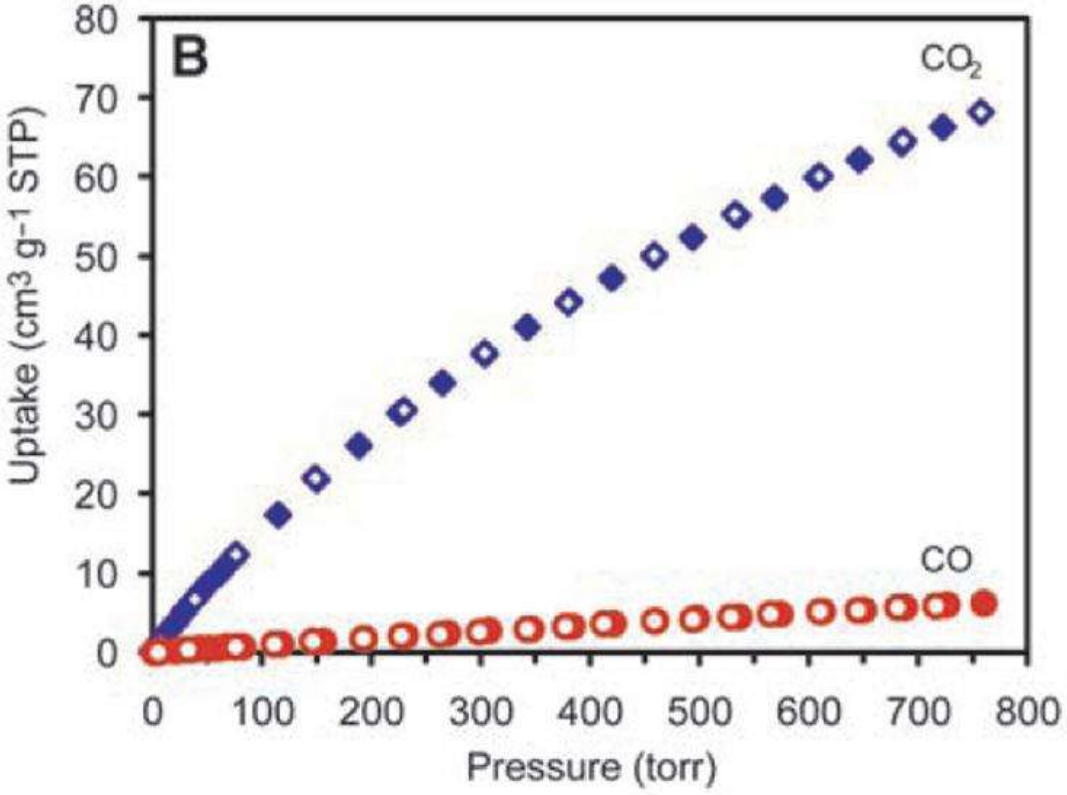

Figure 1.10 The CO_2 and CO adsorption isotherms for ZIF-69 at 273 K[107]

Chapter I provides and introduction to the work. Chapter II provides the overview of state-of-the-art MOF and ZIF membrane fabrication.

Chapter III deals with the experimental procedures for the synthesis and characterization of MOF/ZIF membranes. The research results are presented and discussed in Chapters IV and V, the synthesis and gas permeation of HKUST-1 membranes and ZIF membranes, respectively.

Chapter VI provides the background information on state-of-the-art flame retardant materials and their mechanisms. In Chapter VII, experimental procedures for the synthesis and testing of nanoporous materials containing CO_2 are given. The results are presented and discussed in Chapter VIII.

Finally, Chapter IX summarizes the work presented in this dissertation and presents some suggestions for future work.

CHAPTER II

RESEARCH REVIEW: STATE-OF-THE-ART MOF FILMS AND MEMBRANES

2.1 Introduction

Membrane-base separation have attracted a significant research interest as a potential technology in a wide variety of industrial applications from biomedical to petrochemical because membrane processes generally require low capital investment, low energy consumption, and easy operation in comparison with the conventional processes.[115]

Polymer membranes are currently dominant in membrane-based gas separation markets. This is primarily due to their processability (i.e., an ability to prepare a submicrometer thick selective skin layer using continuous processes) and their cheap material cost. Despite these advantages of polymer membranes, their wider applications are limited because of their limitations such as poor selectivity due to their flexible free volumes and their chemical/thermal instability.

Inorganic zeolite membranes have been developed over the last two decades or so to overcome some of the limitations of polymer membranes. Zeolites membranes offer unique opportunities in gas separation due to their uniform pore size in the molecular scales and thermal/chemical stabilities. Despite a considerable advancement in the development of zeolite membranes, their wider applications are also limited due to their limited number of available frameworks as well as their high manufacturing cost.

Metal-organic framework (MOF) materials are of great interest as membrane materials due to their unique structure and chemistry. MOFs, therefore, offer unique opportunities to overcome some of challenges that both zeolite and polymer membranes are facing. Recently the fabrication of MOF thin films [116, 117, 113, 118, 119, 120] and membranes[99, 121, 122] have been studied intensively. Both continuous thin films and membranes of MOFs have been prepared by in situ growth method[99, 118, 122] and secondary growth method.[119, 121, 123]

More recently membranes of thermal and chemical more stable ZIFs have been synthesized for gas separation. Bux et al.[1] and Li et.al[124] report the fabrication of the first ZIF-8 and ZIF-7 membranes using in situ and secondary growth methods. Liu et. al[125] success in the fabrication of ZIF-69 that show good selectivity of carbon dioxide over carbon monoxide.

Despite the early success of MOF and ZIF membranes (discussed below in more detail), there are several challenges that one has to overcome in order to realize the promises of these exciting materials for membrane-based gas separations to the full. Some of these challenges include: 1) thermal/chemically less stable than zeolites, 2) difficult heterogeneous nucleation and growth, 3) no general synthesis strategy available, and 4) difficult to scale up the synthesis procedures.

2.2 Synthesis of MOF/ZIF films and membranes

MOF and ZIF materials as thin films and membranes are of particular interest for membrane-based separation and other advanced applications such as sensors due to their

exceptionally high adsorption ability and high porous properties. There are some works related to MOF films for different applications with various MOFs, some of which include HKUST-1,[119, 126] MOF-5, [116, 127] ZIFs, [111, 128, 129, 130] MIL-53 and MIL-88B[131].

There are several approaches to prepare MOF thin films: 1) direct growth (or deposition), 2) use of self-assembled monolayers (SAMs), and 3) stepwise layer-by-layer. For the direct/deposition, one can utilize surface charges depending the nature of oxide supports as a simple method for thin film fabrication. For example, the deposition of MOF crystals on the Al_2O_3 (IEP, 8~9) supports is more favorable than that in SiO_2 (IEP, 1.7~3.5).[132] Using this strategy, Zacher et al. [132] prepared a dense coating of HKUST-1 crystals on the alumina supports while not much crystals grown on the silica supports. This was attributed mainly to the electrostatic interaction between positively charged alumina support surfaces and negatively charged organic ligands.

Self-Assembled Monolayers (SAMs) is other method to get thin films. Hermes et al. [116] reported selectively oriented HKUST-1 thin films on SAM modified by Au in the surface. Different terminated groups were tested (COOH-, OH-, CH_3-, and CF_3). The crystallographic preferred orientation was [100] direction. It is speculated that the organic terminated crystal faces might be connected to alkyl-terminated SAM.

Polycrystalline MOF/ZIF membranes can be prepared using two approaches that have been applied to prepare polycrystalline zeolite membranes: in situ[99, 118, 133] and secondary growth.[60, 119, 121] However, it turns out that synthesizing MOF/ZIF membranes is a lot more challenging than synthesizing zeolite membranes due to their unique chemistry (coordination chemistry vs. covalent chemistry).

2.2.1 In situ growth method

In an in situ growth, crystals nucleate and grow on porous supports into continuous well-intergrown membranes. In this method, a porous support is immersed into a precursor solution which contains solvent, metal salts, and organic ligands. Crystals nucleate heterogeneously and grow on the support (see Figure 2.1).

Liu and co-workers[134] used in situ method to prepare the first MOF membrane (MOF-5). They soaked a flat bare α-Al_2O_3 disc for half an hour in a Zn precursor solution. Arnold et al.[117] demonstrated in situ growth of Mn (II) formate crystals on graphite supports.. In the case of ZIF membranes, Box et al.[1] synthesized a ZIF-8 membrane using in situ growth under microwave-assisted solvothermal conditions. They used a titania support to increase the heterogeneous nucleation on the surface.

In general, despite the simplicity (i.e., one step process) of the in situ growth, there are a few limitations: 1) generally unfavorable heterogeneous nucleation of MOFs on porous oxide supports, 2) difficulty in controlling microstructure such as thickness, grain orientation, and grain boundary, and 3) reproducibility.

2.2.2 Secondary (or seeded) growth method

In contrast to in situ method, secondary growth decouples the nucleation step from the growth step. Tsapatsis and co-workers[135] first reported the synthesis of MFI membranes by the secondary growth method.

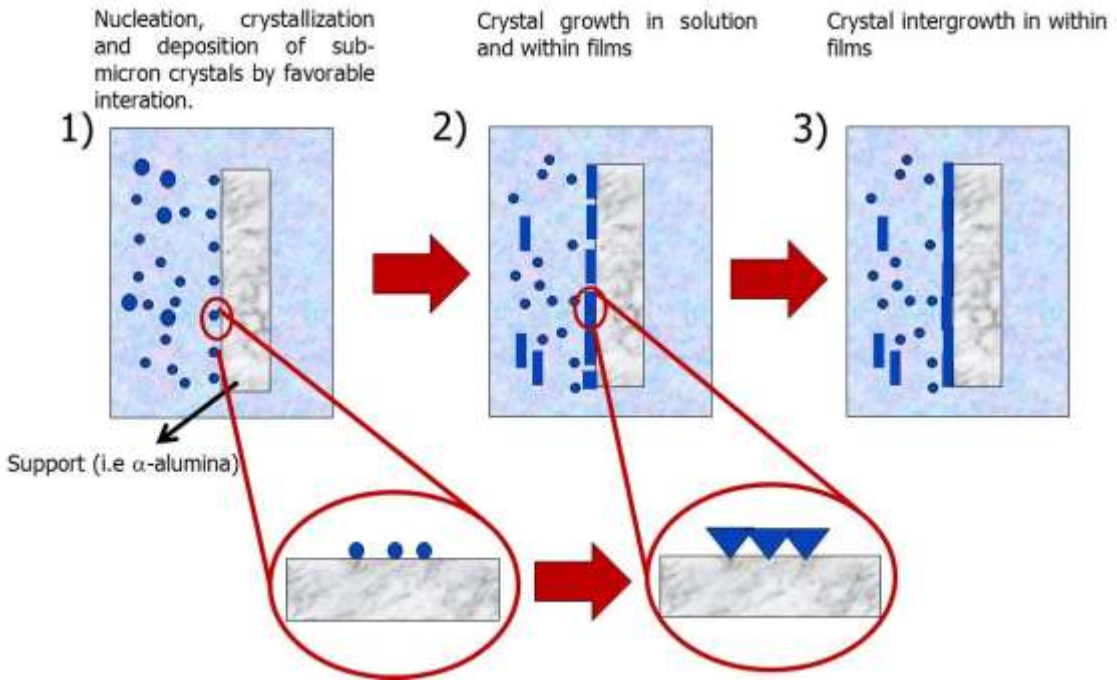

Figure 2.1 Illustration of in situ growth method for MOF films and membranes

By decoupling the nucleation and the growth steps, with secondary method it is a lot easier to control microstructure of membranes. The secondary growth method consists of two steps as illustrated in Figure 2.2.

The first step of this method is to prepare seed crystals by conventional hydrothermal synthesis. The size of seed crystals could be hundreds of nanometers. Seed crystals are then deposited on porous supports. The seed crystals could be preferentially oriented or randomly oriented (see Figure 2.2). Finally the seed layers are subjected to hydrothermal growth to make continuous defect-free membranes. Secondary growth has several advantages over the in situ method: 1) easy to control microstructure and 2) less dependent on the substrate types by decoupling nucleation and growth.

2.2.2.1 Seeding

To synthesize continuous MOF membranes by secondary growth, it is essential to achieve uniformly coated seed layers on the porous supports. There have been reported various seeding methods such as spin coating,[119] dip coating,[135-138] slip coating,[139] and manual assembly by rubbing[140].

In the spin-coating method the support is placed under vacuum and spinned after the solution containing MOF seed crystals is dropped on the surface several times, until the surface is uniformity coated with the crystal (see Figure 2.3a). Slip coating is very similar to dip coating (see Figure 2.3b).

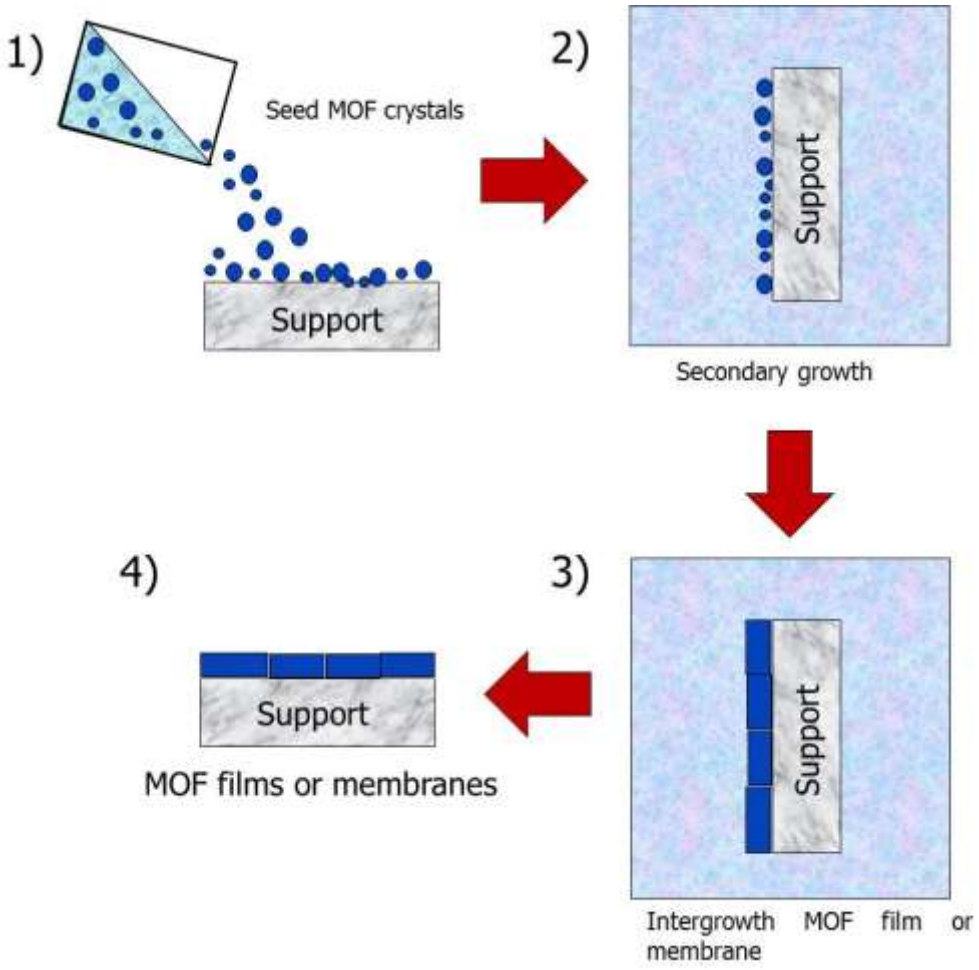

Figure 2.2 Schematic illustration of the procedure of secondary (seeded) growth, 1) deposition of seed crystals, 2) secondary growth, 3) formation of intergrowth film and 4) activation process (drying process)

The rubbing method (manual assembly) was also used in the fabrication of MOF membranes (see Figure 2.3c). Polymeric binding layers were coated on the supports before depositing seed crystals. These polymeric binders strongly attach the seed crystals on the supports via ionic bonding and/or hydrogen bonding.

In the dip-coating method the seed crystals are deposited on the porous support by simple contact with a suspension of MOF crystals as shown in the Figure 2.3d. The porous supports are brought to the surface of suspension. The horizontal surface of the polished support is in contact with the suspension, which can adhere to the porous support due to the surface tension and capillary force. During the drying process, solvents are evaporated and seed crystals can attach to form seed layers on the porous supports. The main driving force to attach the seeds on the porous support is the capillary force. Once water is filled on the support pores, capillary forces acting on seed crystals guided on the surface of the support disappear and seed crystals in the suspension are stopped to move to the support. If seed layers are formed by just one time dip coating, chances are likely to have the seed layers with defects. In order to obtain the high density and coverage of seed layers, it is necessary to repeat the drying and it takes a long time to coat using the dip coating technique.

The upper size limit for self-assembly is approximately around 3 μm because larger crystals are very difficult to disperse in the solution. Direct attachment with the hands normally organizes big crystals (> 3 μm) and its lower size limit is around 0.5 μm.

.

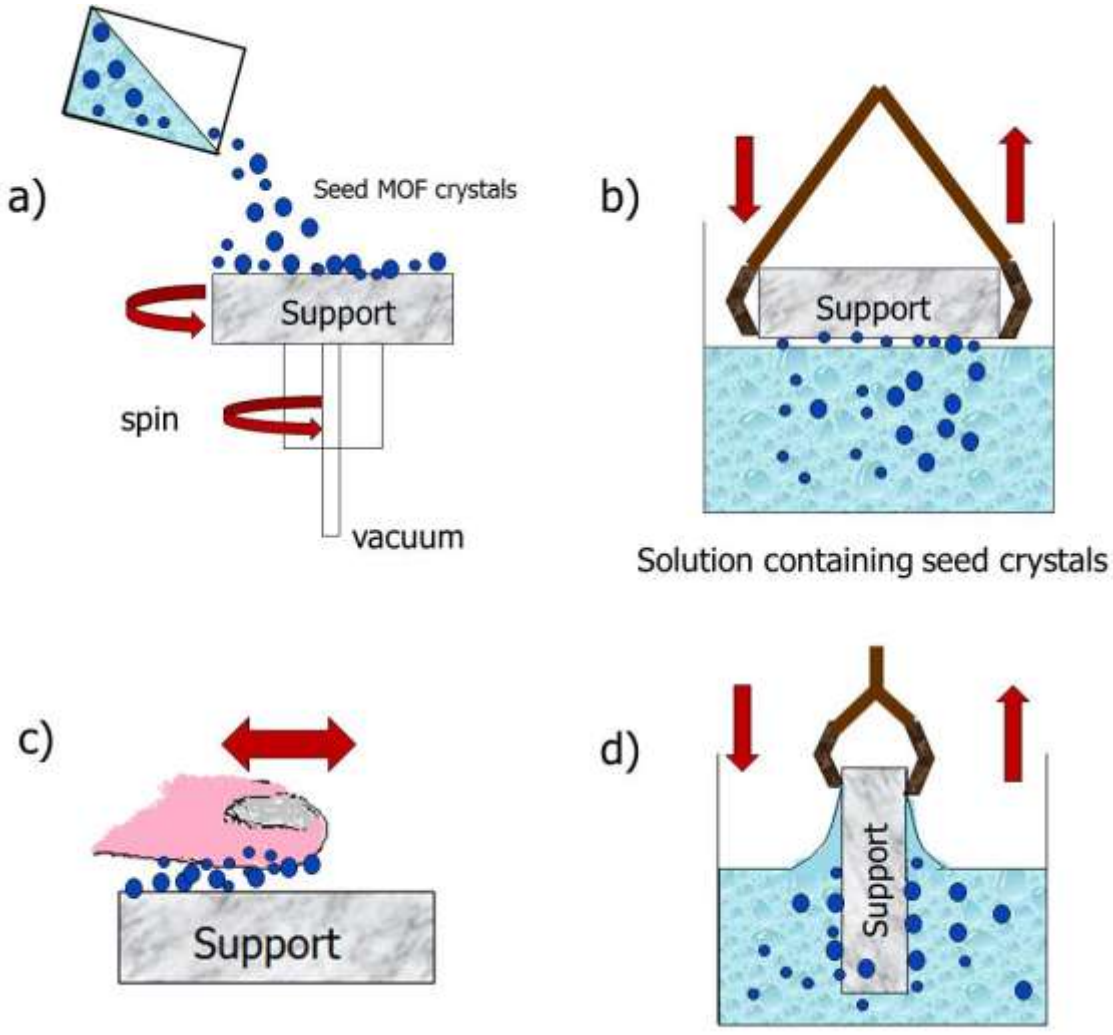

Figure 2.3 Illustration of different seeding methods a) spin coating, b) dip coating, c) rubbing and d) slip coating[199]

In the overlapping range of crystal size from 0.5 μm to 3 μm, direct attachment is desirable to deposit zeolite monolayer in terms of process time, large area deposition, close packing density, and uniform orientation of the crystals.

2.2.2.2 Secondary growth

The porous supports deposited with MOF seed crystals are then solvothermally treated in Teflon-lined autoclaves, leading to the inter-growth of the seed crystals filling the gap between seed crystals, resulting in continuous membranes. In order to synthesize crack-free continuous MOF membranes, it is often necessary to optimize solvothermal synthesis conditions such as molar composition of the precursor solutions, synthesis temperature and time. It is worthy of mentioning here that often the precursor concentrations in the growth step must be lowered as compared to those for the bulk crystal synthesis. By diluting the precursor concentrations, once can promote the heterogeneous nucleation while reducing the homogeneous nucleation.

Recently, microwave (MW)-assisted synthesis has been widely used due to its fast, simple, and energy-efficient nature. One of the main advantages of the MW-assisted synthesis of MOF and ZIF membranes is that one can reduce synthesis time, thereby cost. Rapid heating rate driven from thermal lag and short induction period in MW-assisted synthesis enable to produce a rapid nucleation and growth as well as fast supersaturation of the reaction mixture.[141]

2.3 Gas transport (diffusion) and separation through membranes

Transport and separation of gas molecules through MOF and ZIF membranes are based on interfacial processes and intracrystalline diffusion. Barrer et al.[142] described that transport through porous crystal membranes can be carried out by five consecutive steps: 1) adsorption on the external surface, 2) transport from the external surface into the pores, 3) intracrystalline transport, 4) transport out of the pores to the external surface, and 5) desorption from the external surface (see Figure 2.4).[142]

All of these five steps are activated processes, which assume that molecules jump between low-energy sites. Steps 1, 2, 4, and 5 are referred to as interfacial processes and step 3 as intracrystalline diffusion. The operating conditions (temperature, partial pressure) and characteristic of membranes and gas molecules (pore diameter, channel shape, molecular weight, and average molecular diameter) determine the rate determining step among five steps.

2.3.1 Interfacial processes

Interfacial processes include step 1, 2, 4, and 5 (see Figure 2.4). In the first step, adsorption on the external surface is affected by adsorbent-adsorbate interaction (often determined by gas isotherms) and temperature.

For weak adsorbent-adsorbate interaction or at high temperature, the first step might be negligible and gas molecules enter directly into the pores.

.

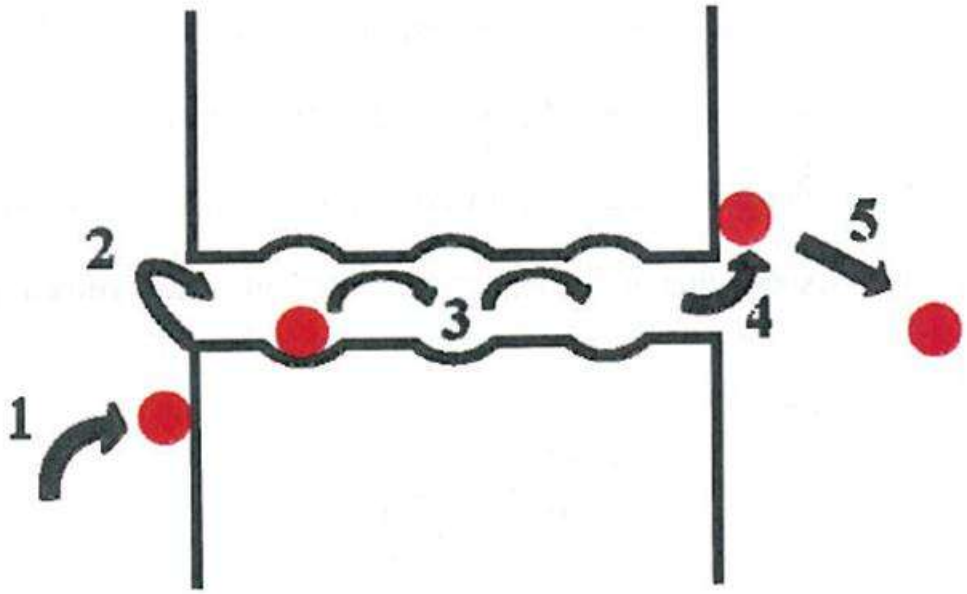

Figure 2.4 Five step model for mass transfer through crystal membranes. Step1: adsorption from the gas phase on the external surface; step 2: transport from the external surface into the pore; step 3: intracrystalline diffusion; step 4: transport out of the pore to the external surface; step 5: desorption from the external surface into the gas phase[143]

In the second step, transport from the external surface into the pores is confronted with high energy barrier for entering inside pores as a result of higher activation energy for this process. In general, the second and the third steps are rate-determining.

Adsorption on the external surface is usually less than adsorption inside crystal such that the fourth and fifth steps are not rate-limiting steps. Barrer derived the equation (1) for the importance of interfacial effects.[142]

$$\frac{N_i^{abs}}{N_i^{id}} = \frac{1}{1 + \left(\frac{1 - k_{P_{i,0}}^{ext}}{1 - k_{P_{i,0}}} + \frac{1 - k_{P_{i,\delta}}^{ext}}{1 - k_{P_{i,\delta}}}\right)\frac{d}{\delta}\exp\left\{\frac{\Delta E_a}{RT}\right\}} \qquad (1)$$

N_i^{id} is the flux when intracystalline transport is rate controlling, and N_i^{abs} is the experimentally observed flux. ΔE_a is the activation energy of diffusion. K^{ext} , and K represent the Langmuir parameters for adsorption on the external and internal surface, respectively. Assume that K^{ext}, and K are identical. Then the equation 1 is simplified to:

$$\frac{N_i^{abs}}{N_i^{id}} = \frac{1}{\frac{1}{1 + 2\frac{d}{\delta}}\ exp\left\{\frac{\Delta E_a}{RT}\right\}} \qquad (2)$$

When N_i^{abs}/ N_i^{id} is one, interfacial processes are negligible. According to the equation (2), it is clear that at high temperature interfacial processes become less important for the low activation energy and thick membranes.

2.3.2 Intracrystalline diffusion

There are five types of transport mechanisms for intracrystalline pore diffusion through membranes as described in Figure 2.5. These mechanisms can be described by different pore sizes. and materials. Viscous flow is the result of the convective flow in the direction of an absolute pressure gradient. This type of diffusion normally occurs when the pores are above 20 nm. The permeance is proportional to the pore size and the partial pressure, and inversely proportional to the temperature. The permeance for the convective flow can be calculated with the following equation:

$$\prod_i = \frac{1}{RT} \cdot \frac{g}{\delta} \cdot \frac{r_p^2}{8_{\pi_i}} \cdot \bar{p}_i \qquad (3)$$

Where Π is permeance, R is gas constant, T is temperature, g is geometrical factor, δ is membrane thickess, r_p is pore radius, η dynamic viscosity, p is partial pressure, D is diffusivity, M is molecular weight, θ_i is occupancy, E_a is activation energy, q is the adsorbed phase concentration, and q_{sat} is the saturation concentration in crystals.

Molecular diffusion is simply called as bulk diffusion that is dominated by molecular-molecular collisions in the gas phase. Like viscous flow, molecular diffusion takes place in the pores of above 20 nm.

.

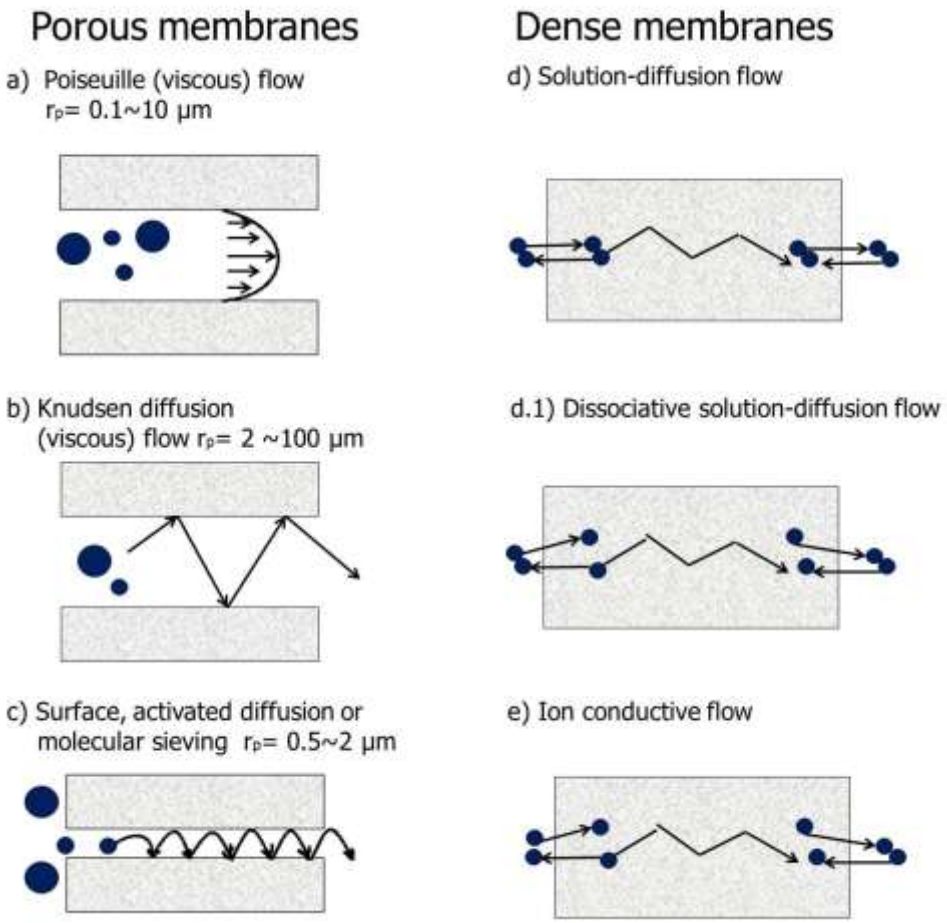

Figure 2.5 Gas diffusion mechanism via various pore size and materials, according to Shi [144], a) Poiseuille (viscous) flow, b) Knudsen diffusion, c) surface, activated diffusion, d) solution-diffusion flow, d.1) dissociative solution-diffusion flow, e) ion conductive flow

The permeance by molecular diffusion can be calculated by equations 4 and 5 (the symbols have the same meaning as those in equation 3).

$$\prod_i = \frac{1}{RT} \cdot \frac{g}{\delta} \cdot D_{ij} \tag{4}$$

$$D_{ij} = \frac{0.001858\, T^{\frac{3}{T}}}{P\sigma_{ij}^2 \Omega_D} \left[\frac{1}{M_i} + \frac{1}{M_j}\right]^{1/2} \tag{5}$$

Knudsen diffusion occurs in a long pore with a narrow diameter with a range from 2 nm to 10 nm by molecule-wall collisions. The Knudsen diffusion coefficient is proportional to the pore radius and the mean molecular velocity. In silicate-1 membranes, intercystalline diffusion through non-zeolitic pores such as defects or cracks is observed and described by the Knudsen diffusion. The Knudsen permeance can be calculated by equations 6 and 7.

$$\prod_i = \frac{1}{RT} \cdot \frac{g}{\delta} \cdot D_i^{KN} \tag{6}$$

$$D_t^{kn} = d \cdot \sqrt{\frac{8RT}{\pi M_i}} \tag{7}$$

Surface diffusion is an activated transport process that the molecules adsorb on the pore surface diffuse without ever escaping from the surface. The permeance from surface diffusion increases as a function of temperature. This can be calculated by equations 8 and 9.

$$\prod_i = \frac{\rho \cdot q_{sat,i} \cdot \mathrm{g} \cdot \mathrm{D_i^s} \nabla \mathrm{lm}(\mathrm{l} - \theta_\mathrm{i})}{\Delta p_i} \quad (8)$$

$$D_i^s = D_i^0 \cdot exp\left[\frac{-E_a^\delta}{RT}\right] \quad (9)$$

Configurational diffusion occurs in micropores, especially in zeolites. Configuration diffusion in zeolites is divided into two mechanisms: surface diffusion and activated gaseous diffusion in micropores. Gas molecules can either retain their gaseous character in the pores (activated gaseous diffusion) or they are adsorbed on the surface (surface diffusion).[145] The permeance by activated gaseous diffusion can be calculated by equations 10 and 11 while that by surface diffusion with equations 12 and 13:

$$\prod_i = \frac{1}{RT} \cdot \frac{1}{\delta} \cdot D_i^\mathrm{g} \quad (10)$$

$$D_t^{kn} = \mathrm{g} \cdot d \sqrt{\frac{8RT}{\pi M}}\ exp\left[\frac{-E_a^\mathrm{g}}{RT}\right] \quad (11)$$

$$\prod_i = \frac{\rho \cdot q_{sat,i} \cdot \mathrm{g} \cdot \mathrm{D_i^s} \nabla \mathrm{lm}(\mathrm{l} - \theta_\mathrm{i})}{\Delta p_i} \quad (12)$$

$$D_i^s = D_i^0 \cdot exp\left[\frac{-E_a^\delta}{RT}\right] \quad (13)$$

The temperature and pressure dependence of the permeance in porous membranes can be used to characterize the pore size of the membranes. Molecular diffusion and activated gaseous diffusion increase with temperature while Knudsen diffusion and viscous flow decrease with temperature.

Knudsen diffusion and activated gaseous diffusion is independent of pressure drop. However, surface diffusion and molecular diffusion decrease with increasing pressure. The dependence of the permeance on the temperature and the pressure is an important measure of the quality of membranes.

2.4 Microstructure of MOF membranes

Microstructure of MOF membranes refers to grain size, shape, thickness, orientation, and grain boundary. Since MOF membranes are polycrystalline in nature their microstructure plays important roles in determining the performance of membranes. It is, therefore, very important to understand and control the microstructure of polycrystalline MOF membranes. There are few reports[134, 146] on the efforts to control the grain size, orientation, membrane thickness and structure of grain boundary.

Here, we would like to review a couple of techniques (permporosimetry and fluorescence confocal optical microscopy (FCOM)) that have been developed to characterize the microstructure of zeolite membranes and its effect on the membrane performance. It is not unreasonable to apply these techniques for MOF membranes.

Hedlund et al.[147] used the permporometry analysis of zeolite membranes In permporosimetry, the permeance of non-adsorbing gas such as helium through zeolite membranes is measured as a function of pressure of a strongly adsorbing compound such as n-hexane in the case of silicate-1 membranes. The adsorbing compound effectively blocks the transport of the non-adsorbing gas even at the very low activity of the adsorbing compound. The plot of the permeance of the non-adsorbing gas as a function

of the relative pressure of the adsorbing compound is denoted a permporometry pattern.. An adsorption-branch permporometry experiment is simple and straightforward. In short, after activating the membrane by removing adsorbed species at 300 ^{o}C in a flow of dry gas, a full permporometry pattern is recorded. It has been shown that the distribution of flow-through defects can be estimated from the permporometry pattern using a simple model for permeation based on Knudsen diffusion. The estimated defect distribution is supported by SEM observations.

Fluorescence confocal optical microscopy (FCOM) is another technique that can be used to study the grain boundaries in MOF membranes. Bonilla et al.[148] applied this technique to observe the size and the density of the grain boundary defects in MFI membranes without destroying the membranes. Snyder et al.[149] later confirmed these results using optical reflectance imaging of dye-saturated c-oriented MFI membranes in combination with SEM images of an identical region of the membrane.

2.5 Characterization of MOF and ZIF membranes

X-ray diffraction (XRD) analysis of MOF and ZIF membranes is used to characterize the phase and the orientation of the crystals in membranes. Scanning electron microscopy (SEM) is a classical technique to evaluate the morphology, thickness, and grain size. Atomic force microscopy (AFM) can be also used to study the growth of MOF and ZIF films. Transmission electron microscopy (TEM) has been less used in the characterization of MOF membranes as compared to the case for zeolite membranes due to the fact that MOFs are not stable under intense electron beams.

Rapid identification of the defects or cracks in the MOF and ZIF membranes is of critical importance for research productivity. Sources of defects include incomplete growth of crystals, a non-uniform seeding, and thermal/capillary stresses during cooling/drying step. The permeation of helium or hydrogen as a function of its feed pressures can be used to make a quick assessment whether or not the membranes under examination have macroscopic defects. If membranes are free of macroscopic defects, the permeance will be independent of the feed pressure.

The measurement of the permeance and selectivity of gas or vapor molecules through the membranes can evaluate the quality of the zeolite membranes. The types of the measurement and methods will be discussed in the next chapter.

2.6 Summary

MOF membranes are of great interest due to their unique properties: 1) flexible pores, 2) chemical functionalities, and 3) a large number of frameworks.. Despite their potentials, there have been a limited number of reports regarding MOF membranes. This is primarily due to the unique challenges to synthesize MOF membranes whatever method used, either in situ growth or secondary growth. Some of these challenges include: 1) promoting heterogeneous nucleation, 2) attaching MOF seed crystals on supports, and 3) preventing crack formation during growth and drying process. In addition, the performance of polycrystalline MOF membranes also depends on the grain boundary defects. It is critical to characterize the grain boundary structure of MOF membranes and to understand their effects on the membrane performance.

CHAPTER III

EXPERIMENT METHODS

3.1 Introduction

This chapter describes general information of membrane performance and characterization. The permeance will be measured using the time lag method for single gas molecules (see Section 3.2). Also analytical methods for films and membranes characterization will be discussed in Section 3.3 (XRD, SEM, XPS, and TGA).

3.2 Permeance measurements

3.2.1 Time lag method for single gas permeance

The permeance of single gas molecules were measured in a custom-made permeation cell using a time-lag method. The time-lag is the amount of time required for a gas to permeate through a membrane.

There are two methods for obtaining the time-lag; one is a differential technique and the other is an integral method. In this study, we used the integral method to obtain the permeance of the gas molecules. The integral method monitors increasing pressure caused by accumulation of permeation gas through membrane in the evacuated chamber as a function of time. The chamber is initially degassed by vacuum and separated from the gas in feed side by a membrane.

The setup for single gas permeation is schematically shown in Figure 3.1. The permeation cell is separated two parts (feed side and permeate side) by a zeolite

membrane. At the permeate side, one port is connected to volume chamber which is subsequently lined to vacuum pump, and the other port is cupped. The pressure of the volume chamber is monitored by computer. Before measurement of permeance, the feed side is flushed with the gas molecules at about 1~2 bar and the permeate side is evacuated to a vacuum. The experiment is started when the inlet gas stream at the feed side is shut off. From this time, the pressure in the volume chamber at the permeate side increase and is monitored by a computer. The permeance (II) of gas molecules through MOF and ZIF membranes can be calculated using following equations.

The flux (J) of gas molecules through the membrane is given by the following expression:

$$J = \frac{slope}{RT} . \frac{V}{A}$$

The slope within the steady-state region is obtained during a permeation experiment by plotting the pressure of the chamber as function of time (see Figure 3.2). In the equation (1), V is the volume of the chamber, A is the area of membrane, R is the ideal gas constant, and T is the temperature of the experiment. Then, the permeance of gas molecules is calculated by the equation (2).

In the equation (2), ΔP is the pressure difference between at the feed side (P_2) and at the permeate side (P_1).

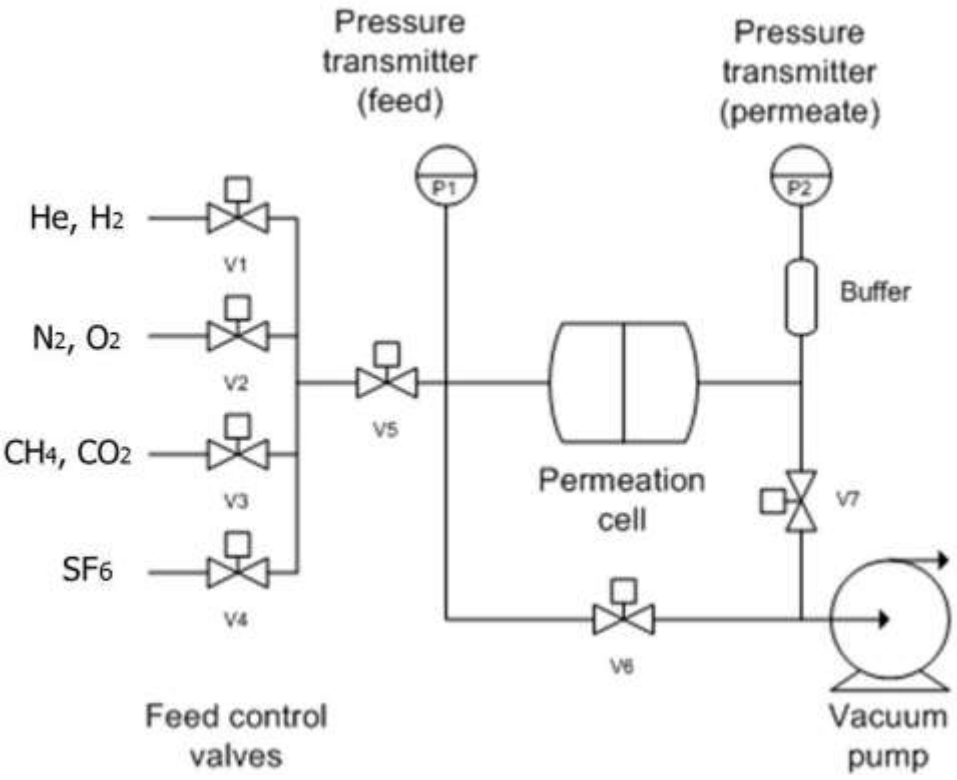

Figure 3.1 Illustration of the single gas permeation setup

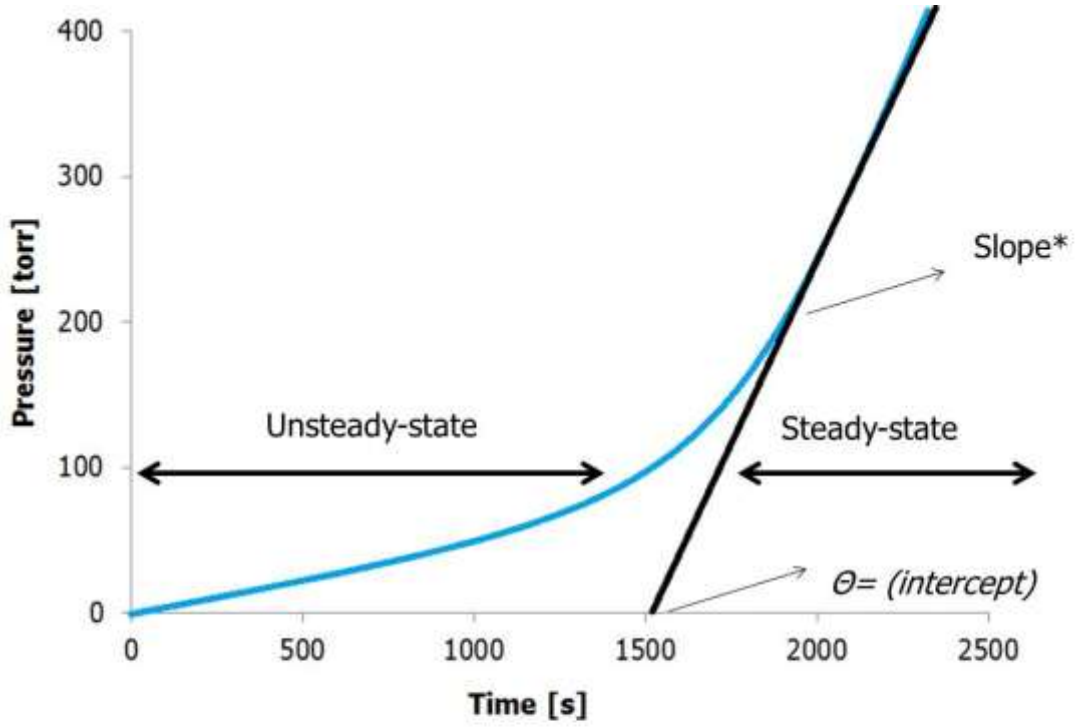

$$* J = P\frac{\Delta p}{l} \cong P\frac{p_{feed}}{l} = \frac{slope}{RT} * \frac{V}{A}$$

$$** \theta(intercept) = \frac{l^2}{6D}, D = \frac{P}{S}$$

Figure 3.2 Illustration of the time lag method

The pressure of permeate side (P_1) is much smaller than one of the feed side because the permeate side is evacuated to a vacuum. Thus, P1 can be ignored in the equation so that ΔP can be replaced to P_2.

3.3 Analytical methods

3.3.1 Electron microscopy

Scanning Electron Microscopy (SEM, JEOL, JSM-6400) was taken the images of MOF and ZIF membranes, thickness, and grain size. Also the SEM images confirm the quality of the MOF (HKUST-1) and ZIF-8 and 7 membranes membrane by close up the crystals and the intergrowth in the films. To observe the seed nanocrystals on the surface of the support in the HKUST-1 membranes.

3.3.2 X-ray diffraction (XRD)

X-ray diffraction analysis of HKUST-1 and ZIF (8 and 7), was used to confirm the structure of the membrane crystals. X-ray diffraction (XRD) measurements were carried out on a RigaKu MiniFlex^{TM} II with Cu-Kα radiation (λ=1.54 Å).

3.3.3 Optical microscopy

The observe as a first approache the quality of the HKUST-1 and ZIF membranes an optical microscope (Axiovert 200M, Zeiss) was used, and also to observe the polish work in the support discs.

3.3.4 X-ray photoelectron spectroscopy (XPS)

High-resolution XPS spectra were calibrated by sp^2-hybridized carbons centered at 284.5 eV. to prove the generation of bonds between N-Al during the surface modification of the porous supports. Scaning electron micrographs were taken with JEOL JSM-7500F field emission scanning electron microscope operating using the gentle beam mode, at 3keV acceleration voltage and 8 mm lens distance. The gentle beam mode improves the image quality of nanoconducting samples by decelerating incident electrons near the sample surface. Samples were coated with 3nm of Pt/Pd to mitigate charging.

3.3.5 Thermal gravimetric analysis (TGA)

Thermal gravimetric analysis (TGA, Netzsch TG 209c) was performed on powder samples of HKUST-1. The samples were heated from 25 ^{o}C to 350^{o} C under nitrogen at 1 ^{o}C min^{-1} heating rate.

CHAPTER IV

FABRICATION OF HKUST-1 MEMBRANES USING THERMAL SEEDING AND SECONDARY GROWTH*

4.1 Introduction

Nanoporous metal organic frameworks. (MOFs) have drawn substantial interest for their potential applications in gas storage,[78, 150] gas separation,[81, 82] gas sensing,[83, 151] and catalysis.[84-86, 152] One of the most striking features of metal organic frameworks is that one can fine-tune size, shape, and chemical functionality of their cavities and internal surfaces.[76, 153] This unique structural feature offers unprecedented opportunities in engineering frameworks for specific applications, particularly in gas storage and separation.

MOF materials as thin films and membranes are of particular interest for membrane-base separation and other advanced applications such as sensors.[113] Despite substantial efforts in the synthesis of MOFs, there have been relatively few reports on the fabrication of MOF thin films[116-120, 132, 154, 155] and membranes.[99, 121, 122, 133] Continuous films and membranes of MOFs were prepared by both in situ [99, 116, 118, 134] and secondary growth (i.e., seeded growth). [119, 121, 122]

---

*Reprinted with permission from "HKUST-1 membranes on porous supports using secondary growth" by V. Varela-Guerrero, Y. Yoo, M.C. McCarthy, H.K. Jeong, Journal of Materials Chemistry **2010**, 20, 3938-3943. Copyright 2010 by The Royal Society of Chemistry.

Liu et al.[133] and Yoo et al.[121] reported MOF-5 (also known as IFMOF-1) membranes grown by in situ and secondary growth, respectively. Gascon et al. [119] produced continuous films of HKUST-1 (also known as CuBTC) on porous supports using secondary growth by hydrothermally growing the seed crystals spin-coated on porous supports. However, no separation results were reported presumably due to the fact that the films were not well inter-grown. Guo et al.[99] recently reported the in situ preparation of HKUST-1 using "dual copper source" on copper nets. Despite their promising separation performance (separation factor of 7 for H_2/N_2), the membranes might have long-term mechanical stability problems since they are virtually free-standing. Ranjan and Tsapatsis[122] most recently reported microporous metal organic framework (MMOF) membranes on porous supports using secondary growth. The seed crystals were manually deposited on supports and subsequently grown into continuous membranes. Bux et al.[1] synthesized membranes of ZIF-8 (Zeolitic Imidazolate Framework) on porous supports showing hydrogen selectivity by molecular sieving.

HKUST-1, originally reported by Chui et al.[97], consists of Cu_2 (H_2O) dimer units linked by benzene-1,3,5-tricarboxylate groups, forming a 3D open framework. HKUST-1 contains intersecting three dimensional channels of ~9 Å in diameter surrounded by tetrahedral side pockets of ~5 Å in diameter (see Figure. 4.1). Owing to their microporous structure and robustness as well as open coordination sites, HKUST-1 has been widely studied experimentally [98, 99] and computationally [100, 101, 156] for gas purification and separation.

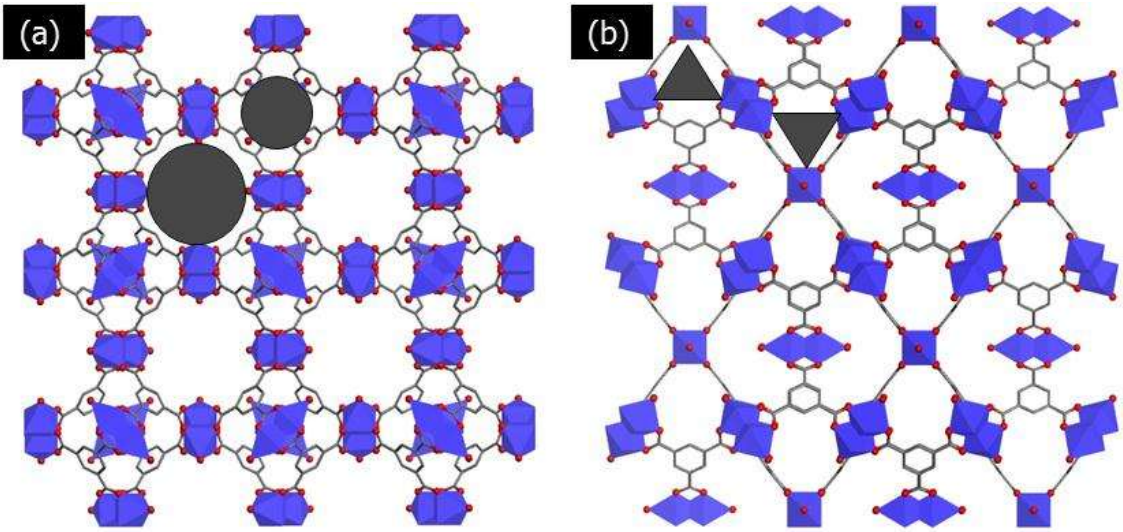

Figure 4.1 The crystal structure of HKUST-1 viewed (a) along the <100> direction showing the main channels of ~9 Å in diameter and the side pockets of ~ 5 Å in diameter and (b) along the <110> direction showing the triangular windows of ~3.5 Å in diameter connecting the main channels and the side pockets

Here we report the synthesis of continuous crack-free HKUST-1 membranes on porous α-alumina supports using the secondary growth method. A new seeding method was developed to strongly anchor seed crystals on the porous supports. The formation of cracks and fractures in the films was eliminated by slowly cooling and drying the membranes. The gas separation performance of the HKUST-1 membranes was measured in a single-gas permeation setup.

4.2 Experimental

HKUST-1 membranes on α-alumina were synthesized by our novel seeding method and secondary growth. The synthesis of seed crystals, seeding, and secondary growth are described in the following section.

4.2.1. Synthesis of HKUST-1 membranes

4.2.1.1. Materials

All chemicals were used as received without further purification. Copper (II) nitrate hydrate ((Cu(No3)2 3H2O, 98%, Sigma-Aldrich), benzene-11,3,5-tricarboxylic acid (trimesic acid, 98% Sigma-Aldrich, hereafter BTC), Ethanol (EtOH, 99%, Sigma-Aldrich) and DI water.

4.2.1.2.Preparation of HKUST-1 seed crystals

HKUST-1 seed crystals were synthesized by following the previously reported procedure.[119] In a typical synthesis, 0.875 g (3.6 mmol) of copper (II) nitrate hydrate

((Cu(No3)2 3H2O, 98%, Sigma-Aldrich) was dissolved in 12 ml of DI water (solution A) and 0.42g (0.2 mmol) of benzene-1,3,5-tricarboxylic acid (trimesic acid, 98% Sigma-Aldrich, hereafter BTC) in 12 mil of ethanol (solution B). The solutions A and B were mixed and stirred for about 30 min. The precursor solution was then poured in a Teflon-lined autoclave and heated at 120 ^{o} C for 6 h in a convective oven. The autoclave was naturally cooled down to room temperature. The resulting solution containing HKUST-1 crystals (solution C) was stored for seeding.

4.2.1.3. Thermal seeding of HKUST-1 seed crystals on porous supports

Porous α-alumina supports (2 mm thickness and 22 mm diameter) were prepared by following the previously reported procedure.[157] Prior to seeding, the bare α-alumina supports were heated in a convective oven at 200 ^{o}C for 15 min. While the supports were still inside the oven, the solution C containing HKUST-1 crystals as well as un-related ligands and copper species was dropped using a disposable pipette on the surface of the hot supports until the support surface was completely covered. To make sure the solvent evaporated completely, the supports were kept inside the oven for about 15 min. This "thermal seeding" process was repeated three times to completely cover the support surface with seed crystals. The seeded supports were then thoroughly washed with a copious amount of ethanol and sonicated for 1 min to remove crystals loosely attached to the supports. The entire process (i.e., three times dropping of the solution C and washing and sonication) was repeated until the supports were uniformly coated with strongly

bound seed crystals (typically four times) when evenly coated, the seeded supports display a uniformly greenish color.

4.2.1.4. Secondary growth of HKUST-1 seed crystals

To prepare the precursor solution for the growth of HKUST-1 seed crystals, 3.5 g of $(Cu(NO_3)_2\ 3H_2O$ was dissolved in 96 ml of DI water (solution A) and 1.68 g of BTC in 96 ml of ethanol (solution B). The solutions A and B were mixed for 10 min under stirring. Meanwhile, as seeded support was placed in an autoclave using a homemade Teflon holder. The sample was placed nearly vertically with the seeded surface very slightly facing down. The growth solution was then poured into the autoclave. After being heated at 120 ^{o}C for 6 h in a convective oven, the autoclave was slowly cooled down to 60 ^{o} C at 1 ^{o} C min^{-1} inside the oven. The autoclave was then removed from the oven and allowed to naturally cool down to room temperature. The membrane was thoroughly washed with a copious amount of DI water.

4.2.1.5. Drying process after secondary growth

As-synthesized HKUST-1 membranes were placed in a convective oven at 40 ^{o}C along with a beaker filled with DI water. The membranes were dried very slowly under nearly saturated conditions for 3 days. The color of the membrane samples changed from dark blue to light blue. Indicating partial removal of water from the pores of the framework.

4.3 Results and discussion

Figure 4.2 illustrates the procedure for the preparation of HKUST-1 membranes using the secondary growth method. Secondary growth was chosen over in situ growth because by decoupling the nucleation and the growth steps: (1) it is easier to control membrane microstructure such as thickness, grain size/ orientation, and grain boundary structure and (2) the nature of supports is less important. When using secondary growth however, it is of critical importance to anchor seed crystals on the supports (often porous oxide supports such as porous α-alumina).

For instance, zeolite seed crystals can be strongly attached on oxide supports by reacting surface hydroxyl groups of both zeolites and supports via simple calcination. However, this is not the case for MOFs due to the lack of such surface functional groups and/or the thermal stability of the materials. In order to achieve strong binding between HKUST-1 seed crystals and alumina supports, we have developed a new seeding method, “thermal seeding”, where the seed crystals in the synthesis solution (not-separated after synthesis) were seeded on the oxide supports at elevated temperature. The size of the seed crystals in the solution varies in the range of several nanometers to micrometres (see Figure 4.3).

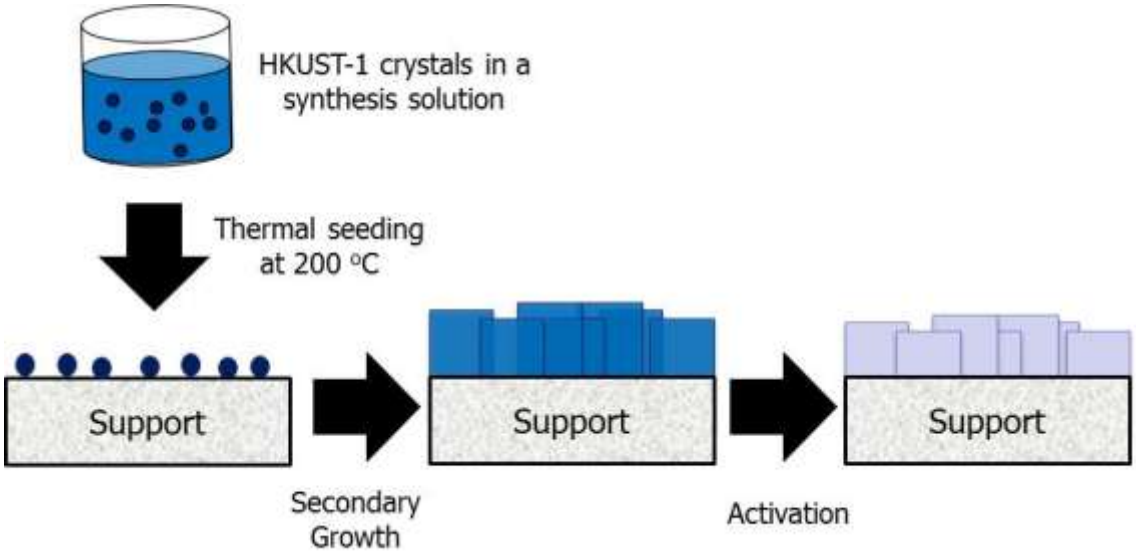

Figure 4.2 Schematic illustration of the synthesis procedure of HKUST-1 membranes by the thermal seeding and the secondary growth methods

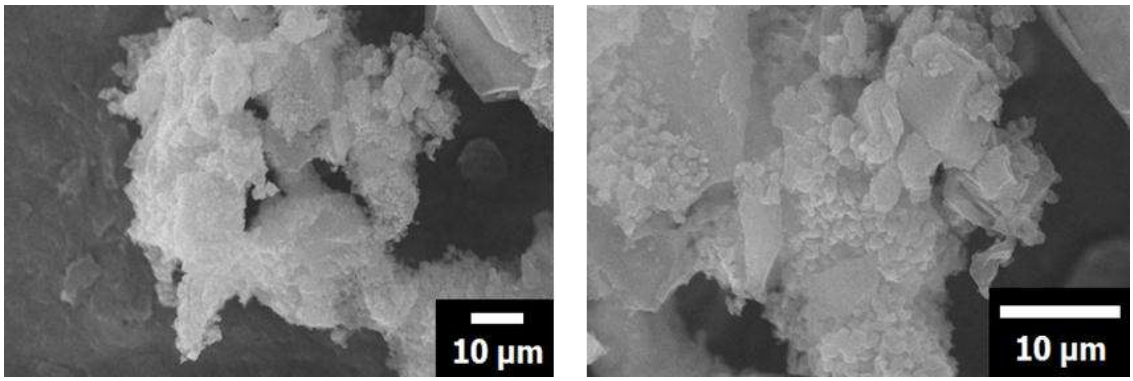

Figure 4.3 SEM micrographs of HKUST-1 seed crystals showing crystals of various sizes

Figure 4.4a compares XRD patterns of a HKUST-1 seeded support at 200 C (denoted as SSHT_S) and a seeded support at RT (denoted as SSRT_S) with the simulated powder diffraction pattern. Note that both samples were thoroughly washed and sonicated for 1 min after seeding to remove loosely bound crystals from the supports. While the SSRT_S sample shows no diffraction peaks, the SSHT_S sample shows well-defined diffraction patterns of HKUST-1, indicating that the seed crystals of SSHT_S are rather strongly bound on the support surface. Electron micrographs in Figure 4.4b show the presence of nanocrystals of HKUST-1 attached to the support in the SSHT_S sample.

To examine how strongly the seed crystals are attached to the supports, the binding strength of the HKUST-1 crystals was tested using a sonication method. As shown in Figure 4.5a 30% of the seed crystals of SSHT_S sample remain attached to the surface even after 1 h of sonication, suggesting rather strong bonds (likely coordination bonds) formed between the HKUST-1 crystals and the support. Since coordination bonds are not as kinetically strong as covalent bonds, the HKUST-1 seed crystals are not as strongly bound to the support as zeolite seed crystals.

The synthesis solution contains not only HKUST-1 nano-/micro-crystals (see Figure 4.3) but also un-reacted ligands and Cu species (likely in the form of Cu(II) paddle-wheel complex). It is hypothesized that these un-reacted ligands and Cu complex serve as binders for the ginding between HKUST-1 crystals and the alumina supports. In order to test our hypothesis, several control experiments were conducted.

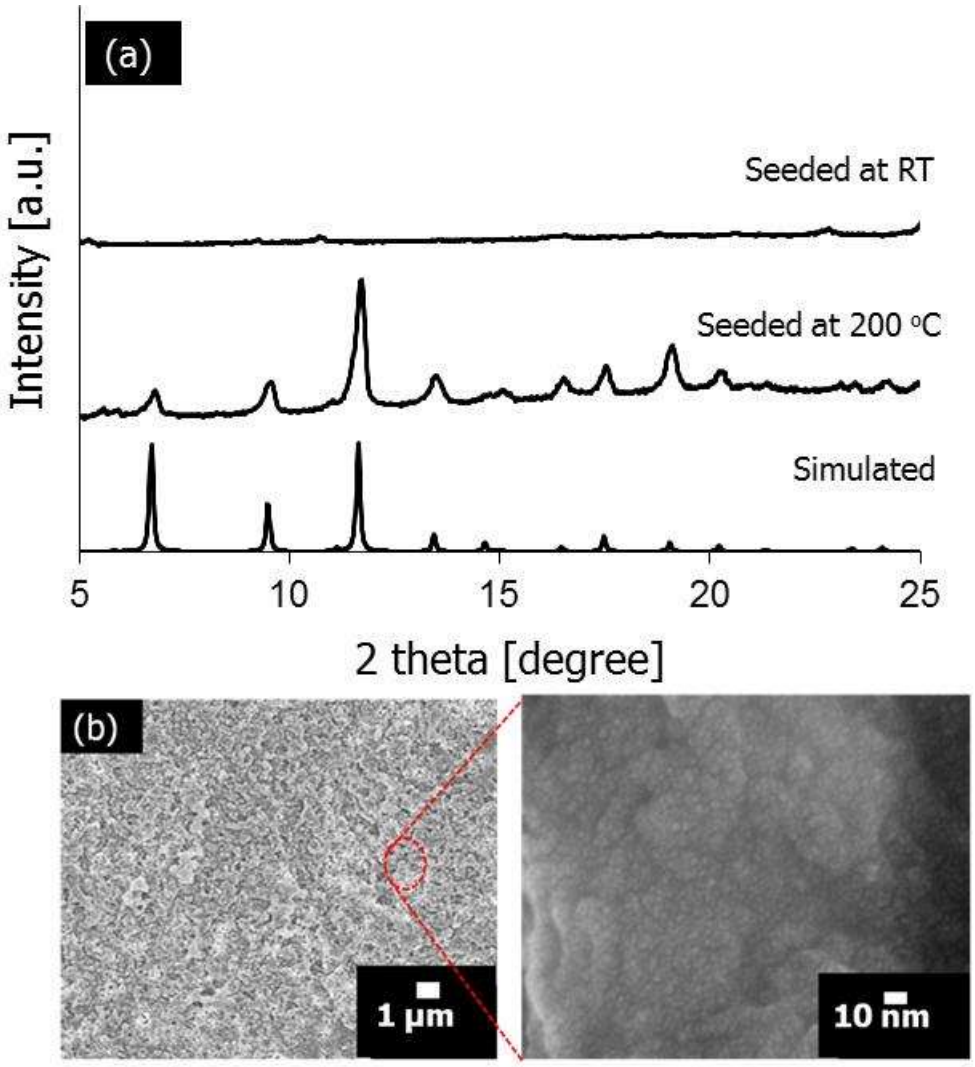

Figure 4.4 (a) X-ray diffraction patterns and (b) SEM micrographs of HKUST-1 seed prepared at RT (SSRT_S, top image) and at 200 ^{o}C (SSHT_S, bottom image). Note that the seeded supports were washed and sonicated for 1 min after seeding

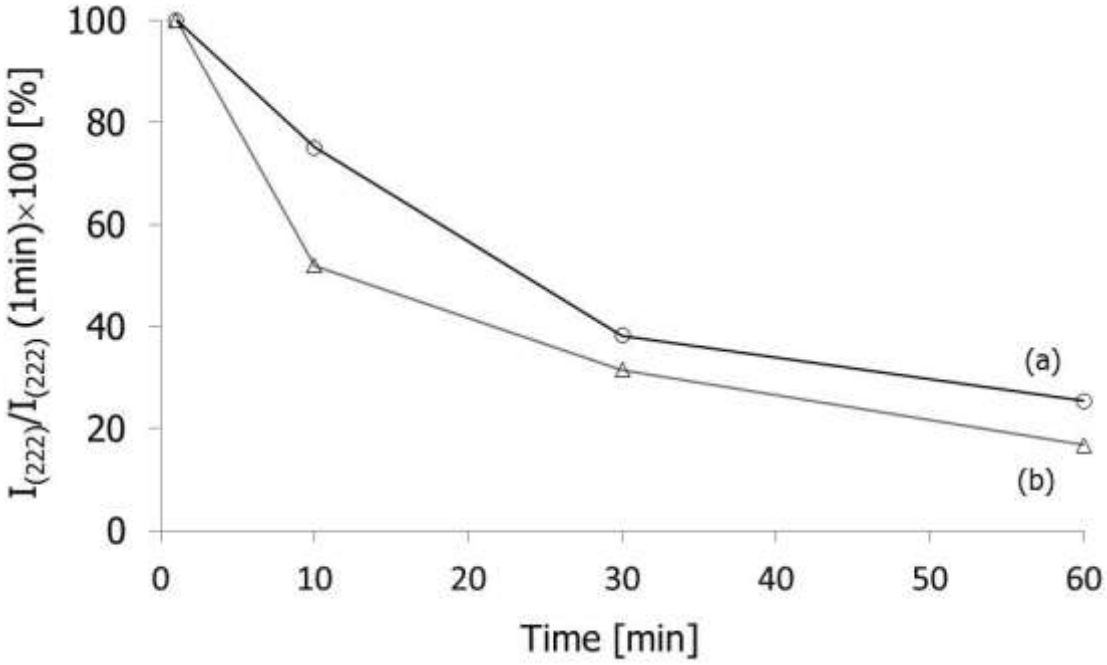

Figure 4.5 Binding strength of HKUST-1 seed crystals on the alumina supports; (a) seeded with crystals in a synthesis solution (SSHT_S) and (b) seeded with re-dispersed crystals in a solution of water/ethanol with both ligands and copper nitrate salt (SSHT_LC). The intensity of the (222) peak was normalized with respect to that of the (222) peak of the samples sonicated for 1 min

First, seed crystals were separated from the synthesis solution and re-dispersed in a fresh mixture of DI water and ethanol (1:1 in volume).

Then alumina support were seeded with the crystals were completely removed after sonication for 1 min (see Figure 4.6), indicating the importance of the presence of the organic ligands and/or Cu species in the seed suspension. Second, three samples of seed suspension in a DI water-ethanol mixture were prepared with fresh organic ligands alone (denoted as SSHT_L), copper nitrate salts alone (SSHT_C), and both ligands and salts (SSHT_LC), respectively.

The concentrations of the ligands and the copper salts in the seed suspensions were matched with those of the un-reacted ligands and copper estimated in the synthesis solution. After seeding at 200 ^{o}C for 15 min and subjected to sonication for 1 min, only the seed crystals from the suspension containing both organic ligands and copper salts (SSHT_LC) remained attached on the supports (see Figure 4.6b-d) pointing to ghe cooperative role of the organic ligands and the Cu species as binders. There are a couple of observations to be made. First, the density of the seed crystals of SSHT_S sample was about 20% higher than that of SSHT_LC sample judging from the relative intensity of the (222) reflection after 1 min sonication (not shown).

Second, the binding strength of the seed crystals of SSHT_S sample was greater than that of SSHT_LC samples (see Figure 4.5b).

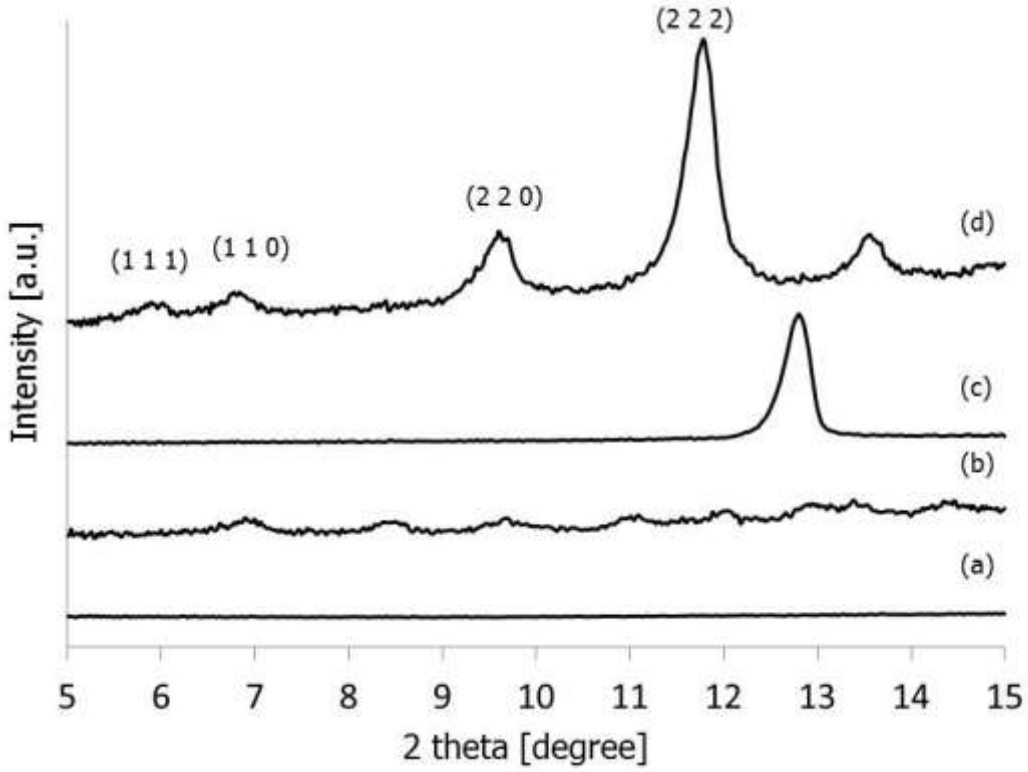

Figure 4.6 XRD patterns of the seeded supports using re-dispersed HKUST-1 samples in water/ethanol mixture containing (a) neither ligands nor copper salts, (b) only ligands (SSHT_l), (c) only copper salts (SSHT_C), and (d) both ligands and salts (SSHT_LC)

These control experiments suggests that both organic ligands and copper species (whether Cu^{2+} ions or Cu(II) paddle-wheel complexes) in the seed solution cooperatively serve as binders enabling the strong binding between the HKUST-1 seed crystals and the alumina supports. Lastly to determine the importance of seeding at 200 ^{o}C, the crystals in the synthesis solution were seeded on a support at room temperature and then treated at 200 ^{o}C for 4 h. After sonication for 1 min, most of the seed crystals were detached (not shown), indicating the importance of seeding at an elevated temperature. Continuous HKUST-1 membranes were formed from the supports seeded at 200 ^{o}C (SSHT_S) after secondary growth as shown in Figure 4.7. On the contrary, only a small amount of crystals were nucleated from the support seeded at room temperature (SSRT_S) (see Figure 4.8a).

For comparison, and attempt was also made to grow HKUST-1 in situ, showing a similar result as with SSRT_S (see Figure 4.8b). Although continuous, the HKUST-1 films exhibit a lot of cracks and fractures formed not only in the grain boundaries but also in the grains as seen in Figure 4.7a. The image of Figure 4.7a shows that some of the crystals were even detached from the support. These cracks and fractures form presumably after crystallization as suggested by the recent in situ and *ex situ* AFM study.[158] The formation of the cracks and fractures was attributed mainly to the stress on the film due to the mismatch between the thermal expansion coefficients of the alumina support and the HKUST-1 film when quenched after crystallization in a water bath after secondary growth.

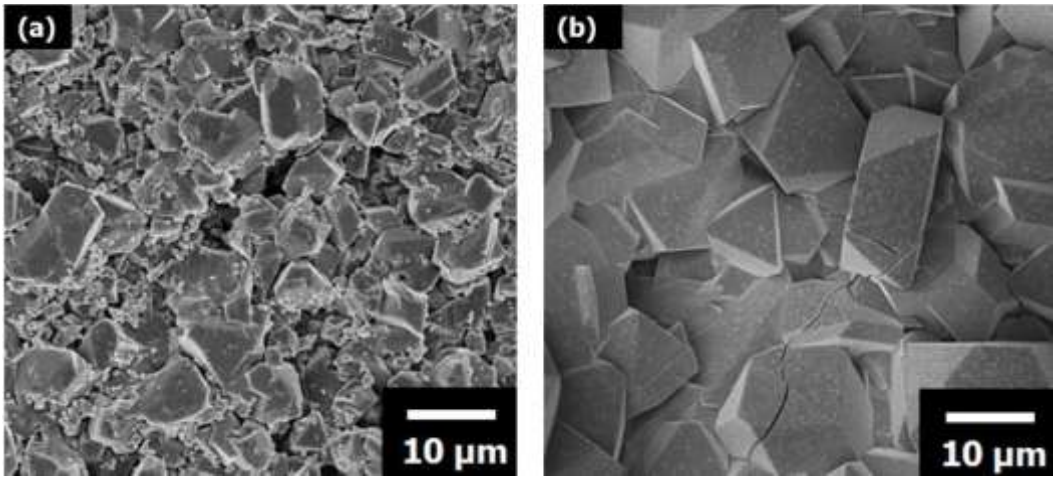

Figure 4.7 SEM images of HKUST-1 membranes using (a) rapid cooling and (b) slowing cooling after secondary growth

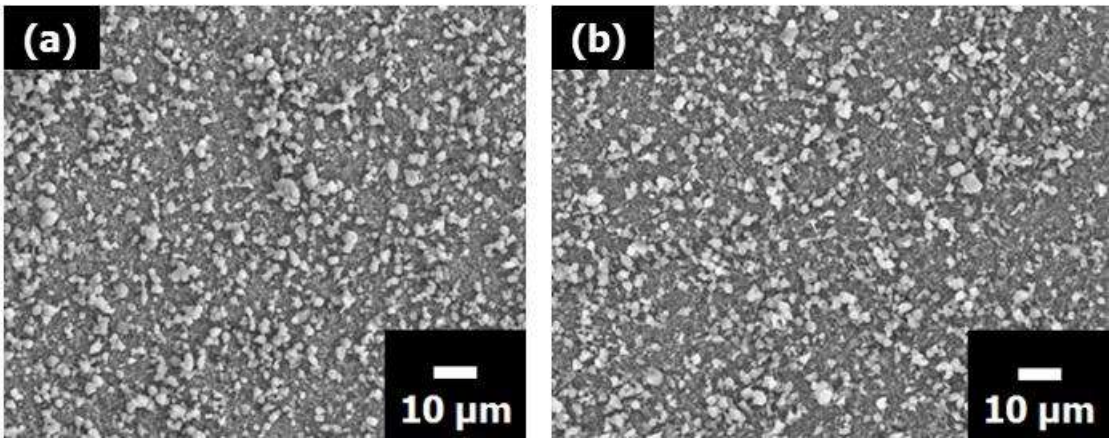

Figure 4.8 SEM micrographs of the samples grown form (a) the seeded support at RT (SSRT_S) and (b) the bare α-alumina support in situ

Due to the nature of bonding (coordination bonds), metal-organic frameworks are more prone to the formation of cracks and fractures than zeolites. By slowly cooling down the autoclaves (see the experimental section for details), the formation of cracks was significantly mitigated and no crystals were detached from the support as shown in Figure 4.7b. It is noteworthy that the cracks in Figure 4.7b are presumably due to the drying process as discussed below (samples were dried at room temperature overnight under vacuum for SEM).

Fully hydrated HKUST-1 membranes contain 13 water molecules (10 in the channels and 3 coordinated with Cu atoms) in formula unit, $[Cu_3(BTC)_2.13H_2O]$. In order to activate the channels, as-synthesized membranes need to be dried. When dried either at room temperature or at elevated temperature under ambient conditions, cracks formed in the membranes as can be seen Figure 4.7b. It is speculated that during the drying process the HKUST-1 films were subjected to capillary stress stemming from the evaporation of water. The magnitude of the capillary stress in the films is proportional to the rate of evaporation. By slowly evaporating water at 40 ^oC under nearly saturated conditions the formation of cracks was completely eliminated (see Figure 4.9a), trough the membranes were not completely dried. Figure 4.9b shows the X-ray diffraction pattern of a partially dried membrane in comparison to that of as-synthesized powder, confirming the phase. It is noteworthy that there was no significant change in the XRD before and after drying, indicating no structural modification upon drying.

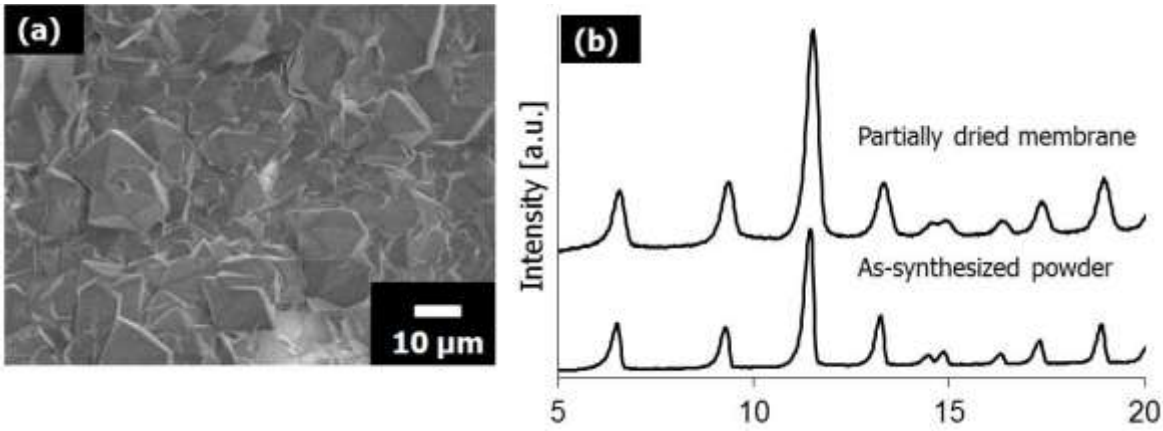

Figure 4.9 SEM image (a) and XRD pattern (b) of HKUST-1 membrane partially dried at 40 ^{o}C for 3 days under nearly saturated condition

In order to estimate how much water remains inside the structure, thermal gravimetric analysis (TGA) was performed on powder samples (see Figure 4.10). The sample dried under nearly saturated conditions exhibits about 17% reduction in mas at 100 C (see Figure 4.10a), which corresponds to about 8 water molecules per formula unit. This suggests that only 20% of the water in the channels was removed during the drying process. It is likely that the water molecules coordinated with the copper atoms still remain inside the framework. However, it is noteworthy that the remaining water molecules, in particular, that are not coordinated with Cu atoms, can be further removed during the permeation measurement. To verify this, we performed TGA on the powder sample that was subjected to the same condition as the membrane samples under the permeation measurement (i.e. repeated flush with dry He under vacuum at different temperatures).

The TGA result (see Figure 4.10b) shows that powder sample subjected under the permeation test conditions contained only about 5% of water in the structure, which corresponds to about 2.4 water molecules, likely rather strongly coordinated with Cu atoms. We speculate that these water molecules might be those that are not removed even after the permeation measurement or adsorbed from the atmosphere while transferring the sample for the TGA measurement.

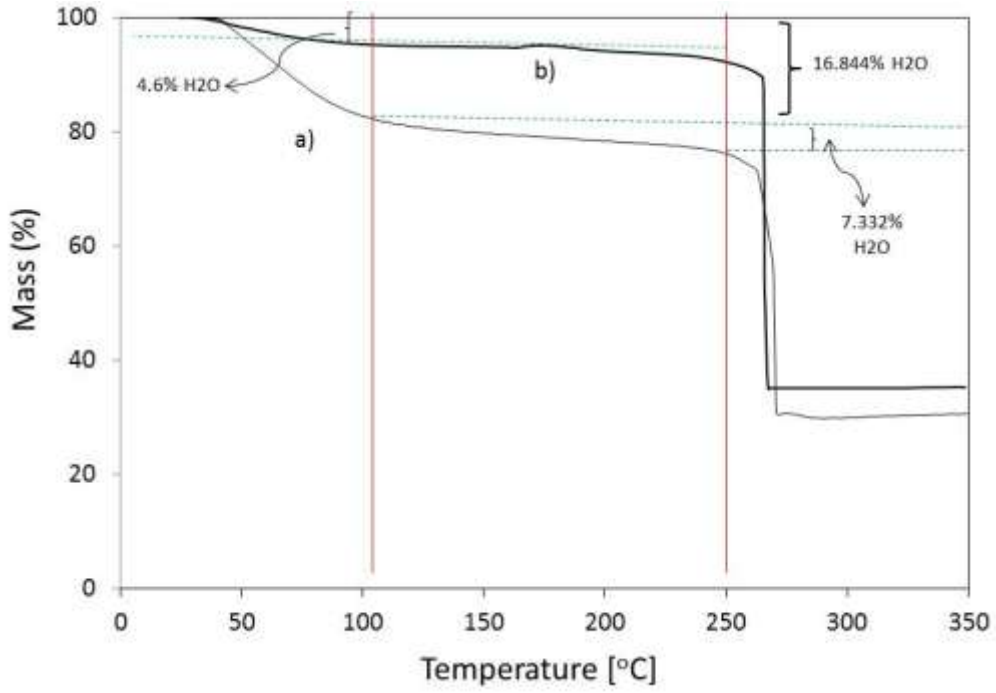

Figure 4.10 Thermal gravimetric analysis of the samples partially dried for 3 days, (a) at 40 ^{o}C under nearly saturated condition and b) after being subjected to the permeation test condition (i.e., flush with dry He under vacuum at different temperatures)

Nonetheless, we verified that after gas permeation test at different temperatures the membrane samples were free of macroscopic cracks (see Figure 4.11a) and structurally intact (see Figure 4.11c). The cross-sectional image in the Figure 4.11b shows the membrane thickness of about 25 μm.

The separation performance of the HKUST-1 membranes was measured as a function of temperature in a single gas permeation set up using time-lag method. To make sure that the gas separation performance of the membranes is not affected by the possible presence of the small amount of water molecules, the permeation measurements were repeated three times at various temperatures. The results showed practically identical results (see Figure 4.12), which can be attributed either to the absence of water molecules or to the negligible effect of the small amount of water on the gas permeation. Figure 4.13a shows the membranes have an ideal selectivity of H_2 over N_2, CH_4, and CO_2 at room temperature of about 3.7, 2.4, and 3.5 respectively, which is smaller than the previously reported values.

This could be due to the effect of the porous supports. In addition, as in the case of zeolite membranes, it is likely that non-selective intercrystalline diffusion through grain boundaries may be playing a role in reducing the selectivity. Since the membranes are tested under dry gases and are periodically flushed with dry helium during the permeation measurement, it is likely that the membranes are being further dried during the measurement even at room temperatures.

This could be due to the presence of water molecules inside. The maximum ideal selectivity of H2 over N2, CH4, and CO2 is around 7.5, 5.7, and 5.1 respectively.

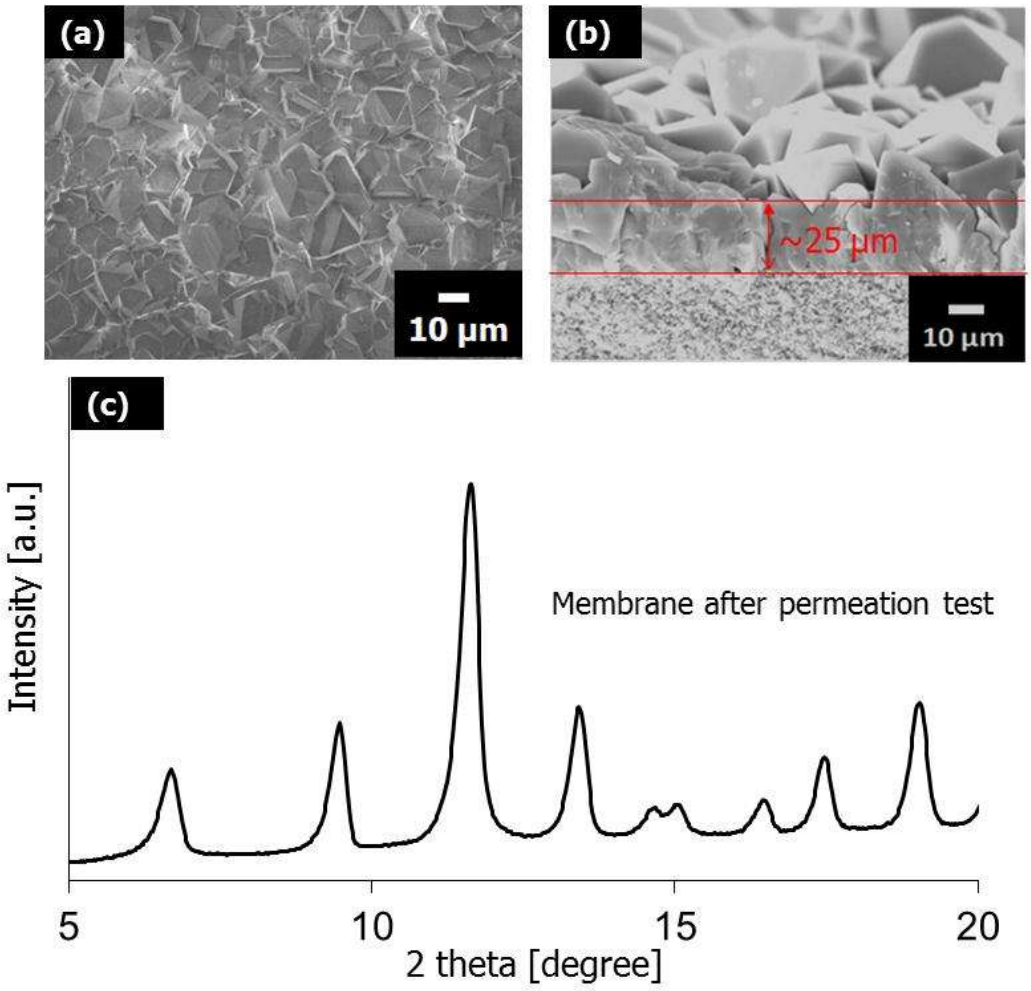

Figure 4.11 SEM images (a) top view and (b) cross sections of HKUST-1 after permeation test, (c) XRD patterns after permeation test

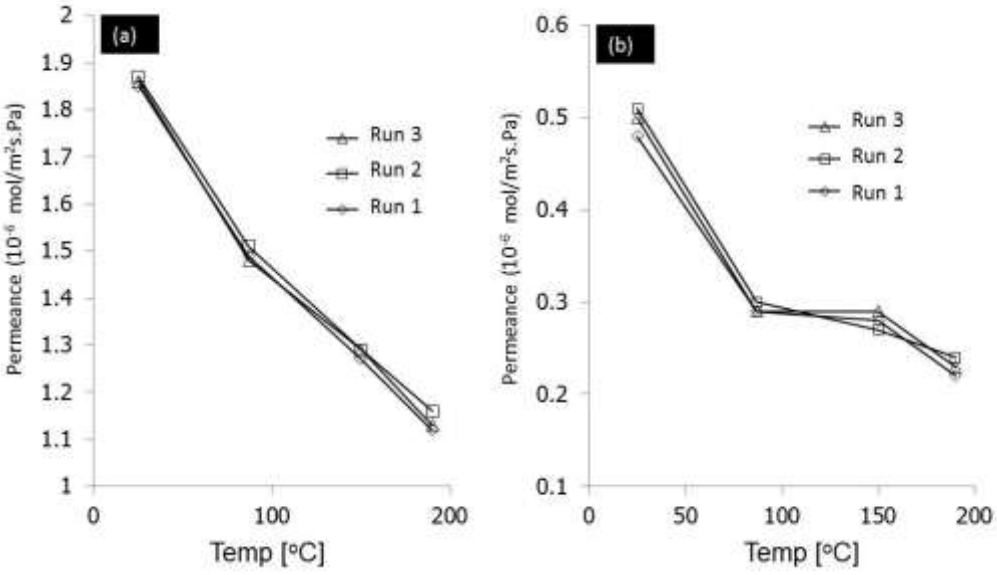

Figure 4.12 Gas permeation results, testing the membrane at different temperatures and cooling down the sample from the highest temperature, repeating the experiment again 2 times (a) Hydrogen permeance, (b) Carbon dioxide

As temperature increases, the selectivity of hydrogen increases initially and then reaches at a plateau. This can be seen more clearly in Figure 4.13b with the increase in the temperature, the permeance value of hydrogen steadily decreases while those of other gases initially drop and then more gradually decrease. Interestingly, as shown in Figure 4.13b, as temperature increases, the permeance value of CO_2 becomes greater than those of CH4 and N2. This can be attributed to the fact that once the open coordination sites of copper atoms are liberated from water molecules CO2 can coordinate with the open coordination sites, thereby increasing its solubility. The temperature-dependent permeance values deviate from the estimated slight decrease for Knudsen diffusion. Future work will focus on measuring the performance of the membranes for gas mixtures as well as on understanding underlying transport mechanisms of gas diffusion through them.

4.4 Conclusions

Continuous crack-free HKUST-1 membranes on porous α-alumina support were tynthesized using the secondary growth method. A new seeding technique ("thermal seeding") was developed to prepare strongly bound HKUST-1 seed crystals on porous alumina supports. The presence of both organic ligands and copper species in the seed solution as well as seeding at elevated temperature proved to be of critical importance to achieve seed crystals strongly bound to the porous supports. The formation of cracks and fractures was prevented by slowly cooling and drying the membranes.

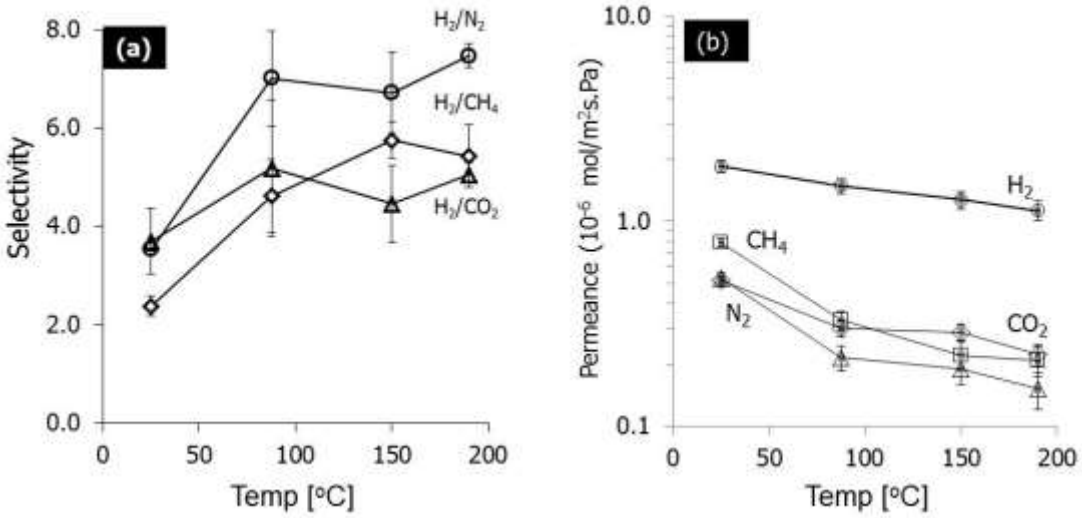

Figure 4.13 Gas permeation results: (a) ideal selectivity and (b) permeance values for various gas molecules as functions of temperature

A gas separation study on this membrane shows moderate ideal selectivity of H_2 over N_2, CH4 and CO_2. As temperature increases, the permeance values generally decrease. The permeance value of CO_2 becomes greater than those of CH_4 and N_2 with temperature increase, suggesting the affinity of the quadrapolar molecule toward the framework. The new seeding method reported here appears to be general and could open up new opportunities to fabricate thin films and membranes of other metal organic frameworks.

CHAPTER V

FABRICATION OF ZIF-8 AND ZIF-7 MEMBRANES USING SURFACE MODIFICATION AND IN SITU SYNTHESIS*

5.1 Introduction

Zeolitic imidazolate frameworks (ZIFs) are members of a new class of hybrid organic-inorganic materials called metal-organic frameworks (MOFs).[105-107] The general structure of MOFs consists of metal atoms or atomic clusters bonded to organic ligands in microporous crystalline lattices.[159] The presence of organic ligands in the structure of MOFs gives them a chemical tenability that is useful for many important applications such as enantioselctive separations[152] or chemical sensor[160]. ZIFs which exhibit zeolite like structures,[106] are med up of metal tetrahedral bonded to imidazolate (or imidazolate derivative) ligands. They have been noted for their thermal and chemical stability, which are unusual for MOFs.[125 106]

For many practical applications, the fabrication of MOFs as thin films is desirable.[120] To date, thin films of various MOFs have been fabricated using a number of synthesis techniques including in situ growth after support surface modification with either organosilane molecules [116, 118, 126, 161] or organic ligands,[117] spin coating,[119] layer-by-layer

---

*Reprinted with permission from "Synthesis of Zeolitic Imidazolate Framework Films and Membranes with Controlled Microstructures" by M.C. McCarthy, V. Varela-Guerrero, G. V. Barnett, H.-K. Jeong, Langmuir **2010**, 26 (18),14636-14641. Copyright 2010 by American Chemical Society.

growth,[131] microwave-induced thermal deposition,[121] electrochemical synthesis,[155] and solvent evaporation.[162] A number of investigators have reported MOF membranes for gas separation.[1, 99, 121, 122, 124, 125, 134] The thermal and chemical stability of ZIFs combined with their regular microporous structures make them very attractive for gas separations in industrial settings.[106, 125] Despite this, there are only a few investigations of ZIF membranes,[1, 124, 125, 163-165] all of which show promising gas separation performance. These investigations focused on four ZIFs: ZIF-7,[124, 146] ZIF-8,[1, 165] ZIF-22,[164] ZIF-90[163] and ZIF-69.[125] Each of these initial reports utilized a different fabrication technique to synthesize ZIF membranes such as secondary growth using microwaves[1] or conventional solvothermal synthesis;[124] however, a general method would save the time and resources commensurate with developing unique membrane frabrication methods for every ZIF of interest.[166] Such a method should be applicable to any ZIF with only minor adjustments and result in continuous, well-intergrown films on porous supports in a relatively short time (a few hours rather than days).

Another challenge to be met in the development of ZIF films and membranes is control of the film microstructure. The microstructure of polycrystalline films and membranes critically impacts their optical, electrical, magnetic, and gas transport properties. For instance, as has been shown in MFI zeolite membranes,[167, 168] grain size and orientation, grain boundary structure , grain boundary density, and membrane thickness all play a role in determining the separation performance of polycrystalline membranes for advanced applications; it would be critical to understand the factors influencing ZIF films microstructure.

Here, we report a potentially general method for ZIF film an membrane fabrication using a simple support modification technique (illustrated in Figure 5.1) followed by rapid solvothermal in situ synthesis. To demonstrate the potential for general applicability of our method, films and membranes of ZIF-7 and ZIF-8 were fabricated and are presented herein. The effect of solvothermal conditions on some aspects of ZIF-8 film microstructure has been investigated and is discussed.

5.2 Experimental

ZIF-8 and ZIF-7 membranes on the porous alumina supports were synthesized by our novel surface modification method and solvothermal in situ growth. The preparation method of the porous alumina disc and solvothermal in situ growth is described in following subsection:

5.2.1. Synthesis of ZIF-8 and ZIF-7 membranes

5.2.1.1. Materials

Zinc chloride (ZnCl2, >95%, Fisher Scientific) and zinc nitrate hexahydrate (ZnNO3, 6H2O, > 98%, Sigma Aldrich) were used as zinc sources. 2-Methylimidazole (C4H6N2,>95%) was purchased from Sigma-Aldrich. Methanol (>95%) and DMF (99%) were obtained from Fisher Scientific. All of the chemicals were used as received without further purification.

5.2.1.2. Support modification

Ligand solutions were synthesized by adding either 3.62 g of 2-methylimidazole (hereafter, m-IM) for ZIF-8 or 3.62 g of benzimidazole (hereafter, b-IM) for ZIF-7 to 50 ml of methanol (>95%, Fisher Scientific) followed by stirring for 20 min at room temperature. Polished α-alumina support was dried in a convection oven at 200 ^{o}C for 2 h. While the supports were still in the oven at 200 o C, the appropriate solution was dropped on the support surface, covering it totally (~0.5-1 ml was used to cover a 2.2 cm^2 α-alumina disk). Immediately after dropping, the oven was closed and the support were allowed to dry for about 20 min; after it was dried, the disk was removed from the oven, and it was sonicated in methanol for approximately 30 s. the disk was returned to the oven, and the process was repeated until the surface exhibited a change in color (dark brown), usually after six repetitions (see Figure 5.1).

5.2.1.3. In situ growth for ZIF-8 membrane

A solid mixture of 1.08 g of zinc chloride, 5.19 g of m-IM, and 2.87 g of sodium formate was dissolved in 80 ml of methanol by stirring for 20 min at room temperature. To prevent precipitation on the surface of the modified support, it was loaded vertically (relative to the autoclave) using a Teflon holder. The support and Teflon holder were immersed in the synthesis solution (~40 ml) in a 45 ml Teflon autoclave and heated in a convection oven at 120 ^{o}C for 4 h. The autoclave was then removed from the oven and allowed to cool naturally to room temperature. After it was cooled, the membrane was washed with methanol and dried in ambient conditions for 1 day.

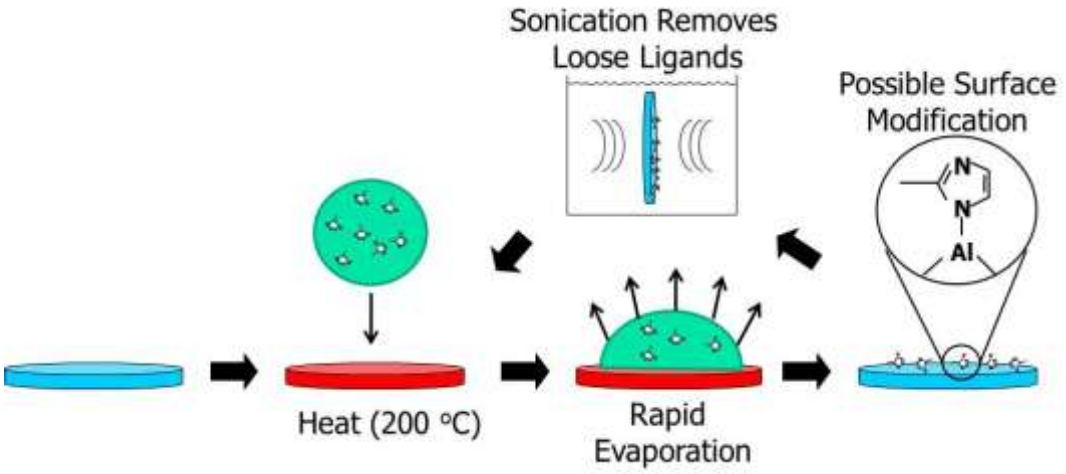

Figure 5.1 Illustration of the substrate modification process

5.2.1.4. In situ growth for ZIF-7 membrane

A solid mixture of 1.53 g of zinc chloride, 0.81 g of b-IM, and 0.70 g of sodium formate was dissolved in 40 ml of dimethylformamide (DMF) by stirring for 20 min at room temperature.This solution was poured into a 45 ml Teflon autoclave. An α-alumina support modified with b-IM was placed in a Teflon holder (45^{o} from vertical relative to the autoclave, modified side down) and immersed in the growth solution. The autoclave was sealed and held at 100 ^{o}C for 4 h. After natural cooling to room temperature, the membrane was immersed in methanol for 1 h and then thoroughly rinsed (also with methanol). ZIF-7 membranes were then dried in ambient conditions overnight.

5.2.1.5. Poorly intergrown ZIF-8 films

A solid mixture of 0.7 g of zinc nitrate hexahydrate and 1.61 g of m-IM was dissolved in 80 ml of methanol by stirring for 20 min at room temperature. To prevent precipitation on the surface of the modified support, it was loaded vertically (relative to the auto-clave) using a Teflon holder. The support and Teflon holder were immersed in the synthesis solution (~40 ml) in a 45 ml Teflon autoclave and heated in a convection oven at 120 ^{o}C for 36 h. The autoclave was then removed from the oven and allowed to cool naturally to room temperature. After it was cooled, the membrane was washed with methanol and dried in ambient conditions for 1 day.

5.2.1.6. Regrowth of poorly intergrown ZIF-8 films

Poorly intergrown ZIF-8 films were used as seeded supports. Growth solutions for the films were similar to those for the well-intergrown film mentioned previously. For the ZIF-8 films, the secondary growth solution consisted of 1.07 g of zinc chloride, 5.22 g of m-IM, and 2.83 g of sodium formate in 80 ml of methanol. The film was tilted about 45^{o} from vertical (relative to the autoclave, modified side down) in a Teflon holder. The support and Teflon holder were immersed in the synthesis solution (~40 ml) in a 45 ml Teflon autoclave and heated in a convection oven at 120 ^{o}C for 1 h. For the poorly intergrown ZIF-8 films, the synthesis was exactly the same but without any sodium formate. After natural cooling to room temperature, both films were washed with methanol and dried in ambient conditions for 1 day.

5.2.2. Performance and characterization

Permeation measurement for single and binary gases is described in subsection 3.4. For the single gas permeance, H_2, He, CO_2, CH_4 and N_2 were measured in different membranes.

The surface of the alumina support was characterized using XPS. The surface morphology and cross sectional view of ZIF-8 and ZIF-7 were characterized by Scanning Electron Microscopy (SEM) and the structure of the crystals was confirmed by XRD.

5.3 Results and discussion

This surface modification process, as shown in Figure 3.1, is similar to the thermal seeding technique previously reported for HKUST-1 membranes[123] but differs significantly in that the seed crystal solution is not used for deposition, only a solution of the organic linker. It should be noted that this is not a seeded or secondary growth technique; crystal nucleation and growth on the α-alumina surface occur in situ.

We observed that solvothermal synthesis without surface modification of the support does not produce ZIF-8 films (not shown here). We have also found that synthesis following room temperature surface modification does not produce ZIF-8 films. The first observation indicates that in these conditions heterogeneous nucleation is not favored on unmodified α-alumina supports. The second observation implies that the interaction (i.e., bonding) between the deposited organic linkers and the α-alumina surface is likely to be an activated process. If the interaction between the deposited m-IM and the support surface was mainly through nonactivated processes such as electrostatic or hydrogen bonding, one would expect that elevated temperature (i.e., ~200 ^{o}C) would be unnecessary for surface modification. The necessity of higher temperature implies that the linkers are attached to the support surface via an activated process, that is, covalent bonding (for instance, Al-N as shown in the inset illustration of Figure 5.1). Further evidence of this is shown by the results of solvothermal growth after sonicating a modified support for 30 min; a well-intergrown film was produced (images not shown here), indicating that the linkers are rather strongly attached.

To further confirm the presence of covalent bonds between the linker and the support, N 1s XPS spectra were taken for α-alumina supports modified at two different temperatures: room temperature and 200 ^{o}C (see Figure 5.2). It is expected that there are no covalent bonds formed between the support and the linker for the sample modified at room temperature. The first sample Figure 5.2a, was modified at room temperature with an m-IM solution and exhibits a single, narrower symmetric peak at ~399.5 eV binding energy, which indicates that there is only one form of nitrogen on the surface. This peak is assigned to the nitrogen in C—N bonds[127, 169] in 2-methylimidazole. The second sample Figure 5.2b, was modified at 200 ^{o}C and exhibits a single, broader asymmetric peak, which, after deconvolution, can be fitted to two Lorentzian—Gaussian peaks, 399.5 and 397.6 eV, with an area ratio of 1.81: 1. The first peak is assigned to the same nitrogen in C—N bonds as in Figure 5.2a, but the second peak is characteristic of the nitrogen in Al—N bonds. [170, 171] This result indicates that nitrogen atoms on the surface of the sample modified at 200 ^{o}C (Figure 5.2b) are chemically bound to the α-alumina surface as evidenced by the presence of Al—N bonds. However, the area ratio between these two N 1s peaks is not 1:1, which suggests that there exit m-IM ligands on the surface that are not covalently bonded to the support (based on the area ratios, about 35% of the ligands are not covalently bonded). This XPS evidence together with the aforementioned experimental evidence indicates that supports modified at 200 ^{o}C have 2-methylimidazole linkers covalently bonded to α-Al_2O_3, whereas on supports modified at room temperature the linkers are only physically attached.

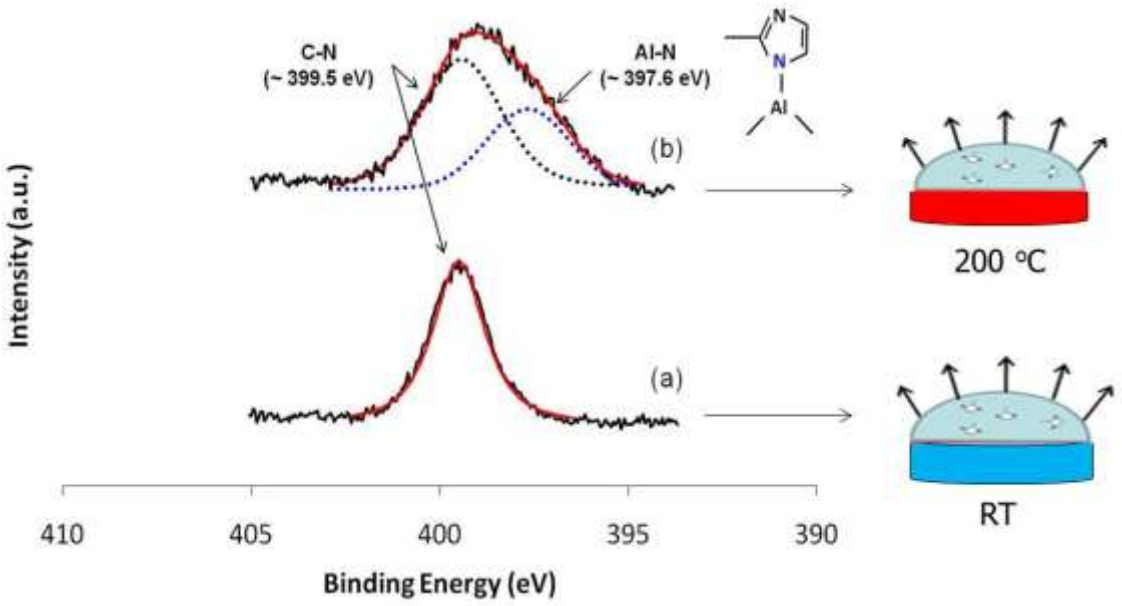

Figure 5.2 N 1s XPS data of α-alumina support modified with m-IM at 25 ^{o}C (a) and 200 ^{o}C (b)

The surmised covalent bonding that happens between the m-IM and the α-Al2O3 supports during thermal deposition can be reasonably explained by a condensation reaction wherein a surface hydroxyl group for α-alumina reacts with neutral m-IM to produce water and an aluminum—nitrogen covalent bond (see inset illustration in Figure 5.1).

In Figure 5.3, the FE-SEM images of continuous ZIF-8 films produced using the surface modification and subsequent in situ solvothermal growth technique are shown. The crystal structure of these films was confirmed using XRD (see Figure 5.4). Although both films consist entirely of ZIF-8 crystals, they exhibit drastically different microstructures. Figures 5.3a,b depicts a continuous film (approximately 20 μm thick) with larger, well-intergrown grains (approximately 5—10 μm). The film in Figure 5.3c,d is continuous but composed of smaller, poorly intergrown crystals (approximately 1—3 μm). Additionally, the thickness of this film is very inhomogeneous; in some places, it is as thin as 2—3 μm, and in others, it is as thick as 12 μm. It should be noted that the microstructure of the ZIF-8 membrane that was synthesized under micro-waves.[1] The microstructure of the ZIF-8 film in Figure 5.3c, d renders the film unsuitable for gas separation by molecular sieving as the crystals are not well intergrown, although they might be useful for other applications such as sensors. The supports for these films were both modified according to the method described in this report. The ZIF-8 membrane in Figure 5.3a was grown solvothermally for 3 h using a methanol solution containing zinc chloride, m-IM, and sodium formate.

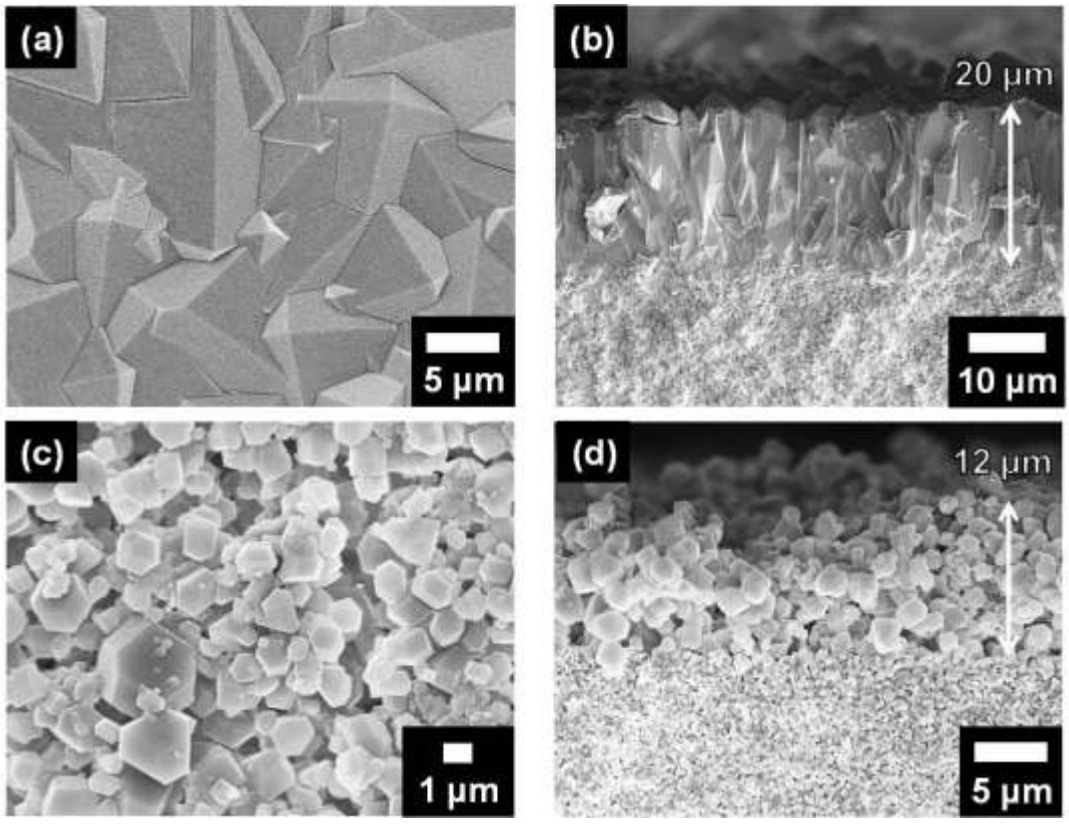

Figure 5.3(a) Top view and (b) cross section FE-SEM images of a ZIF-8 film with larger, well-intergrown crystals. (c) Top view and (d) cross section FE-SEM images of a poorly intergrown ZIF-8 film consisting of relatively small crystals

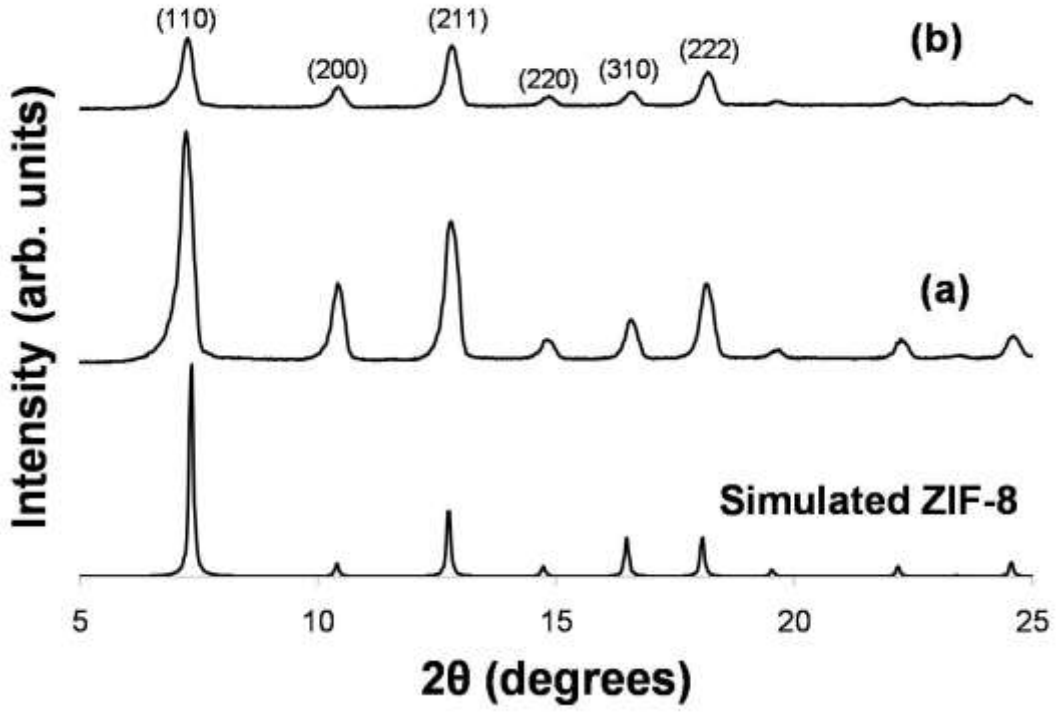

Figure 5.4 (a) XRD pattern of ZIF-8 membrane with large (~5 micron), well intergrown crystals; (b) XRD pattern of ZIF-8 film with smaller, poorly intergrown crystals

The ZIF-8 film in Figure 5.3c was grown under identical conditions except for three important factors: (1) there was no sodium formate in the growth solution, (2) zinc nitrate was used instead of zinc chloride as the zinc source, and (3) synthesis continued for 36 h instead of 3 h. It is important to note that synthesis without sodium formate for 3 h with either zinc source yields no ZIF film. Additionally, synthesis without sodium formate using zinc chloride for 36 h also yields no film. These results suggest that sodium formate plays an essential role in determining film microstructure. The source of zinc also appears to be important in yielding well-intergrown films.

It is our conjecture that the microstructure observed in Figure 5.3c,d is the result of partial deprotonation of organic linkers on the surface of ZIF-8 crystals during solvothermal synthesis. A previous report[172] mentioned that neutral m-IM acts as a capping agent, terminating crystal growth of ZIF-8. Zinc—ligand bonding in ZIF-8 occurs at the nitrogen atom at positions 1 and 3 on m-IM;[106, 172] consequently, crystal growth cannot continue unless the terminal nitrogen atom is deprotonated. On the basis of this reasoning and in light of the drastically different film microstructures observed in Figure 5.3, it seems that the apparently random crystal branching and growth in Figure 5.3c,d is a result of partial deprotonation of surface m-IM. A schematic illustration of this hypothesis is shown in Figure 5.5. We speculate that in the presence of sodium formate, however, 2-methylimidazole linkers at the ZIF-8 crystal surface are likely to be fully deprotonated due to the increase in pH (Le Chatelier's principle), resulting in growth occurring in all directions and yielding larger, well-intergrown crystals (see Figure 5.5).

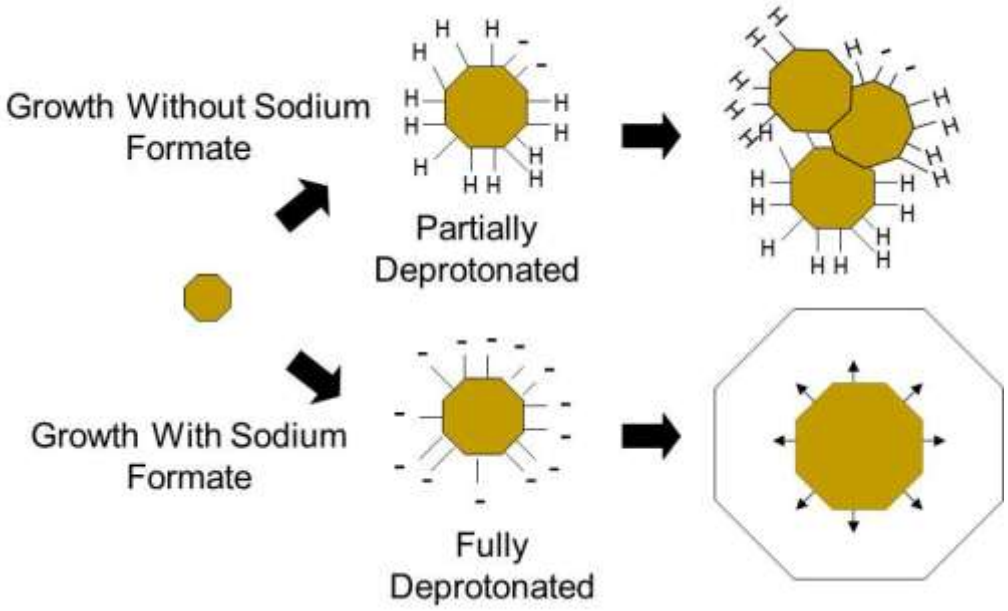

Figure 5.5 Illustration of the possible role of sodium formate in ZIF-8 growth

The pH of the growth solution with sodium formate was found to be ~8.3, and without sodium formate, the pH was ~7.2. The increase in pH, in other words, decreases the concentration of protons in solution, shifting the equilibrium and thereby driving the deprotonation of surface linkers. Consequently, we hypothesize that one important factor in controlling ZIF-8 film microstructure is the degree of surface linker deprotonation (which can be influenced by the growth solution pH).

Further evidence of this was obtained by repeating solvothermal growth (i.e., secondary growth) of poorly intergrown ZIF-8 films (similar to the one shown in Figure 5.3c) using two different growth solutions: one containing sodium formate and another without it. One would expect that if our hypothesis is correct, then secondary growth of the poorly intergrown ZIF-8 film in the presence of sodium formate would result in a well-intergrown film similar to Figure 5.3a and that secondary growth without it would not. Both of these results can be seen in Figure 5.6a,b. These results indicate that a poorly integrown ZIF-8 film can be transformed into a well-intergrown film by introducing a base to the growth solution (Figure 5.6a) and that secondary growth without an added base does not change the microstructure of a poorly intergrown ZIF-8 film (see Figure 5.6b).

To demonstrate the potential for general applicability of our fabrication method, a ZIF-7 film was prepared following the same fabrication method described above for ZIF-8 but having replaced the m-IM linker with b-IM (crystal structure confirmed using XRD, see Appendix A, Figure A1).

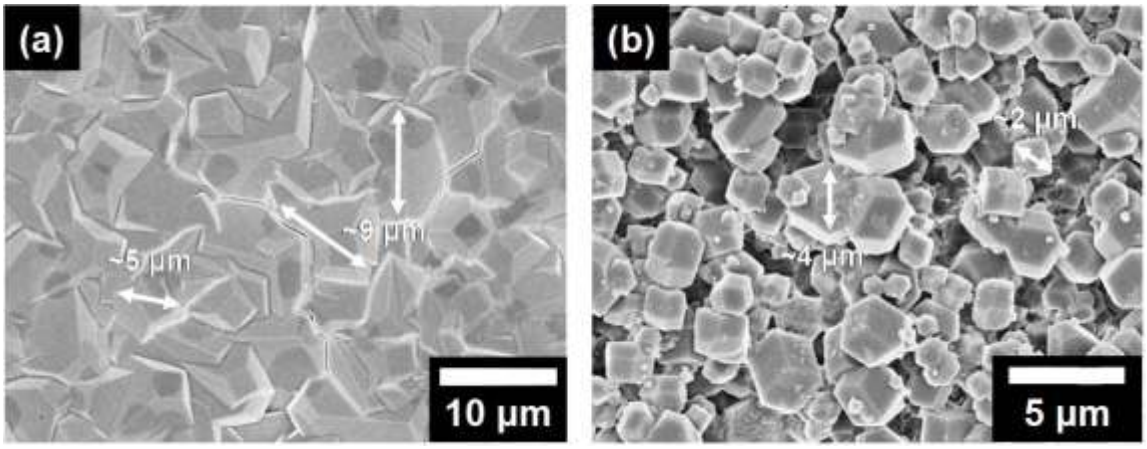

Figure 5.6 (a) ZIF-8 film after secondary growth with sodium formate, (b) ZIF-8 film after secondary growth without sodium formate. Note that these films were re-grown from poorly intergrown ZIF-8 films

As expected, b-IM was also covalently attached on the alumina support via Al—N bonds (see the N 1s spectrum in Appendix A, Figure A2).

As can be seen in Figure 5.7, the ZIF-7 membrane is continuous and consists of well-intergrown, randomly oriented grains. It is also notable that this film is only about 1 μm thick (the permeation test of these membranes is shown in Appendix A, Figure A3).

Finally, the single gas permeation performance of ZIF-8 membranes was tested using several common gases as shown in Figure 5.8 and Appendix A, Table A1. A lack of macroscopic cracks and defects was confirmed by transmembrane pressure-dependent permeation measurements (see Appendix A, Figure A4). The pore aperture size of ZIF-8 is 3.4 Å,[107] which leads one to expect a high selectivity of small molecules such as hydrogen over large molecules such as methane of nitrogen in ZIF-8 membranes. The ideal selectivity for H_2/N_2 is 11.6 and for H_2/CH_4 is 13.0. These values were calculated from single gas permeation test of three different membranes (tested three times each) and are comparable to the first reported ZIF-8 membrane.[1] As previously reported, [1] these ZIF membranes exhibit molecular sieving, favoring smaller molecules except for CO_2 and O_2. Measured permeances of our membranes are ~2—3 times higher than those of the first reported ZIF-8 membrane (probably because our membranes are about ~2—3 times thinner). The permeance of oxygen is greater than that of carbon dioxide, which is contrary to the previous report.[1] This could be attributed to the fact that oxygen might have greater affinity to ZIF-8 as compared to carbon dioxide. As recently noted by Kitagawa et al.,[173] a tetracyanoquinodimethane (TCNQ)-based MOF showed strong adsorption of oxygen in contrast to other gas molecules including carbon dioxide.

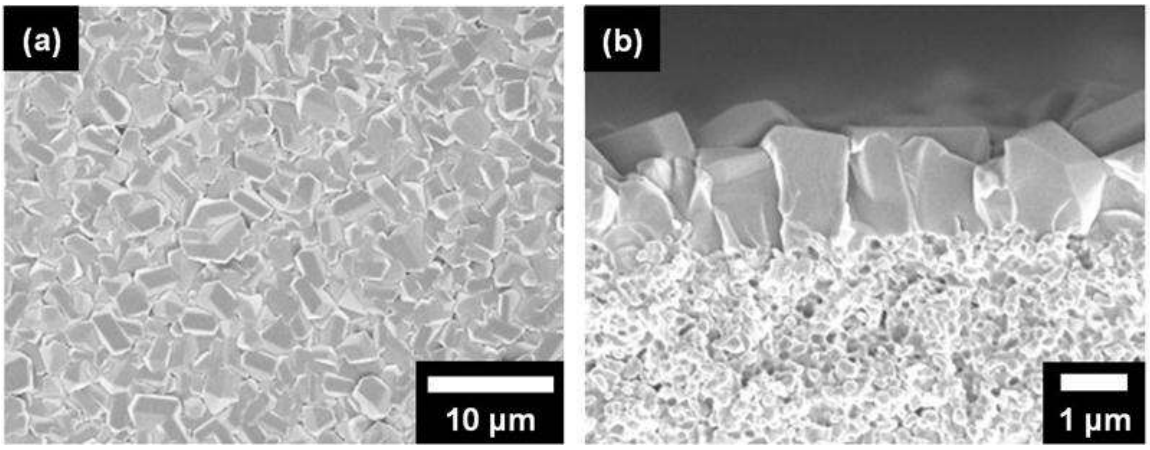

Figure 5.7 (a) Top view and (b) cross section FE-SEM images of ZIF-7 membranes with well-intergrown crystals prepared similarly to ZIF-8 films (same substrate preparation method as ZIF-8 membranes, but modified wit benzimidazole instead of 2-methylimidazole)

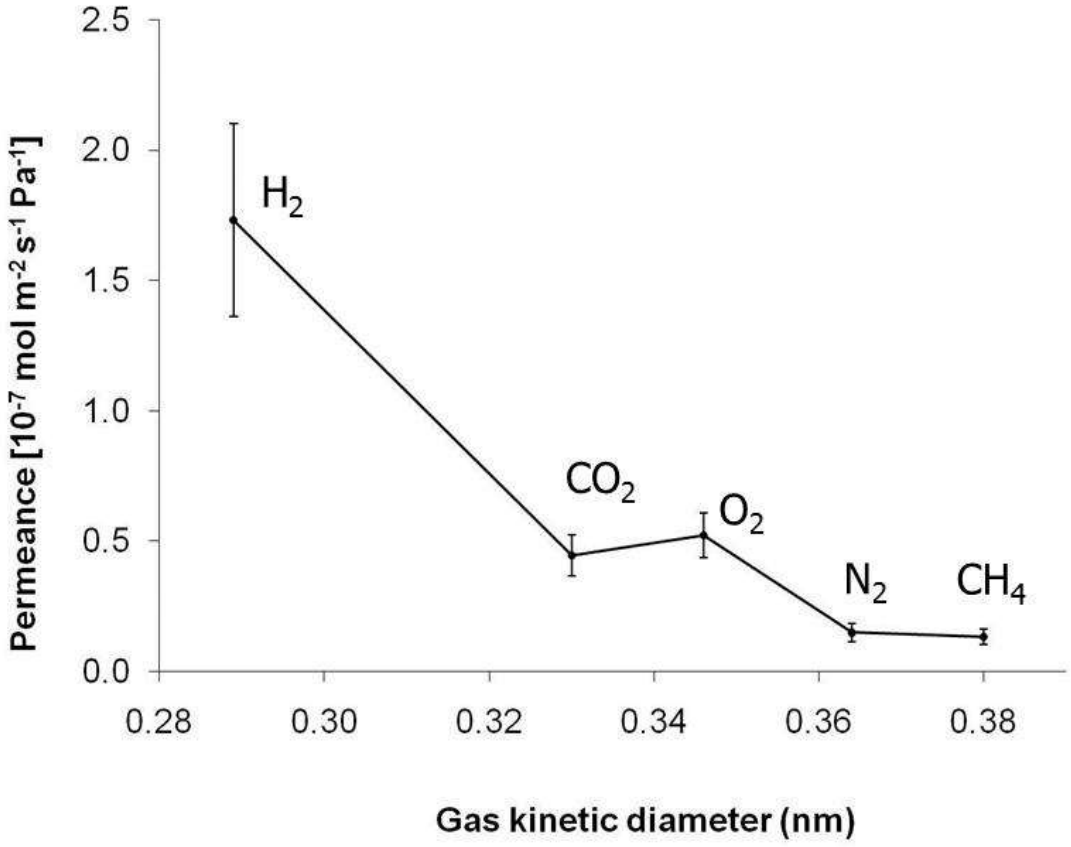

Figure 5.8 Single gas permeance results for well-intergrown ZIF-8 membranes (repeated 3 times on 3 different samples)

They attribute this to the greater electron acceptability of oxygen as compared to other gas molecules. Oxygen can undergo charge transfer with the electron-donating TCNQ of the PCP framework, resulting in high adsorption selectivity toward oxygen. At this time, we cannot explain the higher oxygen permeance observed in Figure 5.8 Preliminary temperature-dependent permeation measurements were also conducted (see Table A1), showing a decrease in permeance as the temperature increases, presumably due to the adsorption effect. A detailed permeation study of these membranes, however, is currently underway and will be reported later.

5.4 Conclusion

In conclusion, we have developed and demonstrated a method for ZIF membrane synthesis that consists of modifying porous supports with the organic ligand of the ZIF of interest followed by conventional solvothermal synthesis. This method is simple, yields continuous, well-intergrown membranes relatively quickly (~4—5 h), and has the potential for general application to other ZIFs. We have demonstrated this method's effectiveness by synthesizing films and membranes of ZIF-7 and ZIF-8 using nearly identical conditions, varying only in the linker used for surface modification and solvothermal synthesis conditions. We have also taken the first step toward understanding the major factors influencing ZIF film microstructure by observing the effects of the presence of absence of a common base on ZIF-8 membranes show molecular sieving, exhibiting ideal selectivities of 11.6 and 13 for H_2/N_2 and H_2/CH_4, respectively.

The results of this investigation will help facilitate future research into ZIF films and membranes by providing important tools for facile ZIF film fabrication and an initial step toward ZIF film microstructure control.

CHAPTER VI

RESEARCH REVIEW: FLAME RETARDANTS

6.1 Introduction

Flame retardant materials are ubiquitous in plastics, paints, electronics, and many other commodities.[174-176] The primary function of these materials is to suppress flame at the early stage of fire incidents, so that flame does not propagate to cause disasters. In order to sustain flames, there are three components involved in the process: 1) a series of chain reactions with free radicals that are generated from raw materials, 2) heat generated from the reactions that enhance the reactions, and 3) constant influx of oxygen. As such, flame retardants and fire extinguishers can generally be classified as follows: 1) those suppressing radical reactions such as brominated additives, 2) thermal quenchers such metal hydroxides, and 3) oxygen barrier such as CO_2 fire extinguishers. Brominated compounds such as polybrominated diphenylethers (PBDEs) are most extensively used as flame retardant additives.[175] Though these brominated flame retardants are very effective, their adverse effects on human health and environmental contamination, however, have raised serious concerns over the last couple of decades. In fact, majority of brominated flame retardants are in the process of being phased out.[176, 177] Therefore, it is imperative to develop alternatives that are environmentally friendly, benign to human health, and effective.

6.2 Flame retardants

Three approaches have been considered to reduce the flammability of polymers: (i) to use inherently flame retarded polymers (e.g. poly(tetrafluoroethylene), polyoxazoles, or polyimides),[178] (ii) to use chemical modify existing polymers also known as reactive flame retardants polymers (RFRP), e.g. copolymerization of flame-retardant monomer into PET chains or organic-inorganic hybrid polymers such as epoxy resin prepared from silsesquioxanes,[179] and (iii) to incorporate flame retardants (additive flame retardants polymers (AFRP)) into polymers via usual procedures (e.g. halogenated flame retardant materials (HFRM)). Out of these three approaches, the use of additive flame retardants is most popular mainly due to its wide applicability and simplicity.

6.2.1 Halogenated additives

Halogenated flame retardants are the most widely used additives in the polymermarket due to its effectiveness. The effectiveness of halogenated flame retardants depends on the type of halogen. Fluorine and iodine-based compounds are not used because they do not interfere with the polymer combustion process. [180] Iodinated compounds are less thermally stable than most commercial polymers and therefor release halogenated species during polymer processing. Owing to their low bonding energy with carbon atoms, bromine and chlorine can readily be released and take part in the combustion process by free radical mechanism occurring in the gas phase. Therefore, bromine- and chlorine-based additives were most widely used

6.2.1.1. Mechanism of halogenated flame retardants

The mechanism is based on the affinity of the halogens, especially chlorine and bromine, to react with H* and OH* free radicals.[181]

$$RX \longrightarrow R^* + X^* \qquad X\ may\ be\ Br\ or\ Cl$$

$$X^* + R'H \longrightarrow R'^* + HX$$

$$HX + H^* \rightarrow H_2 + X^*$$

$$HX + OH^* \rightarrow H_2O + X^*$$

It is worth noting that HX, the effective flame retardant species, is regenerated by the reaction of X* with RH. In addition, being non-flammable, HX can have a physical action on the combustion mechanism (protective gaseous coating, dilution of fuel gases). It also catalyzes the oxidation of the solid phase and the oxidation products tend to cyclize, which lead to the formation of a solid protective layer. It should be noted that X* is much less reactive than OH* and H*.

Tetrabomobisphenol A (TBBPA) is the most widely used halogenate flame retardant. It is mainly incorporated as a additive flame retardant especially in epoxy resins for printed circuit boards. Polybomodiphenylether (PBDE) compounds are the second most used halogenated flame retardant family. They can contain up to 10 bromine atoms attached to a diphenyl ether molecule. The polybromodiphenylethers developed as flame retardant additives are: penta- (5), octa (8), and deca-(10) bromodiphenylethers. They are characterized by high molecular weight and good thermal stability and are mainly used in styrenic polymers, polyolefins, polyesters and nylons.

Hexabomocyclododecane (HBCD) is a cycloaliphatic halogenated flame retardant. It is currently used in expanded or compact PS and textiles. Tetrabomophthalic anhydride (TBPA) is used as a flame retardant additive in unsaturated polyesters and also as a raw material for the production of other flame retardants agents.

The chemical structures of all these halogenated flame retardants are show in the Figure 6.1

6.2.1.2 Halogenated flame retardants in coatings

Flames retardant in coatings are designed for application over a range of combustible or non-combustible surfaces and they offer improved a esthetics. Since coatings with thin films can delay flame spreading (flaming combustion along a surface) and smoke generation, they are often used in living and work spaces where safe egress is essential. On the other hand, if a conventional paint is applied over walls and ceilings of a room and a fire takes place in and object in this space, flames can reach the surface of the wall and, as a consequence, generate more heat and flammable vapors. Flames can then reach the ceiling, and a significant amount of heat is radiated again. When the flammable vapors instantaneously ignite, a flash-over takes place. Flame retardant coatings are distinguished by their ability to release non-flammable gases when contacted by fire or when heat is generated.

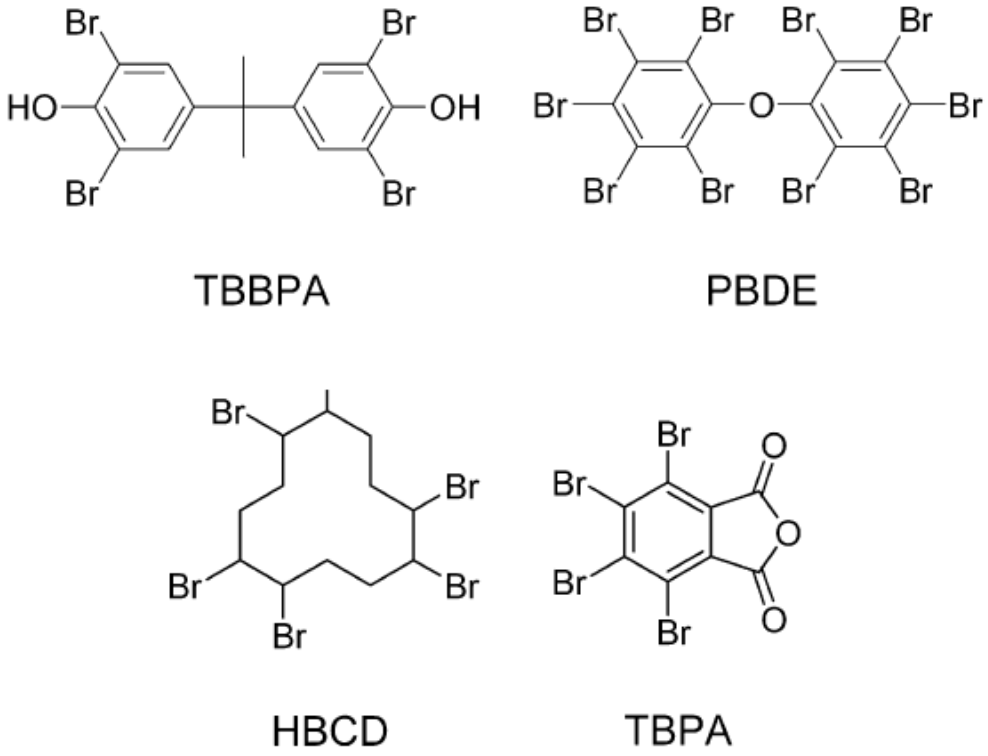

Figure 6.1 Chemical structures of classical halogenated flame retardant products[182]

These gases interfere with the rate of spreading flame and also reduce its intensity. The fire resistance effect can be obtained by adding a halogen source to the composition or by chemically building it into the film-forming polymers. To improve fire retardancy, antimony trioxide and halogenated compounds are usually used as a synergistic additive. The gas-phase flame retardant action of halogenated additives can be improved by the incorporation of antimony oxide (Sb_2O_3). Antimony oxide reacts with the hydracids (HCl or HBr) generated by the halogenated flame ratardants to form antimony oxyhalides, which are much heavier than the native hydroacids, thus prolonging their residence time in the flame. All these oxyhalides lead to the formation of $SbCl_3$ or $SbBr_3$, which act as scavengers of "hot" radicals such as H* see the following equations[176]:

$$SbCl_3 + H^* \rightarrow HCl + SbCl_2^* \quad (1)$$

$$SbCl_2 + H^* \rightarrow HCl + SbCl^* \quad (2)$$

$$SbCl + H^* \rightarrow HCl + Sb^* \quad (3)$$

Moreover, antimony oxide and Sb* can also react by a parallel oxidation mechanism and participate in the scavenging of "hot" radicals:

$$Sb^* + OH^* \rightarrow SbOH \quad (4)$$

$$SbOH^* + H^* \rightarrow SbO^* + H_2 \quad (5)$$

$$SbO^* + H^* \rightarrow SbOH \quad (6)$$

Synergistic effects can also be obtained by combining the gas phase action of halogen species with the condensed-phase action of phosphorus-based compounds. Improved fire performances can thus be achieved by the use of mixtures of halogenated and phosphorated flame retardant compounds or by incorporation of substances containing both phosphorus and halogen groups in their molecular structure. Indeed, Phosphorus halides or oxyhalides are excellent free-radical scavengers, better than hydrogen halides (HX), and can release more halogen-based radicals due to the P-X bond being weaker than the C-X bond. In addition, the phosphorus caontained in phosphorus halides or oxyhalides can also act in the condensed phase to promote the formation of a protective char layer.[183]

6.2.1.3 Concerns about halogenated flame retardants

Brominated flame retardants (BFRs) represent major industrial chemicals whose use has increased dramatically over the past few decades. They are produced to prevent fires and thus can have a direct and obvious benefit. However, concerns are being raised because of their persistence, bioaccumulation and potential for toxicity, both in animals and in humans.[182]

For example, halogenated phenolic properties would suggest that it could uncouple oxidative phosphorylation. It means that could destroy mitochondria in the human cells. Other effect could be perturbation of thyroid homeostasis in the mother that has been associated with cognitive deficits in their children.

It is necessary to develop alternative additive flame retardants without potential toxicity in animals and humans, in particular, for polymers such as polystyrene foams, high-impact polystyrene, and epoxy resins. These polymers are then used in a medley of consumer products, including computers, electronics and electrical equipment, televisions, textiles, foam furniture, insulating foams, paint and other building materials. Some alternative materials will be discussed in the following section.

6.2.3. Alternative flame retardant additives

Gilman et al.[184] reported that the presence of dispersed montmorillonite (MMT) clay in polymeric matrices produces a substantial improvement in fire performance. Gilman and other groups extended this approach to develop hybrid polymeric materials including organomodified clays,[185-187] nanoparticles of TiO_2,[188] nanoparticles of silica,[189] layered double hydroxides (LDH),[190, 191] carbon nanotubes (CNT), [192, 193] of polyhedral silsesquioxanes (POSS).[194-196] All of these materials exhibit low flammability in terms of heat release rate (HRR). Typically, the peak of HRR is decreased by 50-70% in cone calorimeter experiment. However, the UL-94 and LOI results of polymer nanocomposites are poor.[197] Typical fire behavior of polymer nanocomposite during UL-94 of LOI testing does not exhibit dripping and the formation of a char layer can be observed at the surface of the material. Usually, the carbonaceous layer is not effective enough to stop the flame and the material continues to burn slowly failing the test.

The first issue to be considered in the polymer nanocomposites is the nanodispersion (since the filler must be nanodispersed to talk about nanocomposites) and its influence

on flame retardancy. The obvious aspect of nanodispersion when investigating flame retardancy is not always commented on in the literature and it is often assumed when incorporating the so=called nanoparticles that a polymer nanocomposite is formed. To observe the effect of this issue on the flammability of the polymers, several research groups using cone calorimetry experiments conclude that better nanodispertion increase lowest flammability should occurred.[198, 199] Zheng and Wilkie[200] extended this conclusion in a more general ways suggesting base on experience and on literature that no reduction or a slight reduction in the HRR peak can be taken as an indication that nanocomposite formation has not occurred.

Recently El-Wahab et al.[201] produced a flame retardant solvent base and emulsion paints using hexaclorodiphosh (V) azane of types (I-III). These additives were physically incorporated into the paint formula through grinding in a pebble mil until all particles have a size below 38 μm. Experimental coatings were manufactured on a laboratory scale, applied by brush on wood and steel panels. Results of an oxygen index value indicated that coating with these compounds containing chlorine, nitrogen and phosphorous exhibit very good flame retardant effect when mixed with solvent base alkyd and emulsion paint. Giudice et al.[202] used zinc borates for substituting antimony trioxide on the performance of chlorinated alkyd, flame- retardant coatings. The films were manufactured on a laboratory scale, applied by brush on wood panels (Araucaria Angustifolia) and finally tested in a limiting oxygen chamber (LOI values), in a flame cabinet (intermittent bunsen burner rating) and in a two-foot flame tunnel (flame-spread index, panel consumption, after-flaming and after-glow). The results indicated that

coatings with a chlorine-containing resin used the fill-forming material, zinc borates can act as a flame retardant.

6.2.4 Nanoporous materials containing CO_2 as an alternative

Here we propose a novel use of nanoporous materials containing CO_2 for flame retardancy. Zeolite 5A and amine-functionalized ordered mesoporous silica (hereafter amine-OMS) containing CO_2 are proposed as a micro-fire extinguishers for polymers. The incorporation of these materials in the polymeric matrix will prevent the propagation of the fire by blocking the flow of oxygen via CO_2 released upon the increase of temperature.

6.3 Flame retardant characterization

For the characterization of the flame retardant materials, several methods have been using recently to attempt to measure the ignitability, flame-spread rate and heat release rate (flammability properties). There are numerous small-, intermediate- or full-scale flammability test used in industril or academic laboratories for either screening materials during product development or testing manufactured products. Commonly the UL 94v test [203], the limiting oxygen index [204,205] and the cone calorimeter[206] methods are using to measure these properties.

6.3.1 Limited Oxygen Index

Limited Oxygen Index (LOI).[204] This test was first proposed in 1966 by Fenimore and Martin and is used to indicate the relative flammability of materials (Standardized in the United States by ASTM D2863). The value of the LOI is defined as the minimal oxygen concentration [O_2] in the oxygen/ nitrogen mixture [O_2/N_2] that either maintains flame combustion of the material for 3 min or consumes a length of 5 cm of the sample, with the sample placed in a vertical position (the top of the test sample is inflamed with a burner). The LOI is expressed as:

$$LOI = 100 * \frac{[O_2]}{[O_2] + [N_2]} \quad (7)$$

The LOI is measured on (80 x 10 x 4 mm^3) specimens placed vertically at the center of a glass chimney (see Figure 6.2). The mixture of gases flows upstream through this chimney and is homogenized by being passed through layers of glass beads. After a 30 s purge of the column, the top of the specimen is ignited, like a candle. As air contains 21% oxygen, materials with an LOI below 21 are classified as "combustible" whereas those with an LOI above 21 are classified as "self-extinguishing", because their combustion cannot be sustained at ambient temperature without and external energy contribution. The higher the LOI the better the flame retardant property. Although this test is nowadays considered to be relatively unsophisticated due to the development and standardization of more elaborate methods, it remains one of the mos important screening and quality control methods used in the plastics industry.

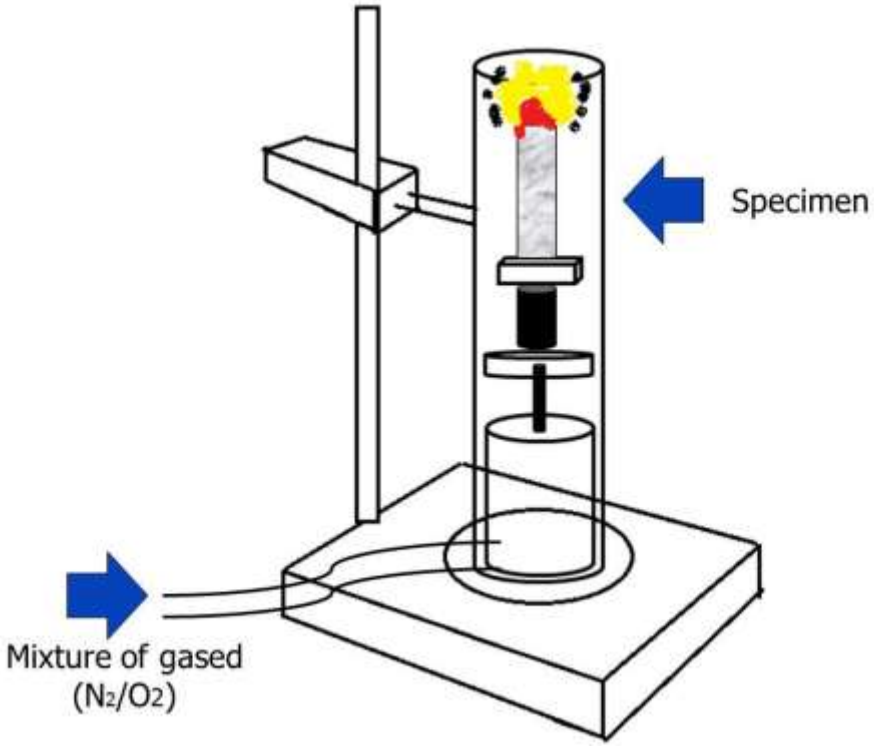

Figure 6.2 Experimental set-up for LOI measurement[176]

6.3.2 UL94 test

The set of UL94[203] test has been approved by the "underwriters" "Laboratories" as test of the flammability of plastic materials for parts in devices and appliances. It includes a range of flammability test (small and large flame vertical test, horizontal test for bulk and foamed materials, radiant panel flame-spread test).

In terms of practice and usage, the most commonly used test is UL94V for measuring the ignitability and flame-spread of vertical bulk materials exposed to a small flame. This test is the subject of an international standard (IEC 60695-11-10) for small flames (50W). It is a simple test of vertical combustion that classifies materials as V-0, V-1 or V-2. The corresponding experimental device is shown in the Figure 6.3.

The burner is controlled to produce a blue flame with a 20 mm high central cone and a power of 50 W. The flame is applied to the bottom of the specimen and the top of the burner has to be located at 10 mm from the bottom edge of the specimen. The flame iw applied for 10s and removed. The after flame time t_1 (the time required for the flame to extinghish) is noted. After extinction, the flame is applied for another 10s. The afterflame time t_2 is noted, together with the afterglow time t_3 (the time required for the fire glow to disappear). During the application of the flame, the distance between burner and specimen must remain constant. If drops fall, the burner must be tilted through a maximum angle of 45^o or slightly isolated from the specimen flame. During the test, the presence of burning drops, causing a piece of cotton located under the sample to ignite, must be noted.

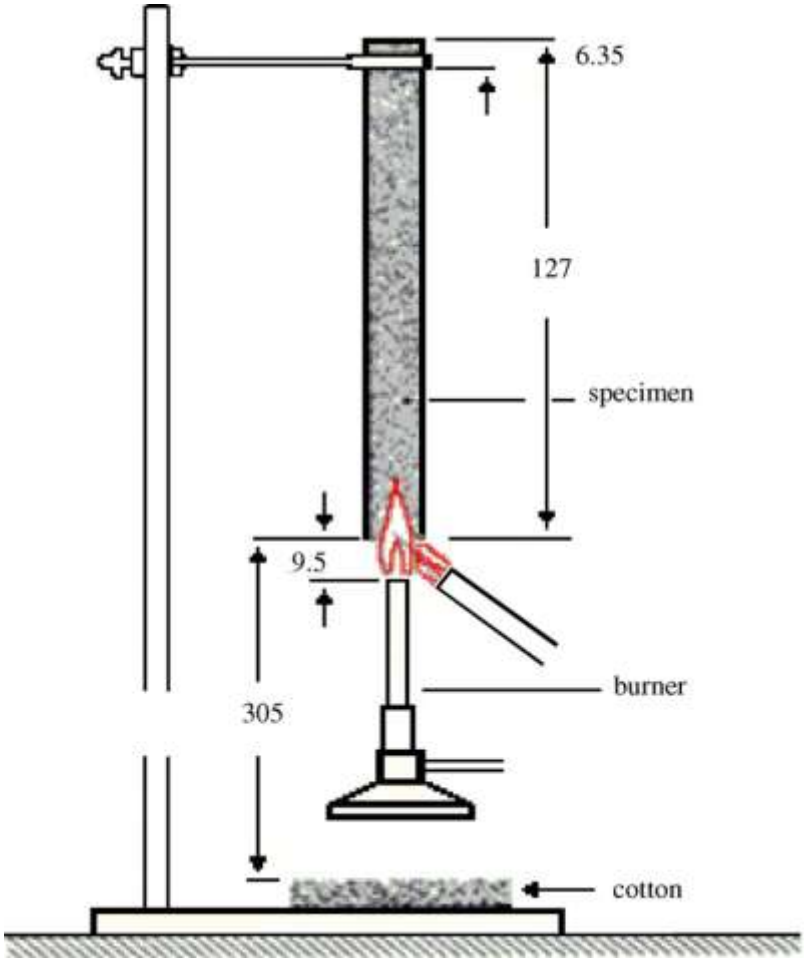

Figure 6.3 Experiment set-up for UL94V flammability test[176]

6.3.3 Cone calorimeter

Cone calorimeter is one of the most effective medium-sized polymer fire behavior tests. The principle of cone calorimeter experiments is based on the measurement of the decreasing oxygen concentration in the combustion gases of a sample subjected to a given heat flux (in general from 10 to 100 kW/m^2). Figure 6.4 illustrates the experimental set-up of a cone calorimeter. Standardized in the United States (ASTM E 1354). The sample (100 x 100 x 4 mm^3) is placed on a load cell in order to evaluate the evolution of mass loss during the experiment. A conical radian electrical heater uniformly irradiates the sample from above. The combustion is triggered by an electric spark. The combustion gases produced pass through the heating cone and are captured by means of and exhaust duct system with a centrifugal fan and a hood. The gas flow, oxygen, CO and CO_2 concentrations and smoke density are measured in the exhaust duct. The measurements of the gas flow and oxygen concentration are used to calculate the quantity of heat realeased per unit of time and surface area; HRR (heat release rate) expressed in kW/m^2. The evolution of the HRR over time, in particular the value of its peak/maximum (pHRR of HRRmas), is usually taken into account in order to evaluate the fire properties. The calculation is based on Huggett's[206] observation that most organic materials release a quantity of heat practically proportional to the quantity of oxygen consumed while burning. The proportionality factor is constant from one material to another and is equal to 13.1 kJ/g consumed oxygen.[206] Integration of the HRR vs. time curve gives the total heat released (THR) expressed in kJ/m^2.

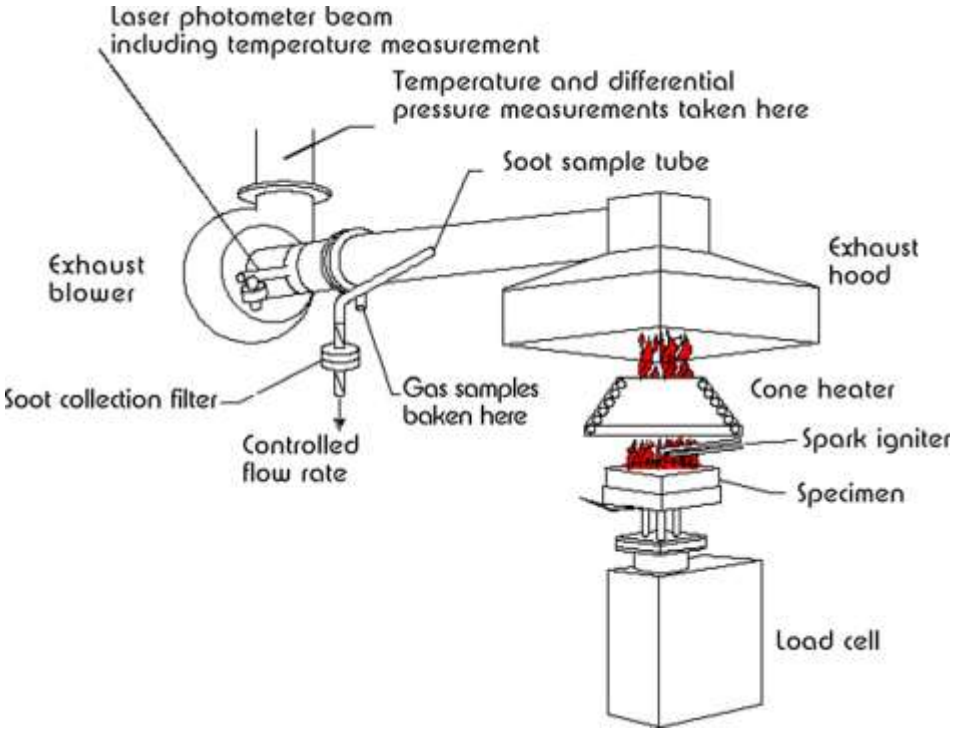

Figure 6.4 Experimental set-up for a cone calorimetry measurement[176]

In addition, the cone calorimeter test also enables characterization of the time to ignition (TTI), time of combustion or extinction (TOF), mass loss during combustion, quantities of CO and CO_2

The cone calorimeter method is based on the evaluation of heat release rate (HRR) subject to the ASTM 1354 standard. The HRR can be determined by measuring the combustion gases and oxygen flux. Also other important parameter such as CO and CO_2 mass loss, total smoke released (TSR), total heat released (THR), time of combustion or extinction (TOE), maximum of heat release (HRRmas) and rate time to ignition (TTI).

6.4 Summary

There are many different types of flame retardants (additive or reactive) for polymers that prevent the fire propagation. Halogenate additive flame retardants are extensively used in the polymer industry. However recent studies show that they are toxic to human health. In consequence its necessary find new flame retardant material to prevent the propagation of the fire in the polymers.

CHAPTER VII

EXPERIMENT METHODS

7.1 Introduction

This chapter describes general information of the materials and procedures for the synthesis of amine-OMS. Here we describe the adsorption method of the CO_2 using amine-OMS and zeolite 5A. The fabrication method of flame retardant paint and the paint films is described. For the flame retardant test, the film of flame retardant paint will be tested using a standard test method (D6413-08).

7.2 Synthesis of amine-ordered mesoporous silica (A-SBA-15)

7.2.1 Materials

All chemicals were used as received without further purification. Tetraethyl orthosilicate (TEOS, 98%, Sigma-Aldrich), pluronic P123 (EO20PO70EO20, MW= 5800, BASF),HCl (Sigma-Aldrich, reagent grade, 37%), 3-(Aminopropyl)triethoxysilane (APTES, 99%, Sigma-Aldrich), Toluene (Sigma-Aldrich 99.5%), Ethanol (Acros, 95%), Zeolite 5A (Sigma-Aldrich) and deionized water (DI water) was used throughout the study.

7.2.2 Synthesis of SBA-15

For the SBA-15 synthesis, 4.0 g of Pluronic P123 was dissolved in 60 ml of 4 M HCl and 85 ml of deionized water by stirring for 5 h at room temperature. Then, 8.5 g of

TEOS was added to that solution and stirred for 24 h at 35^{o}C. The mixture was then aged at 80 ^{o} for 24h without stirring. After completion of the reaction, the solid products were filtered, washed with deionized water, and air-dried overnight. The solid products were calcined to remove pluronic. The calcination procedure was as follows; the air-dried samples were heated from room temperature to 100^{o} C at a rate of 1^{o}C/min; held at 100 ^{o}C for 2 h; increased from 100 to 500 ^{o}C at a rate of 1 ^{o}C/min;; and held at 500 ^{o}C for 8h.

7.2.3. Synthesis of amine-SBA-15

The amine-functionalized SBA-15 samples were prepared using post-synthetic grafting. Unless noted otherwise the target loading of organic is 0.8 mmequiv/g SiO2. One gram of calcined SBA-15 was place in a round-bottomed flask, and ride at 100^{o}C under vacuum for 1 h. Then, 100 mL of anhydrous toluene was added into the flask under nitrogen. An aliquot of APTES 184 μL (0.2 mmol) was added to the solution under nitrogen. This mixture was stirred overnight in a closed flask at room temperature. The product was collected by filtration, washed sequentially with 50 mL of toluene, 50 mL of methanol, and 500 mL of deionized water, and air-dried.

7.3. CO_2 adsorption using zeolite 5A and amine-SBA-15

For the CO2 adsorption, twenty five grams of zeolite 5A/amine-SBA-15 were placed in a round-bottomed flask, and using a heating band dried at 150 ^{o}C under vacuum for 1 day. Then, the round-bottoned flask was cool down until 25 ^{o}C and immediately after CO_2 gas (99% of purity) was introduce in the round-bottoned flask during one day (the

flux of the CO_2 was verify by bobble meter of water and the pressure of the gas in the flask was 10 psi approximately). After the flux of CO_2 was cut and zeolite 5A/Amine-SBA-15 rich in CO2 was maintain in site of the flask until the materials were close to used.

7.4. Preparation of flame retardant paint and paint films

The zeolite 5A/amine-SBA-15 containing CO_2 were mixed with commercial paint solved base (Olympic Fasthide) immediately after remove the zeolite 5A/amine-SBA-15 from the round-bottoned flask. After the addition of the Zeolite 5A and/orAmine-SBA-15 in the paint, the mixture is stirring until homogeneous dispersion of the particles (approx. 30 min).

After the generation of a homogeneous flame retardant paint, one brush was immersing in the paint to paint a support paper with dimension of 12 in per 3 inches. It's important mention that during the process of paint, the person should try to form a homogeneous film in terms of thickness and distribution (ocular observation). Subsequently the film on the paper is dried during 2 days at room temperature (see Figure 7.1 and 7.2).

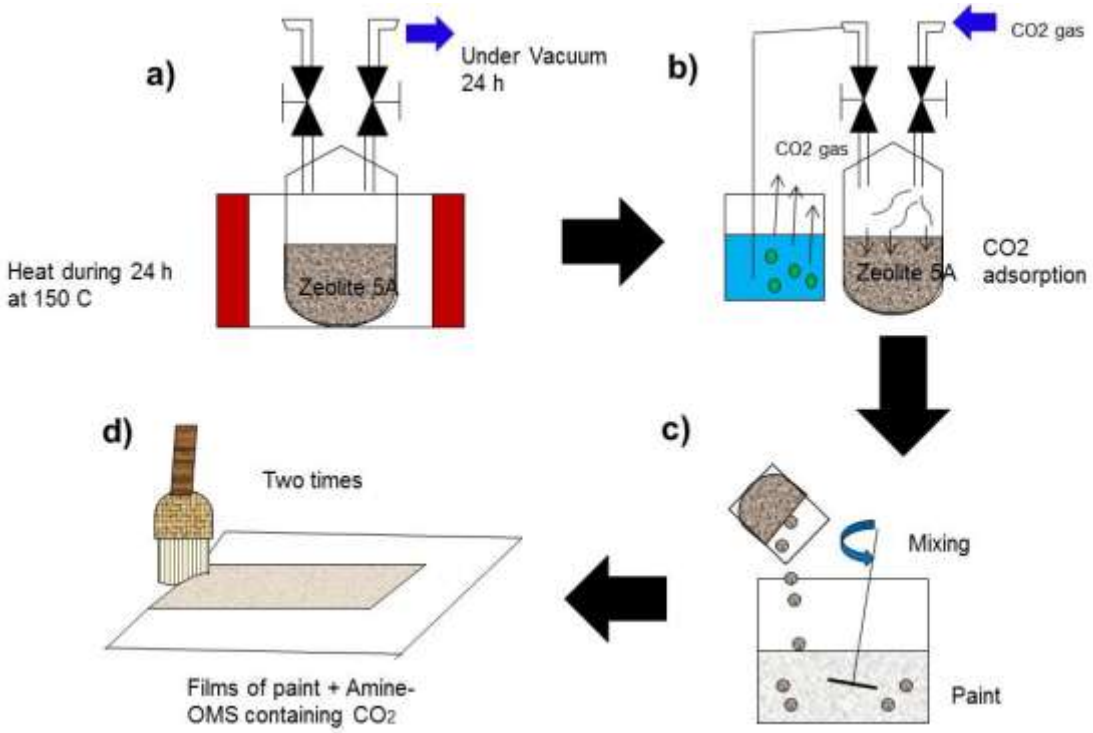

Figure 7.1 Illustrate the fabrication of flame retardant films using zeolite 5A containing CO_2. a) drying process, b) CO_2 adsorption, c) mixing with commercial paint, and d) fabrication of paint films using brush

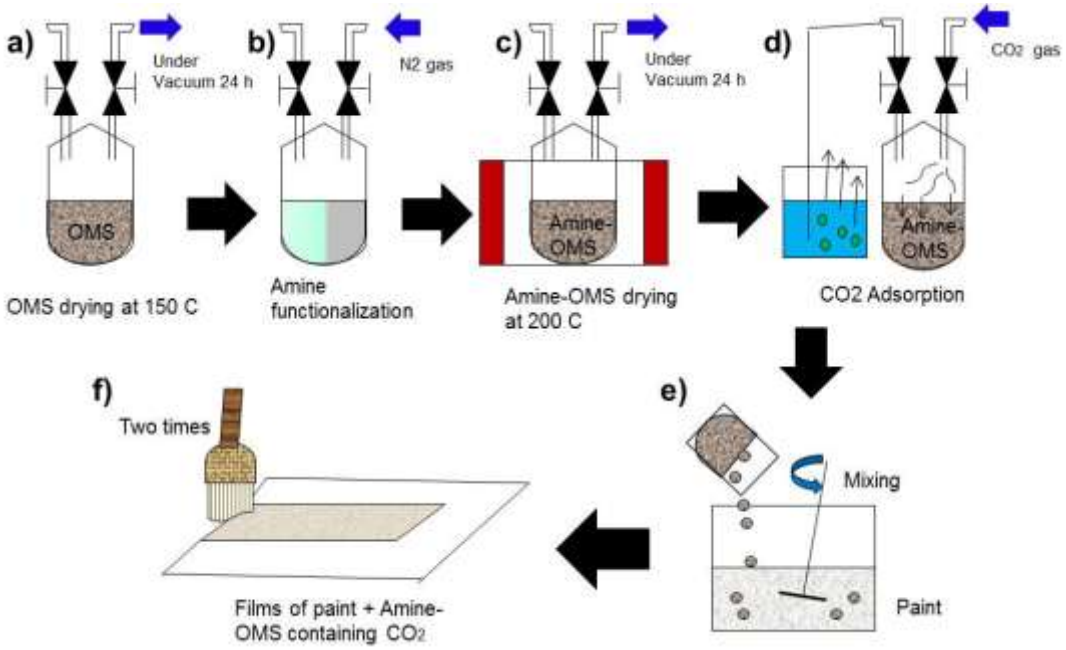

Figure 7.2 Illustrate the fabrication of flame retardant films using amine-SBA-15 storing CO_2. a) drying process, b) Amine functionalization, c) drying process (A-OMS) d) CO_2 adsorption, e) mixing with commercial paint d) fabrication of film using brush

7.5. Flame retardant test for paint films using ASTM D-6413-08 method

This test method is extensively used to measure the vertical flame resistance in textiles. However its possible used it, to test for polymeric films. This standard shall be used to measure and describe the response of materials, products, or assemblies to heat and flame under controlled laboratory conditions and shall not be used to describe or appraise the fire hazard or fire risk of materials, products, or assemblies under actual fire conditions.

For this test is necessary a test cabinet and accessories. Galvanized sheet metal or other suitable metal or other suitable metal can be used. The entire inside back wall of the cabinet shall be painted black to facilitate the viewing of the test specimen and pilot flame (see Figure 7.3). The burner, equipped with a needle valve to adjust flame height. The burner shall be constructed by combining a 10 mm inside diameter barrel 76+/- 6 mm long with a base from an adjustable valve burner. A tirrill burner is recommended, but a Bunsen burner modified to conform to this test method also will suffice. The pilot light tube shall have an inside diameter of approximately 1.5 mm and shall be spaced 3 mm away from the burner edge. On the side of the barrel of the burner, opposite the burner pilot light there shall be a flame height gage constructed of metal spaced approximately 13 mm from the barrel and extending above the burner. The gage shall have two prongs approximately 8 mm long making the distances of 19 mm and 38 mm above the top of the burner.

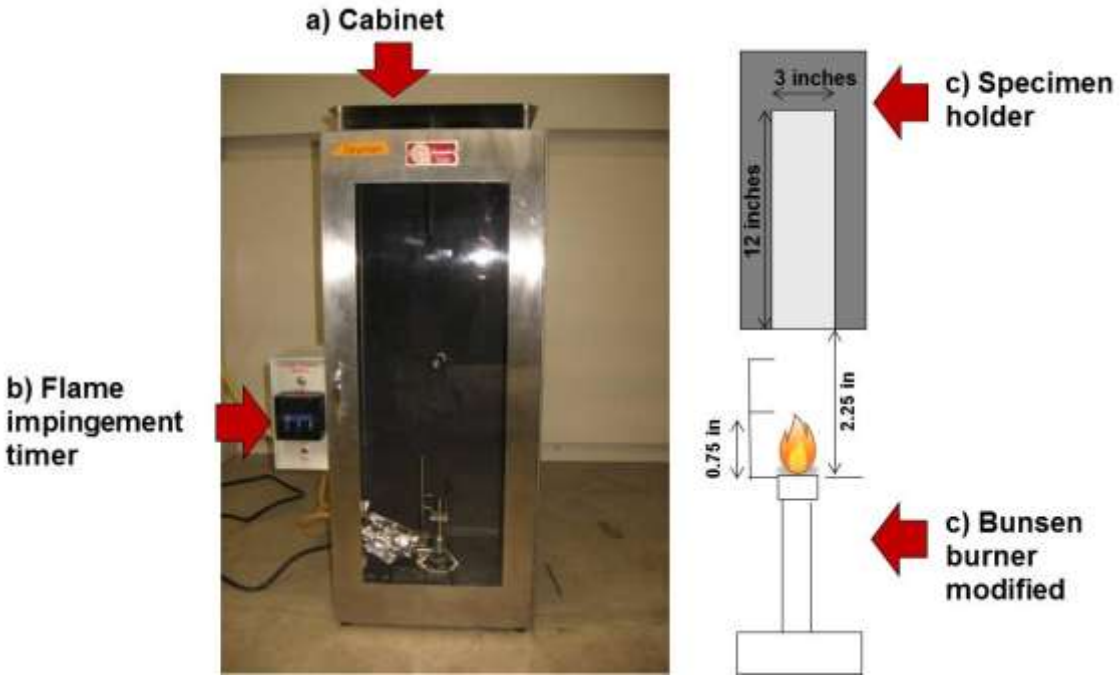

Figure 7.3 Flame retardant test equipment according with ASTM D-8413-08[207]

Test specimen holder and specimen holder clamps, as shown in Figure 3.1, are used to test the specimen correctly. The flame impingement timer, a timer and electrical gas solenoid used to control the interval, which gas is supplied to the burner.

The procedure to test the samples is as follow: 1) Mount and expose each specimen to the flame within 4 min of removal from the conditioning area or storage. 2) Clamp the test specimen between the two halves of the holder, with the bottom of the specimen even the bottom of the holder. With the holder vertically, secure the specimen in the holder with a minimum of four clamps. Position two, clamps near the top of the holder, one on each side to stabilize the specimen. Similarly, position two, clamps at the botton of the holder, one on each side. 3) Turn off the hood ventilation. Insert the specimen holder containing the specimen into the test cabinet and position the burner with the middle of the lower edge of the test specimen centered 19 mm above the burner and leveled with the bottom metal prong. 4) Start the flame impingement timer and expose the specimen for the 12+/- 0.2 s. observe the specimen for melting or dripping during the flame exposure (to the same time record any observation during the hold experiment using video camera). Immediately after the flame is removed, start a stopwatch for measurement of the afterflame and afterglow time. 5) Observe how long the specimen continues to flame after 12 s exposure time. 6) Observe how long the specimen continues to glow after the afterflame ceases or after removal of the flame if there is no afterflame. 7) Remove the specimen holder from the test cabinet. Turn on the hood ventilation to clear the test cabinet of fumes and smoke. Allow the specimen to cool. 8) Take pictures of the specimens. And finally 9) Using the video of the flame retardant

test, estimate the rate of fire propagation and construct a graphic of the results in function of the loading of the nanoporous material containing the CO_2 in the paint.

CHAPTER VIII

PREPERATION AND PERFORMANCE OF FLAME RETARDANT PAINT FILMS USING NANOPOROUS MATERIALS CONTAINING CO_2

8.1. Introduction

Due to the negative environmental and toxic effect in the human life, brominated flame retardants (BFRs), gradually have to be substituted in the industry by new materials inert to the human life.[182] However it is a big challenge because of the widespread production and use of BFRs. Until know several research groups have been used different alternatives to substituted the BFRs but until now the performance of this new alternatives didn't show similar efficiency in comparison with the BFRs. Here we propose a new alternative of flame retardant nanoporous materials to substitute the BFRs commonly used in paint. The zeolite 5A and amine-SBA-15 storing CO_2 will act as micro-fire extinguisher in paint films. A different flame retardant mechanism is propose here, where the formation of protective gas layer (by CO_2) during the combustion block the flux of oxygen and fuel gas to prevent the propagation of the fire.

The performance of the flame retardant paint will describe and analyzed in the following section testing the flame retardant paint using the method described in the section 3.5 (ASTM D-8413-08). The rate of fire propagation (RFP) will be analyzed in function of the nanoporous material present in the paint films.

8.2. Results and discussion

8.2.1 Flame retardant test of paint films containing zeolite 5A storing CO_2

To analyze the performance of the flame retardant paint in terms of the rate of fire propagation (RFP), different paint films were prepared varying the loading of zeolite 5A storing CO_2 (see Table 8.1) and tested by triplicate using the method describe in the section 7.5. The Figure 8.1 show that as we increase the loading of zeolite 5A containing CO_2 in the paint film (from 0 to 12.5% wt), the RFP decrease from 0.6 to 0.4 in/s. This result can be explained by the formation of protective gas layer in the mechanism of flame retardant paint. To prove this hypothesis one sample of flame retardant paint was made using 25% wt of zeolite 5A without CO_2 and tested in the flame retardant test. This sample show similar RFP (0.6 in/s) in comparison with the sample that contain 2.5 % wt of zeolite 5A containing CO_2. It demonstrated that the presence of the CO_2, affect the RFP, even the big difference in the weight percent of zeolite 5A in the samples. (the value of RFP is approximately the same).

The RFP decrease from 0.6 to 0.4 in/s due to bigger concentration of CO_2 allow the formation of a partial protective gas layer (partial oxygen blocking), until the loading of the zeolite 5A containing CO_2 is 15 wt%, in this point our hypothesis is that the amount of CO_2 is enough to form the protective gas layer due to the RFP is cero even after 12s of ignition. After this point the samples show the same result (see Figure 8.1).

Table 8.1 Results of flame retardant test for the paint films containing zeolite 5A storing CO_2

Mixtures			
Weight percent of paint (%)	Weight percent of Zeolite 5A storing CO2 (%)	Time to take the fire consume completely the sample (sec)	Average time (s)
97.5	2.5	Sample 1 = 20 s, Sample 2 = 21 s, Sample 3= 19 s	20
95	5	Sample 1 = 22 s, Sample 2 = 21 s, Sample 3= 18 s	21
92.5	7.5	Sample 1 = 20 s, Sample 2 = 21 s, Sample 3= 19 s	21
90	10	Sample 1 = 20 s, Sample 2 = 21 s, Sample 3= 19 s	22
87.5	12.5	Sample 1 = 25 s, Sample 2 = 27 s, Sample 3= 29 s	27
85	15	Sample 1 = 0 s, Sample 2 = 0 s, Sample 3= 0 s	0
82.5	17.5	Sample 1 = 0 s, Sample 2 = 0 s, Sample 3= 0 s	0

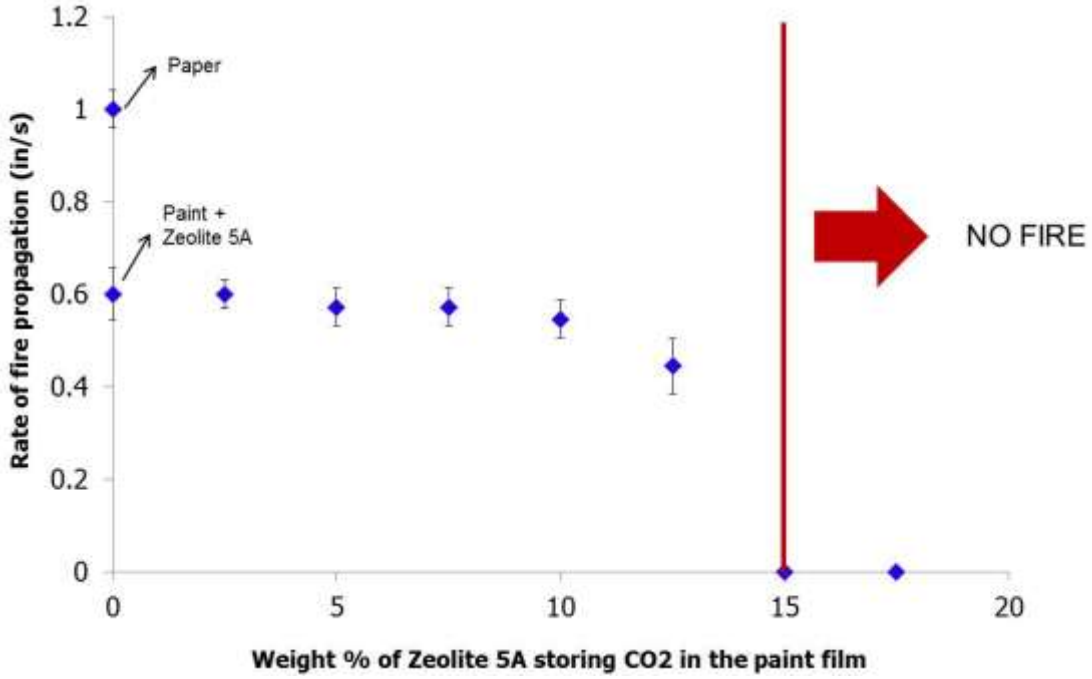

Figure 8.1 Results of flame retardant test for the paint films containing zeolite 5A storing CO_2 in terms of rate of fire propagation (RFP) and loading of zeolite 5A in the commercial paint. Two samples of reference were tested; paint film containing 25 wt% of zeolite 5A without CO_2 and just the support (paper)

Other important observation is that the propagation of fire stops completely but the area of ignition any way was damage. This observation confirms that the fire propagates slowly in the film but amount of the CO_2 is enough to decrease the rate of propagation.

8.2.2. Flame retardant test of paint films containing amine-SBA-15 storing CO_2

The results of the flame retardant test of the paint films with different loadings of amine-SBA-15 storing CO_2 are showing in the Table 8.2 and Figure 8.2. As in the case of the zeolite 5A, the RFP in the films decrease as the loading of the amine-SBA-15 storing CO_2 increase (see Figure 8.2). To prove the influence of CO_2 in the flame retardant mechanism, one sample containing 25 wt% of amine-SBA-15 without CO_2 was tested in the flame retardant test in similar way that in the case of zeolite 5A. This experiment shows that the RFP of the samples containing 25 wt% of the material is very similar to the samples containing 2.5 wt% of amine-SBA-15 storing CO_2 (~0.52 in/s). This experiment proves that the presence of CO_2 in the material during the combustion is very important to decrease the rate of fire propagation (see Figure 8.2).

The samples that contain 10% in weight of amine-SBA-15 containing CO_2 were able to extinguish the fire even after 12 s of ignition. This result its different respect to the results from the films containing zeolite 5A storing CO_2 because the fire propagation stop at 15% in weight respect to the paint. This difference is probably due to the enthalpy of desorption of CO_2 that in the case of zeolite 5A is lower in comparison with the amine-SBA-15.

Table 8.2 Results of flame retardant test for the paint films containing amine-SBA-15 storing CO_2

Mixtures			
Weight percent of paint (%)	Weight percent of Zeolite 5A storing CO2 (%)	Time to take the fire consume completely the sample (sec)	Average time (s)
97.5	2.5	Sample 1 = 20 s, Sample 2 = 22 s, Sample 3= 24 s	22
95	5	Sample 1 = 24 s, Sample 2 = 23 s, Sample 3= 25 s	24
92.5	7.5	Sample 1 = 25 s, Sample 2 = 26 s, Sample 3= 27 s	26
90	10	Sample 1 = 0 s, Sample 2 = 0 s, Sample 3= 0 s	0
87.5	12.5	Sample 1 = 0 s, Sample 2 = 0 s, Sample 3= 0 s	0
85	15	Sample 1 = 0 s, Sample 2 = 0 s, Sample 3= 0 s	0
82.5	17.5	Sample 1 = 0 s, Sample 2 = 0 s, Sample 3= 0 s	0

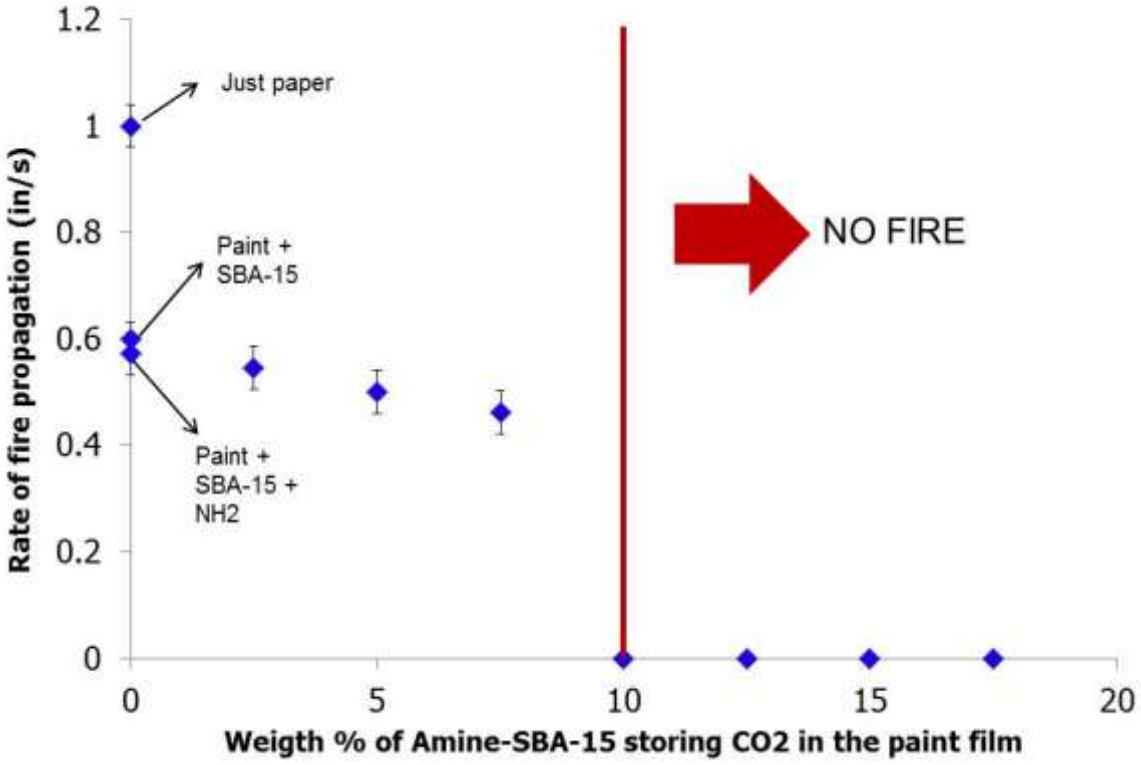

Figure 8.2 Results of flame retardant test for the paint films containing amine-SBA-15 storing CO_2 in terms of rate of fire propagation (RFP) and different loading of amine-SBA-15 storing CO_2. Three samples of reference were tested; paint film containing 25 wt% of SBA-15, paint film containing 25 wt% amine-SBA-15 without CO_2 and just the support (paper)

Our hypothesis is that desorption of the CO_2 in the zeolite will occur before the amine-SBA-15 because the desorption require lower heat allowing premature desorption of CO_2 and reducing the possibility to form a protective gas layer during the combustion. In consequence the formation of the protective gas layer will occur until the amount of CO_2 is enough to overcome this problem. Now in the case of the amine-SBA-15 due to the higher enthalpy require for the CO_2 desorption. The desorption will not occur premature and the formation of the protective gas layer blocking the flux of oxygen will be sooner.

For this reason is necessary lower concentration of amine-SBA-15 in the paint films because in the case of zeolite 5A the concentration of CO_2 strongly depends of the loading of zeolite 5A storing CO_2 to find an equilibrium point to form a protective gas layer to block the flux of oxygen and fuel gas to the fire. It's important mention that there is a possibility the formation of protective solid layer by the nanoporous material (zeolite and amine-SBA-15). However the contribution of this is minimal because to observe reduction in the RFP is necessary add bigger loadings that 25 wt% in the paint of these nanoporous materials (reference sample in the figures 8.1 and 8.2). This confirm that the influence of the CO_2 in the mechanism is more important that the solid participation.

8.2.3. Proposed mechanism

As mentioned before, the flame retardant additives lead to the formation of a protective solid (physical action of zeolite or silica) or gaseous layer between the

gaseous phase where combustion occurs and the solid phase where thermal degradation takes place. Such a protective layer limits the transfer of matter such as combustible volatile gases and oxygen. As a result, the amount of decomposition gases produced is significantly decreased. Moreover, the fuel gases can be physically separated from the oxygen, which prevents the combustion process being sustained.

Here our hypothesis is that the primary mechanism is by the formation of protective gas layer due to desorption of CO_2 from the nanoporous materials though there might be a slight chance that the formation of protective solid layers when a relatively large amount of materials are used. The particles of nanoprous materials storing CO_2 are dispersed in the paint films. But for the hydrophilic nature of these materials our hypothesis is that tent to agglomerate due to the hydrophobic nature of the polymer matrix. These particles could migrate where the thermal degradation takes place (see Figure 8.3). The endothermic decomposition of the hydrocarbons will increase the temperature of the matrices. This heatdesorbe CO_2 from nanoporous materials. Once CO_2 is released, the combustible gas mixture is diluted which limits the concentration of reagents including oxygen and the possibility of re-ignition. Finally the action of this process will stop the combustion of the polymer (see Figure 8.3 last step).

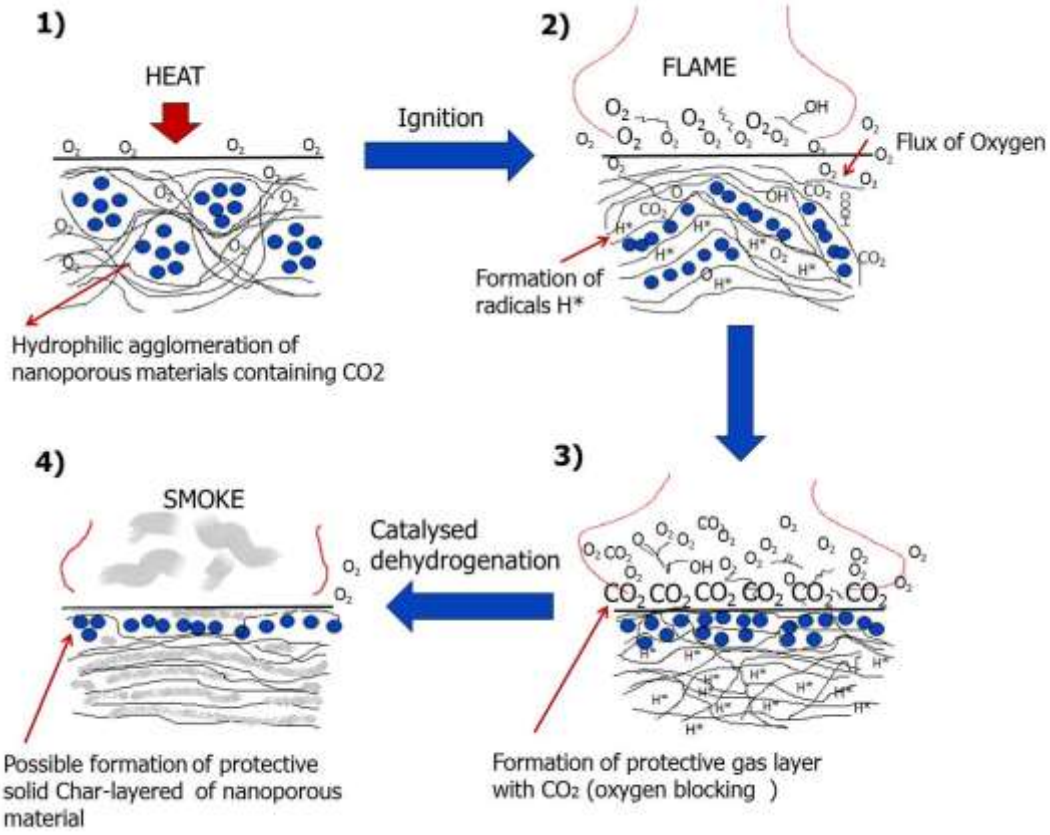

Figure 8.3 Hypothetical flame retardant mechanisms in paint using nanoporous materials storing CO_2 in paint

8.3. Summaries and conclusions

We have demonstrated using a flame retardant test (ASTM D6413-08) that nanoporous materials like zeolite 5A and amine-SBA-15 storing CO_2 can be used as micro fire extinguishers. The experimental results show that the flame retardant effect in the painted papers is correlated with the loadings of zeolite 5A and amine-SBA-15 storing CO_2, as we increase the loading of these nanoporous materials, the rate of fire propagation (RFP) decreases as expected. When the amount of zeolite 5A and amine-SBA-15 storing CO_2 reached critical points, the fire propagation and the combustion were completely prevented. The critical points are 15 wt% and 10 wt% for zeolite 5A and amine-SBA-15, respectively. This difference between these two materials could be explained as follows: due to the low enthalpy of desorption of CO_2 in the zeolite, CO_2 desorption occurs prematurely, thereby requiring more CO_2. In contrast, more strongly adsorbed CO_2 in the amine-SBA-15 releases at higher temperature, thereby most of the CO_2 released contribute to the formation of the protective gas layer blocking the flux of oxygen. This in turn requires less amount of material because the concentration of CO_2 at the flame front will be higher as compared to that in the case of zeolites.

CHAPTER IX

CONCLUSIONS AND FUTURE WORK

9.1 Conclusions

In this dissertation, we explore two different applications for nanoporous materials, related with CO_2 storage and separation. The first objective of this research was explored the novel synthesis methods of MOF and ZIF membranes. In this dissertation, we explored the novel synthesis of HKUST-1 membranes and films with controlled microstructure. A simple and commercially viable seeding technic which we called "Thermal seeding" has been demonstrated to prepare HKUST-1 membranes with controlled microstructure such as thickness, and grain boundary. The synthesis and characterization test were describe in Chapter III. The formation of cracks and fractures in the membranes was prevented by slowly cooling and drying. The performance of HKUST-1 membranes was obtained by measuring permeance and selectivity of N_2, H_2, CH_2, and CO_2 in Chapter IV. The permeance value of CO_2 becomes greater than those of CH_4 and N_2 with temperature increase, suggesting the affinity of the quadrapolar molecule toward the framework. The new seeding method reported here appears to be general and could open up new opportunities to fabricate thin films and membranes of other metal organic frameworks.

In Chapter V, we explored the novel synthesis method of ZIF-8 and ZIF-7 membranes. A simple and viable method which we called "surface modification and in situ synthesis" has been demonstrated to prepare the ZIF-8 and ZIF-7 membranes. The

performance of ZIF membranes was obtained by measuring permeance and selectivity of N_2, H_2, CH_2, and CO_2. The pore aperture size of ZIF-8 membranes. The ideal selectivity for H_2/N_2 is 11.6 and for H_2/CH_4 is 13.0. These values were calculated from single gas permeation test of three different membranes (tested three times each) and are comparable to the first reported ZIF-8 membrane. As previously reported, these ZIF membranes exhibit molecular sieving, favoring smaller molecules except for CO_2 and O_2. Measured permeances of our membranes are ~2—3 times higher than those of the first reported ZIF-8 membrane (probably because our membranes are about ~2—3 times thinner). The permeance of oxygen is greater than that of carbon dioxide, which is contrary to the previous report.

We have also taken the first step toward understanding the major factors influencing ZIF film microstructure by observing the effects of the presence of absence of a common base on ZIF-8 membranes show molecular sieving, exhibiting ideal selectivity of 11.6 and 13 for H_2/N_2 and H_2/CH_4, respectively.

The second objective of this dissertation is used zeolite 5A and Amine-SBA-15 containing CO_2 as a flame retardants in commercial paint. This idea has been demonstrated to prepare flame retardant paint by mixing the nanoporous material and the paint. Our second objective in this regard was to demonstrate the ability of zeolite 5A and amine-SBA-15 storing CO_2 to reduce the rate of fire propagation (RFP) in commercial paint. This issue was addressed in Chapter VIII, flame retardant paint films were prepare by mixing nanoporous materials storing CO_2 with paint and preparing the films using paper as support. These films show flame retardant behavior when these

contained 15 wt% loading in the case of zeolite 5A and 10% wt loading in the case of amine-SBA-15. This experiment demonstrated the ability and functionality of nanoporous materials containing CO_2 to act as micro fire extinguishers in paint.

9.2 Future work

9.2.1. Preparation and characterization of MOF membranes

Based on the results of the first part of this dissertation, there are suggestions and directions for the future work. Here we suggest the study and analysis of the microstructure of MOF and ZIF membranes by porosymetry measurements and laser confocal microscope. These technics also were used for the characterization of zeolite membranes to study the size of the grain boundaries between the zeolite crystals in MFI membranes (see section 9.2.1.1). There are not previous studies about the grain boundaries size between the MOF and ZIF crystals and how the size of the grain boundary can affect the quality of the membrane. Other possible study could be investigated the performance of the ZIF-8 and ZIF-7 membranes using hydrocarbons and SF_6 (propane/propylene) during the permeation test. Due that the “thermal seeding” and “surface modification looks apparently general for possible applications in other MOFs and ZIFs materials. One option could be investigated the preparation of other kind of MOF and ZIF membranes using these two methods.

9.2.1.1 Microstructure of MOF and ZIF membranes

Microstructure of MOF and ZIF membranes refers to grain size, shape, thickness, orientation, and grain boundary. Since MOF and ZIF are crystalline in nature, their microstructure plays important roles in the determining the pereformance of membranes such as peremeance and separation. Controlling the microstructure of MOF and ZIF membranes has a great implication. There are not many reported efforts to control the grain size, orientation, membrane thickness, and structure of grain boundary.

.

9.2.1.2 Study of grain boundary structure

The study of MOF and ZIF membranes will be base in previous studies in zeolite membranes. Due to a challenge to commercialize zeolite membranes free of defects and cracks formed in grain boundaries. Defects in grain boundaries are formed in response to stresses that are induced by thermal treatment during TPA removal. Non-selective transport pathways through defects in grain boundaries make molecular sieve membranes to lose the separation performance. There are successful approaches to minimize defects formed in grain boundaries. Control of the microstructure of zeolite membranes plays and important role to obtain good membrane performance.

Rapid identification of the defects or cracks in the MOF, ZIF and zeolite membranes is the key factor for the large-scale industrial applications. Defects are classified according to origin and size. Sources of defects include incomplete growth of crystals, a non-uniform seeding, and thermal stresses during the drying process. The

orientation of crystals, the thickness of the membranes, and the structure of grain boundary may affect the formation of defects.

In this way Bonilla et al.[148] used for first time Fluorescent confocal optical microscopy (FCOM) was used to characterize MFI membranes made by secondary growth. It was demonstrated that FMCO is a powerful tool for the non-destructive evaluation of zeolite membranes. Using this technique, it is possible to observe the three-dimensional network of the crystalline grain boundaries. In addition, internal defects in the membrane that are not observable with SEM can be identified. This technique has potential improviding quantitative information on interzeolitic pathways and on the degree of intergrowth of the membranes.

In 2004, M.A. Snyder et al.[149] used again FCOM, for relatively thick (10-25 μm), well-oriented membranes, the reflectance image reveals the crystalline grains at the membrane surface (see Figure 9.1). It provides low-resolution isight reminiscent of SEM, and augments FCOM techniques enabling direct correlation of the fluorescing regions of the membrane with the peripheries of the crystal grains (i.e., grain boundaries).

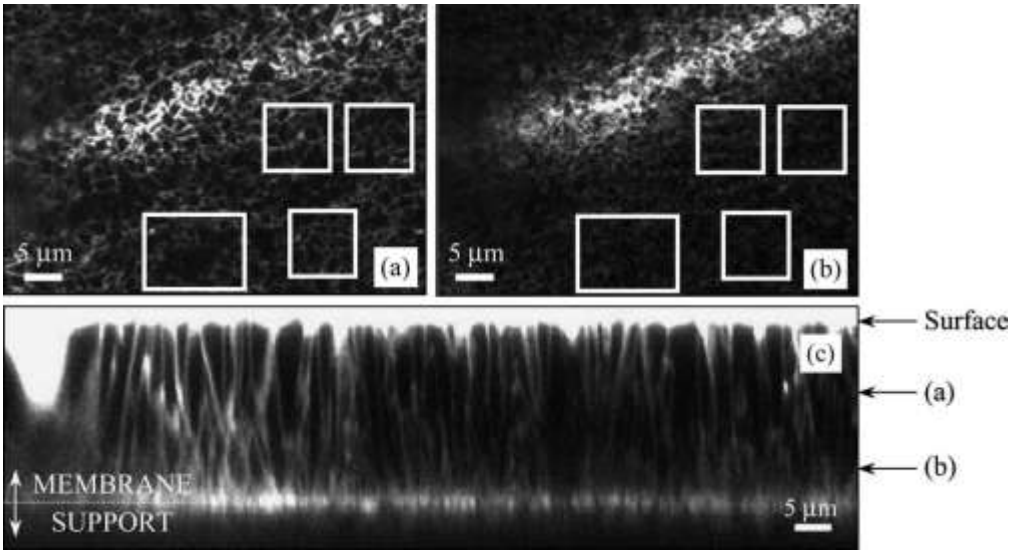

Figure 9.1 Two optical slices (a and b) at approximately 10 and 20 µm below the membrane surface depict the increasing density of the fluorescing grain boundaries in approaching the membrane support. A vertical cross-sectional slice through the membrane thickness (c) shows the propagation of the grain boundaries from the membrane surface to the support, with the location of the optical slice of (a) and (b) noted to the right. Squares and rectangles corresponding to those are included for ease of comparison[149]

Direct comparison of reflectance, fluorescence, and SEM images of and identical region of the membrane, rather than qualitative comparison of images from different membranes, conclusively confirms that molecular probes (dyes) of maximum diameter greater than the MFI pore dimensions access grain boundaries within the poly crystalline MFI membranes.

J. Hedlund et al.[208] report a permporometry analysis of zeolite membranes, the permeance of a non-adsorbing gas, such as helium, is measured as a function of pressure of a strongly adsorbing compound, such as n-hexane in the case of silicate-1 membranes. The adsorbing compound effectively blocks the transport of the non-adsorbing gas already at very low activity of the adsorbing compound. The plot of the permeance of the non-adsorbing gas as a function of relative pressure of the adsorbing ccompound is denoted a permporometry pattern. An adsorption-branch permporometry experiment is simple and straightforward and after activation of the membrane by removing adsorbed species at 300 C in a flow of dry gas, a full permporometry pattern is recorded within about 7 h for such membranes. It is shown how the distribution of flow-through defects can be estimated from the permporometry pattern using a simple model for permeation based on Knudsen diffusion. The estimated defect distribution is supported by SEM observations.

9.2.2 Preparation and characterization of flame retardant paint

Based on the results of the second part of this dissertation, there are a suggestions and directions for the future work of nanoporous materials as micro-fire extinghishers in

paint. The first suggestion is study the distribution of the particles in the polymer film using EDX. In this form we could know how the distribution of the nanoporous material storing CO_2 is in the film (this study can confirm that the particles of the nanoporous materials tent to agglomerate in the paint matrix due to hydrophilic nature of this materials and the hydrophobic nature of the polymers). Also we can try to reduce the loading of the nanoporous materials storing CO_2 by the modification of this material to be hydrophobic. However its necessary find and equilibrium in this alternative because this step will complicate the process. Other alternative could be used dendrimers that can provide mayor number of Nitrogen groups to stored bigger amount of CO_2 in the SBA-15 and in this way reduce the loading necessary form the protective gas layer during the combustion.

REFERENCES

1. Bux, H.; Liang, F. Y.; Li, Y. S.; Cravillon, J.; Wiebcke, M.; Caro, J. *Journal of the American Chemical Society* **2009,** 131, (44), 16345-16349.

2. Interngovernmental Panel on Climate Change (IPCC). Cambridge University Press, *Climate Change*, Cambridge, UK **2007**.

3. Earth Policy Institute, Cambridge University Press, *Global Warming*, Cambridge, UK **2009**

4. Ciferno, J. P.; Fout, T. E.; Jones, A. P.; Murphy, J. T. *Chemical Engineering Progress* **2009,** 105, (4), 33-41.

5. Ebner, A. D.; Ritter, J. A. *Separation Science and Technology* **2009,** 44, (6), 1273-1421.

6. U S Deparment of Energy, USDOE/NETL's *Carbon Capture R&D Program for Existing Coal-Fired Power Plants*, Pittsburg, PA, **2009**.

7. Herzog, H; Meldon, J; Hatton, A. Cambridge University Press, *Advanced Post-Combustion CO_2 Capture*; Boston, MA, **2009.**

8. Choi, S.; Drese, J. H.; Jones, C. W. *ChemSusChem* **2009,** 2, (9), 796-854.

9. Ho, M. T.; Leamon, G.; Allinson, G. W.; Wiley, D. E. *Industrial & Engineering Chemistry Research* **2006,** 45, (8), 2546-2552.

10. Rico, M. J. O.; Moreno-Tost, R.; Jimenez-Lopez, A.; Rodriguez-Castellon, E.; Pereniguez, R.; Caballero, A.; Holgado, J. P. *Catalysis Today* **2010,** 158, (1-2), 78-88.

11. Forster, S.; Konrad, M. *Journal of Materials Chemistry* **2003,** 13, (11), 2671-2688.

12. Morris, R. E.; Bu, X. H. *Nature Chemistry* **2010,** 2, (5), 353-361.

13. Adiga, S. P.; Curtiss, L. A.; Elam, J. W.; Pellin, M. J.; Shih, C. C.; Shih, C. M.; Lin, S. J.; Su, Y. Y.; Gittard, S. A.; Zhang, J.; Narayan, R. J. *Nanoporous Materials* **2008,** 60, (3), 26-32.

14. Adiga, S. P.; Jin, C. M.; Curtiss, L. A.; Monteiro-Riviere, N. A.; Narayan, R. J. *Wiley Interdisciplinary Reviews-Nanomedicine and Nanobiotechnology* **2009,** 1, (5), 568-581.

15. Kleps, I.; Miu, M.; Simion, M.; Ignat, T.; Bragaru, A.; Craciunoiu, F.; Danila, M. *Journal of Biomedical Nanotechnology* **2009,** 5, (3), 300-309.

16. Guillet-Nicolas, R.; Marcoux, L.; Kleitz, F. *New Journal of Chemistry* **2010,** 34, (2), 355-366.

17. Kumar, P.; Guliants, V. V. *Microporous and Mesoporous Materials* **2010,** 132, (1-2), 1-14.

18. Zhang, L.; Primera-Pedrozo, J. N.; Hernandez-Maldonado, A. J. *Journal of Physical Chemistry C* **2010,** 114, (35), 14755-14762.

19. Sing, K. S. W.; Everett, D. H.; Haul, R. A. W.; Moscou, L.; Pierotti, R. A.; Rouquerol, J.; Siemieniewska, T. *Pure and Applied Chemistry* **1985,** 57, (4), 603-619.

20. Sing, K. S. W. *Pure and Applied Chemistry* **1982,** 54, (11), 2201-2218.

21. Breck, D. W.; Eversole, W. G.; Milton, R. M.; Reed, T. B.; Thomas, T. L. *Journal of the American Chemical Society* **1956,** 78, (23), 5963-5971.

22. Davini, P. *Carbon* **2002,** 40, (11), 1973-1979.

23. Chew, T. L.; Ahmad, A. L.; Bhatia, S. *Advances in Colloid and Interface Science* **2010,** 153, (1-2), 43-57.

24. Adeogun, M. J.; Hay, J. N. *Chemistry of Materials* **2000,** 12, (3), 767-775.

25. Tsuji, H.; Smith, R.; Bonfield, W.; Ikada, Y. *Journal of Applied Polymer Science* **2000,** 75, (5), 629-637.

26. Cote, A. P.; Benin, A. I.; Ockwig, N. W.; O'Keeffe, M.; Matzger, A. J.; Yaghi, O. M. *Science* **2005,** 310, (5751), 1166-1170.

27. Hoffmann, F.; Cornelius, M.; Morell, J.; Froba, M. *Angewandte Chemie-International Edition* **2006,** 45, (20), 3216-3251.

28. Yaghi, O. M.; Davis, C. E.; Li, G. M.; Li, H. L. *Journal of the American Chemical Society* **1997,** 119, (12), 2861-2868.

29. Yaghi, O. M.; Li, G. M.; Li, H. L. *Nature* **1995,** 378, (6558), 703-706.

30. Davis, M. E.; Lobo, R. F. *Chemistry of Materials* **1992,** 4, (4), 756-768.

31. Barrer, R. M. *Journal of the Chemical Society* **1948**, 2, (62), 61-72

32. Flanigen, E. M. *Pure and Applied Chemistry* **1980,** 52, (9), 2191-2211.

33. Barrer, R. M.; Denny, P. J. *Journal of the Chemical Society* **1961**, 2, (4), 971-985

34. Montanari, T.; Busca, G. *Vibrational Spectroscopy* **2008,** 46, (1), 45-51.

35. Dai, F. Y.; Suzuki, M.; Takahashi, H.; Saito, Y. *Bulletin of the Chemical Society of Japan* **1988,** 61, (10), 3403-3407.

36. Flanigen, E. M. *Advances in Chemistry Series* **1973**, (121), 119-139.

37. Davis, M. E. *Industrial & Engineering Chemistry Research* **1991,** 30, (8), 1675-1683.

38. Kresge, C. T.; Vartuli, J. C.; Roth, W. J.; Leonowicz, M. E.; Beck, J. S.; Schmitt, K. D.; Chu, C. T. W.; Olson, D. H.; Sheppard, E. W.; McCullen, S. B.; Higgins, J. B.; Schlenker, J. L., M41S: A new family of mesoporous molecular sieves prepared with liquid crystal templates. In Izumi, Y.; Arai, H.; Iwamoto, M., (Eds.), *Science and Technology in Catalysis* **1995**; Vol. 92, pp 11-19. Elsevier Science, Amsterdam.

39. Zhao, W.; Li, Q. Z.; Wang, L. N.; Chu, J. L.; Qu, J. K.; Li, S. H.; Qi, T. *Langmuir* **2010,** 26, (10), 6982-6988.

40. Zhao, D. Y.; Feng, J. L.; Huo, Q. S.; Melosh, N.; Fredrickson, G. H.; Chmelka, B. F.; Stucky, G. D. *Science* **1998,** 279, (5350), 548-552.

41. Zhao, D. Y.; Huo, Q. S.; Feng, J. L.; Chmelka, B. F.; Stucky, G. D. *Journal of the American Chemical Society* **1998,** 120, (24), 6024-6036.

42. Widenmeyer, M.; Anwander, R. *Chemistry of Materials* **2002,** 14, (4), 1827-1831.

43. Barczak, M.; Pikus, S.; Skrzydlo-Radomanska, B.; Dabrowski, A. *Journal of the International Adsorption Society* **2009,** 15, (3), 278-286.

44. Cheng, K.; Landry, C. C. *Journal of the American Chemical Society* **2007,** 129, (31), 9674-9685.

45. Ikeda, S.; Tachi, K.; Ng, Y. H.; Ikoma, Y.; Sakata, T.; Mori, H.; Harada, T.; Matsumura, M. *Chemistry of Materials* **2007,** 19, (17), 4335-4340.

46. Yang, C. M.; Lin, H. A.; Zibrowius, B.; Spliethoff, B.; Schueth, F.; Liou, S. C.; Chu, M. W.; Chen, C. H. *Chemistry of Materials* **2007,** 19, (13), 3205-3211.

47. Ji, A.; Shi, L. Y.; Cao, Y.; Wang, Y., Functionalization of silica by in-situ grafting hydrotalcite. In, Sayari, A.; Jaroniec, M., (Eds). *Nanoporous Materials* 2005; Vol. 156, pp 917-924. Elsevier, Amsterdam.

48. Chong, A. S. M.; Zhao, X. S. *Journal of Physical Chemistry B* **2003,** 107, (46), 12650-12657.

49. Chong, A. S. M.; Zhao, X. S.; Kustedjo, A. T.; Qiao, S. Z. *Microporous and Mesoporous Materials* **2004,** 72, (1-3), 33-42.

50. Bent, S. F. *Surface Science* **2002,** 500, (1-3), 879-903.

51. Stein, A.; Melde, B. J.; Schroden, R. C. *Advanced Materials* **2000,** 12, (19), 1403-1419.

52. Guan, B.; Ciampi, S.; Le Saux, G.; Gaus, K.; Reece, P. J.; Gooding, J. J. *Langmuir* **2011,** 27, (1), 328-334.

53. Yu, D.; Wang, Z. Y.; Ergang, N. S.; Stein, A.,Stud. Surf. Sci. Catal. **2007**, 165, (2), 365-368.

54. Wu, S. S.; Liu, P.; Leng, Y.; Wang, J. *Catalysis Letters* **2009,** 132, (3-4), 500-505.

55. Wang, Q. Q.; Shantz, D. F. *Journal of Catalysis* **2010,** 271, (2), 170-177.

56. Williams, J. J.; Wiersum, A. D.; Seaton, N. A.; Duren, T. *Journal of Physical Chemistry C* **2010,** 114, (43), 18538-18547.

57. Gonzalez, B.; Colilla, M.; de Laorden, C. L.; Vallet-Regi, M. *Journal of Materials Chemistry* **2009,** 19, (47), 9012-9024.

58. Zhao, H. L.; Hu, J.; Wang, J. J.; Zhou, L. H.; Liu, H. L. *Acta Physico-Chimica Sinica* **2007,** 23, (6), 801-806.

59. Liu, S. H.; Wu, C. H.; Lee, H. K.; Liu, S. B. *Topics in Catalysis* **2010,** 53, (3-4), 210-217.

60. Guerrero, V. V.; Shantz, D. F. *Industrial & Engineering Chemistry Research* **2009,** 48, (23), 10375-10380.

61. Srinivas, D.; Saikia, L. *Catalysis Surveys from Asia* **2008,** 12, (2), 114-130.

62. Fiorilli, S.; Onida, B.; Bonelli, B.; Garrone, E. *Journal of Physical Chemistry B* **2005,** 109, (35), 16725-16729.

63. Hicks, J. C.; Dabestani, R.; Buchanan, A. C.; Jones, C. W. *Inorganica Chimica Acta* **2008,** 361, (11), 3024-3032.

64. Barczak, M.; Skwarek, E.; Janusz, W.; Dabrowski, A.; Pikus, S. *Applied Surface Science* **2010,** 256, (17), 5370-5375.

65. Muller, C. A.; Schneider, M.; Mallat, T.; Baiker, A. *Applied Catalysis a-General* **2000,** 201, (2), 253-261.

66. Etienne, M.; Goubert-Renaudin, S.; Rousselin, Y.; Marichal, C.; Denat, F.; Lebeau, B.; Walcarius, A. *Langmuir* **2009,** 25, (5), 3137-3145.

67. Liu, X. X.; Hua, Y.; Villemure, G. *Microporous and Mesoporous Materials* **2009,** 117, (1-2), 317-325.

68. Zelenak, V.; Badanicova, M.; Halamova, D.; Cejka, J.; Zukal, A.; Murafa, N.; Goerigk, G. *Chemical Engineering Journal* **2008,** 144, (2), 336-342.

69. Serna-Guerrero, R.; Belmabkhout, Y.; Sayari, A. *Chemical Engineering Journal* **2010,** 161, (1-2), 173-181.

70. Basaldella, E. I.; Legnoverde, M. S.; Ponzi, E. N.; Tara, J. C.; Firpo, N.; Soto, E. L., Stud. Surf. Sci. Catal, **2008**, 174, (3), 619-622.

71. Notz, R.; Tonnies, I.; Scheffknecht, G.; Hasse, H. *Chemie Ingenieur Technik* **2010,** 82, (10), 1639-1653.

72. Davison, J.; Thambimuthu, K. *Proceedings of the Institution of Mechanical Engineers Part a-Journal of Power and Energy* **2009,** 223, (A3), 201-212.

73. Dave, N.; Do, T.; Puxty, G.; Rowland, R.; Feron, P. H. M.; Attalla, M. I., CO_2 capture by aqueous amines and aqueous ammonia - A comparison. In Gale, J.; Herzog, H.; Braitsch, J., (Eds), *Greenhouse Gas Control Technologies 9*,. **2009**; Vol. 1, pp 949-954. Elsevier, Amsterdam.

74. Belmabkhout, Y.; Sayari, A. *Energy & Fuels* **2010,** (24), 5273-5280.

75. Khatri, R. A.; Chuang, S. S. C.; Soong, Y.; Gray, M. *Industrial & Engineering Chemistry Research* **2005,** 44, (10), 3702-3708.

76. Rowsell, J. L. C.; Yaghi, O. M. *Microporous and Mesoporous Materials* **2004,** 73, (1-2), 3-14.

77. Li, H.; Eddaoudi, M.; Groy, T. L.; Yaghi, O. M. *Journal of the American Chemical Society* **1998,** 120, (33), 8571-8572.

78. Rosi, N. L.; Eckert, J.; Eddaoudi, M.; Vodak, D. T.; Kim, J.; O'Keeffe, M.; Yaghi, O. M. *Science* **2003,** 300, (5622), 1127-1129.

79. Rowsell, J. L. C.; Millward, A. R.; Park, K. S.; Yaghi, O. M. *Journal of the American Chemical Society* **2004,** 126, (18), 5666-5667.

80. Bae, T. H.; Lee, J. S.; Qiu, W. L.; Koros, W. J.; Jones, C. W.; Nair, S. *Angewandte Chemie-International Edition* **2010,** 49, (51), 9863-9866.

81. Snurr, R. Q.; Hupp, J. T.; Nguyen, S. T. *AICHE Journal* **2004,** 50, (6), 1090-1095.

82. Li, J. R.; Kuppler, R. J.; Zhou, H. C. *Chemical Society Reviews* **2009,** 38, (5), 1477-1504.

83. Bauer, C. A.; Schroeder, F.; Skulan, A. J.; Hermes, S.; Talin, A. A.; Anderson, R. J.; Fischer, R. A.; Simmons, B. A.; Allendorf, M. D. *Abstracts of Papers of the American Chemical Society* **2006,** 231.

84. Cho, S. H.; Ma, B. Q.; Nguyen, S. T.; Hupp, J. T.; Albrecht-Schmitt, T. E. *Chemical Communications* **2006**, (24), 2563-2565.

85. Lee, J.; Farha, O. K.; Roberts, J.; Scheidt, K. A.; Nguyen, S. T.; Hupp, J. T. *Chemical Society Reviews* **2009,** 38, (5), 1450-1459.

86. Ma, L. Q.; Abney, C.; Lin, W. B. *Chemical Society Reviews* **2009,** 38, (5), 1248-1256.

87. Cheetham, A. K.; Rao, C. N. R.; Feller, R. K. *Chemical Communications* **2006**, (46), 4780-4795.

88. Tranchemontagne, D. J.; Mendoza-Cortes, J. L.; O'Keeffe, M.; Yaghi, O. M. *Chemical Society Reviews* **2009,** 38, (5), 1257-1283.

89. Ramanan, A.; Whittingham, M. S. *Crystal Growth & Design* **2006,** 6, (11), 2419-2421.

90. O'Keeffe, M. *Chemical Society Reviews* **2009,** 38, (5), 1215-1217.

91. Hoffmann, R. *Scientific American* **1993,** 268, (2), 66-73.

92. Eddaoudi, M.; Kim, J.; Rosi, N.; Vodak, D.; Wachter, J.; O'Keeffe, M.; Yaghi, O. M. *Science* **2002,** 295, (5554), 469-472.

93. Panella, B.; Hirscher, M.; Putter, H.; Muller, U. *Advanced Functional Materials* **2006,** 16, (4), 520-524.

94. Serpaggi, F.; Loiseau, T.; Taulelle, F.; Ferey, G. *Microporous and Mesoporous Materials* **1998,** 20, (1-3), 197-206.

95. Ferey, G. *Chemical Society Reviews* **2008,** 37, (1), 191-214.

96. Ferey, G.; Mellot-Draznieks, C.; Serre, C.; Millange, F.; Dutour, J.; Surble, S.; Margiolaki, I. *Science* **2005,** 309, (5743), 2040-2042.

97. Chui, S. S. Y.; Lo, S. M. F.; Charmant, J. P. H.; Orpen, A. G.; Williams, I. D. *Science* **1999,** 283, (5405), 1148-1150.

98. Wang, Q. M.; Shen, D. M.; Bulow, M.; Lau, M. L.; Deng, S. G.; Fitch, F. R.; Lemcoff, N. O.; Semanscin, J. *Microporous and Mesoporous Materials* **2002,** 55, (2), 217-230.

99. Guo, H. L.; Zhu, G. S.; Hewitt, I. J.; Qiu, S. L. *Journal of the American Chemical Society* **2009,** 131, (5), 1646-1652.

100. Keskin, S.; Liu, J. C.; Johnson, J. K.; Sholl, D. S. *Microporous and Mesoporous Materials* **2009,** 125, (1-2), 101-106.

101. Yang, Q. Y.; Xue, C. Y.; Zhong, C. L.; Chen, J. F. *Aiche Journal* **2007,** 53, (11), 2832-2840.

102. Ma, S. Q.; Sun, D. F.; Yuan, D. Q.; Wang, X. S.; Zhou, H. C. *Journal of the American Chemical Society* **2009,** 131, (18), 6445-6451.

103. Ma, S. Q.; Yuan, D. Q.; Zhou, H. C. *Abstracts of Papers of the American Chemical Society* **2008,** 235, 383-INOR.

104. Kuznicki, S. M.; Bell, V. A.; Nair, S.; Hillhouse, H. W.; Jacubinas, R. M.; Braunbarth, C. M.; Toby, B. H.; Tsapatsis, M. *Nature* **2001,** 413, (6856), 652-652.

105. Hayashi, H.; Cote, A. P.; Furukawa, H.; O'Keeffe, M.; Yaghi, O. M. *Nature Materials* **2007,** 6, (7), 501-506.

106. Park, K. S.; Ni, Z.; Cote, A. P.; Choi, J. Y.; Huang, R. D.; Uribe-Romo, F. J.; Chae, H. K.; O'Keeffe, M.; Yaghi, O. M. *Proceedings of the National Academy of Sciences of the United States of America* **2006,** 103, (27), 10186-10191.

107. Banerjee, R.; Phan, A.; Wang, B.; Knobler, C.; Furukawa, H.; O'Keeffe, M.; Yaghi, O. M. *Science* **2008,** 319, (5865), 939-943.

108. Phan, A.; Doonan, C. J.; Uribe-Romo, F. J.; Knobler, C. B.; O'Keeffe, M.; Yaghi, O. M. *Accounts of Chemical Research* **2010,** 43, (1), 58-67.

109. Banerjee, R.; Furukawa, H.; Britt, D.; Knobler, C.; O'Keeffe, M.; Yaghi, O. M. *Journal of the American Chemical Society* **2009,** 131, (11), 3875-3880.

110. Morris, W.; Leung, B.; Furukawa, H.; Yaghi, O. K.; He, N.; Hayashi, H.; Houndonougbo, Y.; Asta, M.; Laird, B. B.; Yaghi, O. M. *Journal of the American Chemical Society* **2010,** 132, (32), 11006-11008.

111. Zhou, M.; Wang, Q.; Zhang, L.; Liu, Y. C.; Kang, Y. *Journal of Physical Chemistry B* **2009,** 113, (32), 11049-11053.

112. Guo, H. C.; Shi, F.; Ma, Z. F.; Liu, X. Q. *Journal of Physical Chemistry C* **2010,** 114, (28), 12158-12165.

113. Zacher, D.; Shekhah, O.; Wöll, C.; Fischer, R. A. *Chemical Society Reviews* **2009,** 38, 1418-1429.

114. Millward, A. R.; Yaghi, O. M. *Journal of the American Chemical Society* **2005,** 127, (51), 17998-17999.

115. Mulder, M., *Basic Principles of Membrane Technology*. Kluwer Academic Publishers: Dordrecht, Netherlands **1996**.

116. Hermes, S.; Schroder, F.; Chelmowski, R.; Woll, C.; Fischer, R. A. *Journal of the American Chemical Society* **2005,** 127, (40), 13744-13745.

117. Arnold, M.; Kortunov, P.; Jones, D. J.; Nedellec, Y.; Karger, J.; Caro, J. *European Journal of Inorganic Chemistry* **2007**, (1), 60-64.

118. Biemmi, E.; Darga, A.; Stock, N.; Bein, T. *Microporous and Mesoporous Materials* **2008,** 114, (1-3), 380-386.

119. Gascon, J.; Aguado, S.; Kapteijn, F. *Microporous and Mesoporous Materials* **2008,** 113, (1-3), 132-138.

120. Yoo, Y.; Jeong, H. K. *Chemical Communications* **2008**, (21), 2441-2443.

121. Yoo, Y.; Lai, Z.; Jeong, H. K. *Microporous Mesoporous Mater.* **2009,** (123), 100-106

122. Ranjan, R.; Tsapatsis, M. *Chemistry of Materials* **2009**, (20), 4920-4924

123. Guerrero, V. V.; Yoo, Y.; McCarthy, M. C.; Jeong, H. K. *Journal of Materials Chemistry* **2010,** 20, (19), 3938-3943.

124. Li, Y. S.; Liang, F. Y.; Bux, H. G.; Yang, W. S.; Caro, J. *Journal of Membrane Science* **2010,** 354, (1-2), 48-54.

125. Liu, Y. Y.; Hu, E. P.; Khan, E. A.; Lai, Z. P. *Journal of Membrane Science* **2010,** 353, (1-2), 36-40.

126. Biemmi, E.; Scherb, C.; Bein, T. *Journal of the American Chemical Society* **2007,** 129, 8054-8055.

127. Yoo, Y.; Jeong, H. K. *Crystal Growth & Design* **2010,** 10, (3), 1283-1288.

128. Perez-Pellitero, J.; Amrouche, H.; Siperstein, F. R.; Pirngruber, G.; Nieto-Draghi, C.; Chaplais, G.; Simon-Masseron, A.; Bazer-Bachi, D.; Peralta, D.; Bats, N. *Chemistry-A European Journal* **2010,** 16, (5), 1560-1571.

129. Demessence, A.; Boissiere, C.; Grosso, D.; Horcajada, P.; Serre, C.; Ferey, G.; Soler-Illia, G.; Sanchez, C. *Journal of Materials Chemistry* **2010,** 20, (36), 7676-7681.

130. Lu, G.; Hupp, J. T. *Journal of the American Chemical Society* **2010,** 132, (23), 7832-7840.

131. Shekhah, C.; Wang, H.; Kowarik, S.; Schreiber, F.; Paulus, M.; Tolan, M.; Sternemann, C.; Evers, F.; Zacher, D.; Fischer, R. A.; Woll, C. *Journal of the American Chemical Society* **2007,** 129, 15118-15128.

132. Zacher, D.; Baunemann, A.; Hermes, S.; Fischer, R. A. *Journal of Materials Chemistry* **2007,** 17, (27), 2785-2792.

133. Liu, Y. Y.; Ng, Z. F.; Khan, E. A.; Jeong, H. K.; Ching, C. B.; Lai, Z. P. *Microporous and Mesoporous Materials* **2009,** 118, (1-3), 296-301.

134. Liu, Y.; Ng, Z.; Khan, E. A.; Jeong, H.-K.; Ching, C.-b.; Lai, Z. *Microporous Mesoporous Mater.* **2009,** 118, (1-3), 296-301.

135. Lovallo, M. C.; Gouzinis, A.; Tsapatsis, M. *AICHE Journal* **1998,** 44, (8), 1903-1913.

136. Xomeritakis, G.; Tsapatsis, M. *Chemistry of Materials* **1999,** 11, (4), 875-882.

137. Xomeritakis, G.; Gouzinis, A.; Nair, S.; Okubo, T.; He, M. Y.; Overney, R. M.; Tsapatsis, M. *Chemical Engineering Science* **1999,** 54, (15-16), 3521-3531.

138. Xomeritakis, G.; Nair, S.; Tsapatsis, M. *Microporous and Mesoporous Materials* **2000,** 38, (1), 61-73.

139. Motuzas, J.; Julbe, A.; Noble, R. D.; van der Lee, A.; Beresnevicius, Z. J. *Microporous and Mesoporous Materials* **2006,** 92, (1-3), 259-269.

140. Lee, I.; Buday, J. L.; Jeong, H. K. *Microporous and Mesoporous Materials* **2009,** 122, (1-3), 288-293.

141. Cundy, C. S.; Cox, P. A. *Microporous and Mesoporous Materials* **2005,** 82, (1-2), 1-78.

142. Barrer, R. M. *Journal of the Chemical Society-Faraday Transactions* **1990,** 86, (7), 1123-1130.

143. Barrer, R. M.; Craven, R. J. B. *Journal of the Chemical Society-Faraday Transactions* **1990,** 86, (3), 545-552.

144. Shi, D. *Nanotechnology Focus*, Springer, New York, **2001**.

145. Xiao, J. R.; Wei, J. *Chemical Engineering Science* **1992,** 47, (5), 1143-1159.

146. Li, Y. S.; Bux, H.; Feldhoff, A.; Li, G. L.; Yang, W. S.; Caro, J. *Advanced Materials* **2010,** 22, (30), 3322-3330.

147. Hedlund, J.; Korelskiy, D.; Sandstrom, L.; Lindmark, J. *Journal of Membrane Science* **2009,** 345, (1-2), 276-287.

148. Bonilla, G.; Tsapatsis, M.; Vlachos, D. G.; Xomeritakis, G. *Journal of Membrane Science* **2001,** 182, (1-2), 103-109.

149. Snyder, M. A.; Lai, Z.; Tsapatsis, M.; Vlachos, D. G. *Microporous and Mesoporous Materials* **2004,** 76, (1-3), 29-33.

150. Li, H.; Eddaoudi, M.; O'Keeffe, M.; Yaghi, O. M. *Nature* **1999,** 402, (6759), 276-279.

151. Zou, X. Q.; Zhu, G. S.; Hewitt, I. J.; Sun, F. X.; Qiu, S. L. *Dalton Transactions* **2009**, (16), 3009-3013.

152. Seo, J. S.; Whang, D.; Lee, H.; Jun, S. I.; Oh, J.; Jeon, Y. J.; Kim, K. *Nature* **2000,** 404, (6781), 982-986.

153. Kitagawa, S.; Kitaura, R.; Noro, S. *Angewandte Chemie-International Edition* **2004,** 43, (18), 2334-2375.

154. Horcajada, P.; Serre, C.; Grosso, D.; Boissiere, C.; Perruchas, S.; Sanchez, C.; Ferey, G. *Advanced Materials* **2009,** 21, (19), 1931-1935.

155. Ameloot, R.; Stappers, L.; Fransaer, J.; Alaerts, L.; Sels, B. F.; De Vos, D. E. *Chemistry of Materials* **2009,** 21, (13), 2580-2582.

156. Skoulidas, A. I. *Journal of the American Chemical Society* **2004,** 126, (5), 1356-1357.

157. Lai, Z. P.; Tsapatsis, M.; Nicolich, J. R. *Advanced Functional Materials* **2004,** 14, (7), 716-729.

158. Shoaee, M.; Anderson, M. W.; Attfield, M. P. *Angewandte Chemie-International Edition* **2008,** 47, (44), 8525-8528.

159. Yaghi, O. M.; O'Keeffe, M.; Ockwig, N. W.; Chae, H. K.; Eddaoudi, M.; Kim, J. *Nature* **2003,** 423, (6941), 705-714.

160. Allendorf, M. D.; Bauer, C. A.; Bhakta, R. K.; Houk, R. J. T. *Chemical Society Reviews* **2009,** 38, (5), 1330-1352.

161. Hermes, S.; Zacher, D.; Baunemann, A.; Woll, C.; Fischer, R. A. *Chemistry of Materials* **2007,** 19, (9), 2168-2173.

162. Ameloot, R.; Gobechiya, E.; Uji-i, H.; Martens, J. A.; Hofkens, J.; Alaerts, L.; Sels, B. F.; De Vos, D. E. *Advanced Materials* **2010,** 22, (24), 2685-2692.

163. Huang, A. S.; Dou, W.; Caro, J. *Journal of the American Chemical Society* **2010,** 132, (44), 15562-15564.

164. Huang, A. S.; Bux, H.; Steinbach, F.; Caro, J. *Angewandte Chemie-International Edition* **2010,** 49, (29), 4958-4961.

165. Venna, S. R.; Carreon, M. A. *Journal of the American Chemical Society* **2010,** 132, (1), 76-78.

166. Haldoupis, E.; Nair, S.; Sholl, D. S. *Journal of the American Chemical Society* **2010,** 132, (21), 7528-7539.

167. Choi, J.; Jeong, H. K.; Snyder, M. A.; Stoeger, J. A.; Masel, R. I.; Tsapatsis, M. *Science* **2009,** 325, (5940), 590-593.

168. Lai, Z. P.; Bonilla, G.; Diaz, I.; Nery, J. G.; Sujaoti, K.; Amat, M. A.; Kokkoli, E.; Terasaki, O.; Thompson, R. W.; Tsapatsis, M.; Vlachos, D. G. *Science* **2003,** 300, (5618), 456-460.

169. Derylo-Marczewska, A.; Goworek, J.; Pikus, S.; Kobylas, E.; Zgrajka, W. *Langmuir* **2002,** 18, (20), 7538-7543.

170. Xiong, R.; Shi, J. *Journal of Materials Science & Technology* **2005,** 21, (4), 541-544.

171. Bertoti, I. *Surface & Coatings Technology* **2002,** 151, 194-203.

172. Cravillon, J.; Munzer, S.; Lohmeier, S. J.; Feldhoff, A.; Huber, K.; Wiebcke, M. *Chemistry of Materials* **2009,** 21, (8), 1410-1412.

173. Shimomura, S.; Higuchi, M.; Matsuda, R.; Yoneda, K.; Hijikata, Y.; Kubota, Y.; Mita, Y.; Kim, J.; Takata, M.; Kitagawa, S. *Nature Chemistry* **2010,** 2, (8), 633-637.

174. Borms, R.; Georlette, P. *Plast. Eur.* **2004,** 9, 256-265.

175. Mack, A. G. Jon Wiley & Sons, *Kirk-Othmer Encyclopedia of Chemical Technology,* Malden MA, USA **2004.**

176. Laoutid, F.; Bonnaud, L.; Alexandre, M.; Lopez-Cuesta, J. M.; Dubois, P. *Materials Science & Engineering R-Reports* **2009,** 63, (3), 100-125.

177. Gouteux, B.; Alaee, M.; Mabury, S. A.; Pacepavicius, G.; Muir, D. C. G. *Environmental Science & Technology* **2008,** 42, (24), 9039-9044.

178. Bourbigot, S.; Flambard, X. *Fire and Materials* **2002,** 26, (4-5), 155-168.

179. Choi, J.; Yee, A. F.; Laine, R. M. *Macromolecules* **2003,** 36, (15), 5666-5682.

180. S. Levchik, Jon Wiley & Sons, *Flame Retardant Polymer Nanocomposites*. Malden MA, USA **2007**.

181. Faeth, G., C. Kim, and O. Kwon, . *International Journal of Energy for a clean enviroment* **2003,** 4 (2), 117.

182. Birnbaum, L. S.; Staskal, D. F. *Environmental Health Perspectives* **2004,** 112, (1), 9-17.

183. Gunduz, G.; Kisakurek, D.; Kayadan, S. *Polymer Degradation and Stability* **1999,** 64, (3), 501-504.

184. Gilman, J. W.; Kashiwagi, T.; Lichtenhan, J. D. *Sampe Journal* **1997,** 33, (4), 40-46.

185. Bourbigot, S.; Vanderhart, D. L.; Gilman, J. W.; Bellayer, S.; Stretz, H.; Paul, D. R. *Polymer* **2004,** 45, (22), 7627-7638.

186. Qin, H. L.; Su, Q. S.; Zhang, S. M.; Zhao, B.; Yang, M. S. *Polymer* **2003,** 44, (24), 7533-7538.

187. Zhu, J.; Morgan, A. B.; Lamelas, F. J.; Wilkie, C. A. *Chemistry of Materials* **2001,** 13, (10), 3774-3780.

188. Laachachi, A.; Leroy, E.; Cochez, M.; Ferriol, M.; Cuesta, J. M. L. *Polymer Degradation and Stability* **2005,** 89, (2), 344-352.

189. Kashiwagi, T.; Morgan, A. B.; Antonucci, J. M.; VanLandingham, M. R.; Harris, R. H.; Awad, W. H.; Shields, J. R. *Journal of Applied Polymer Science* **2003,** 89, (8), 2072-2078.

190. Zammarano, M.; Franceschi, M.; Bellayer, S.; Gilman, J. W.; Meriani, S. *Polymer* **2005,** 46, (22), 9314-9328.

191. Lefebvre, J.; Le Bras, M.; Bourbigot, S., American Chemical Society, *Fire and Polymers*. Washington, DC USA **2005**.

192. Kashiwagi, T.; Du, F. M.; Douglas, J. F.; Winey, K. I.; Harris, R. H.; Shields, J. R. *Nature Materials* **2005,** 4, (12), 928-933.

193. Kashiwagi, T.; Grulke, E.; Hilding, J.; Groth, K.; Harris, R.; Butler, K.; Shields, J.; Kharchenko, S.; Douglas, J. *Polymer* **2004,** 45, (12), 4227-4239.

194. Chigwada, G.; Jash, P.; Jiang, D. D.; Wilkie, C. A. *Polymer Degradation and Stability* **2005,** 89, (1), 85-100.

195. Bourbigot, S.; Le Bras, M.; Flambard, X.; Rochery, M.; Devaux, E.; Lichtenhan, J. D., The Royal Sciety of Chemistry, *Fire Retardancy of Polymers : New Applications of Mineral Fillers*, Cambridge, UK **2005.**

196. Devaux, E.; Rochery, M.; Bourbigot, S. *Fire and Materials* **2002,** 26, (4-5), 149-154.

197. Jama, C.; Quede, A.; Le Bras, M.; Delobel, R.; Goudmand, P.; Dessaux, O.; Bourbigot, S.; Gilman, J. W.; Kashiwagi, T. *Abstracts of Papers of the American Chemical Society* **2000,** 220, 96-PMSE.

198. Gilman, J. W.; Jackson, C. L.; Morgan, A. B.; Harris, R.; Manias, E.; Giannelis, E. P.; Wuthenow, M.; Hilton, D.; Phillips, S. H. *Chemistry of Materials* **2000,** 12, (7), 1866-1873.

199. Duquesne, S.; Jama, C.; Le Bras, M.; Delobel, R.; Recourt, P.; Gloaguen, J. M. *Composites Science and Technology* **2003,** 63, (8), 1141-1148.

200. Zheng, X. X.; Wilkie, C. A. *Polymer Degradation and Stability* **2003,** 82, (3), 441-450.

201. El-Wahab, H. A.; El-Fattah, M. A.; Gabr, M. Y. *Progress in Organic Coatings* **2010,** 69, (3), 272-277.

202. Giudice, C. A.; Benitez, J. C. *Progress in Organic Coatings* **2001,** 42, (1-2), 82-88.

203. Morgan A.B., *Fire and Materials* **2007**, 31, (2), 257-283.

204. La Rosa, A. D.; Recca, A.; Carter, J. T.; McGrail, P. T. *Polymer* **1999,** 40, (14), 4093-4098.

205. Petsom, A.; Roengsumran, S.; Ariyaphattanakul, A.; Sangvanich, P. *Polymer Degradation and Stability* **2003,** 80, (1), 17-22.

206. Huggett, C. *Fire and Materials* **1980,** 4, (2), 61-65.

207. Shui-Yu L. *Prog. Polym. Sci.* **2002**, 27, (1), 1661-1712

208. Hedlund, J.; *Microporous and Mesoporous Materials* **2002**, 52, (4), 179-189.

APPENDIX A

FIGURES AND TABLE CHAPTER V

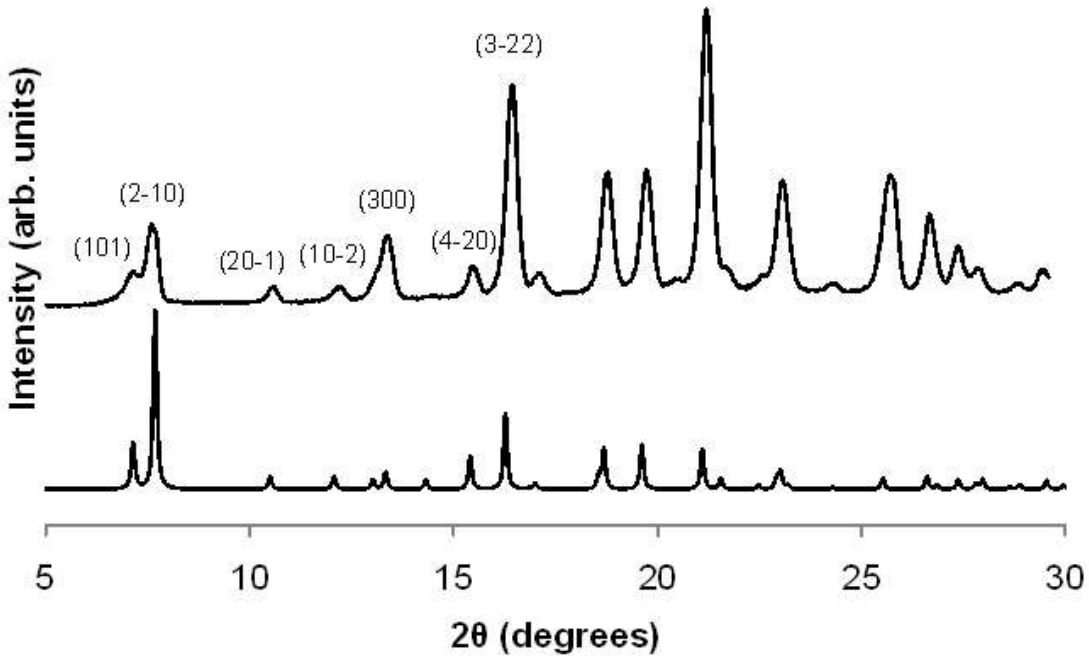

Figure A1. XRD pattern of ZIF-7 film compared to simulated ZIF-7 pattern

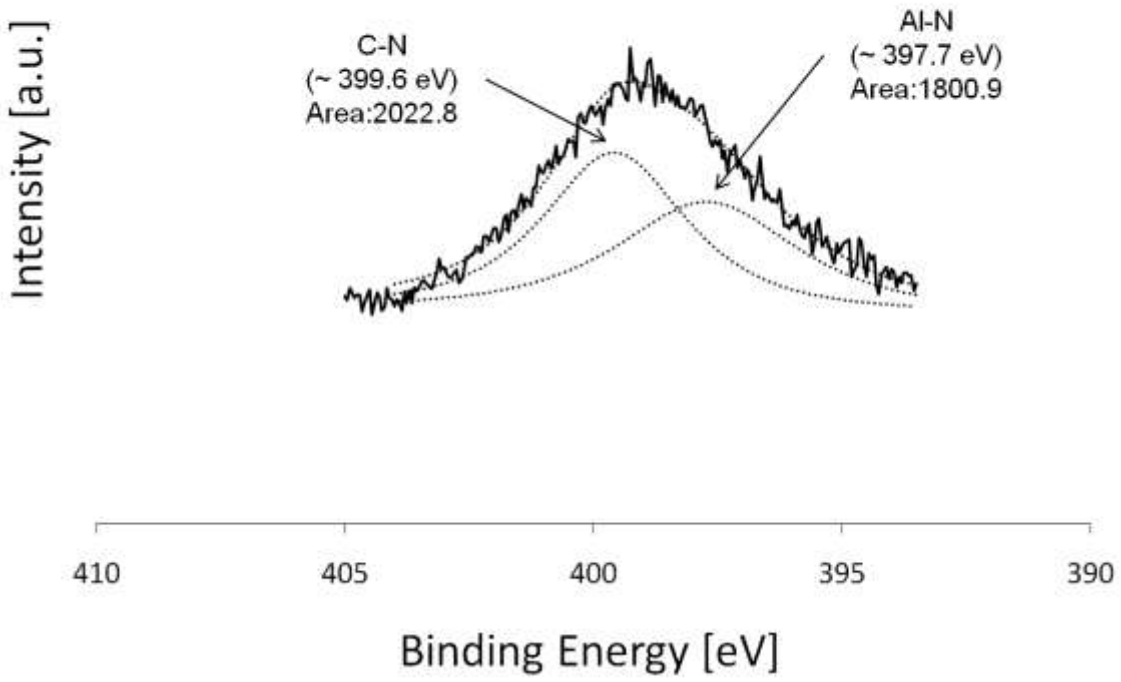

Figure A2: N 1s XPS spectra of benzimidazole modified supports. An asymmetric peaks was again observed at ~397 eV indicating covalently bound organic ligands

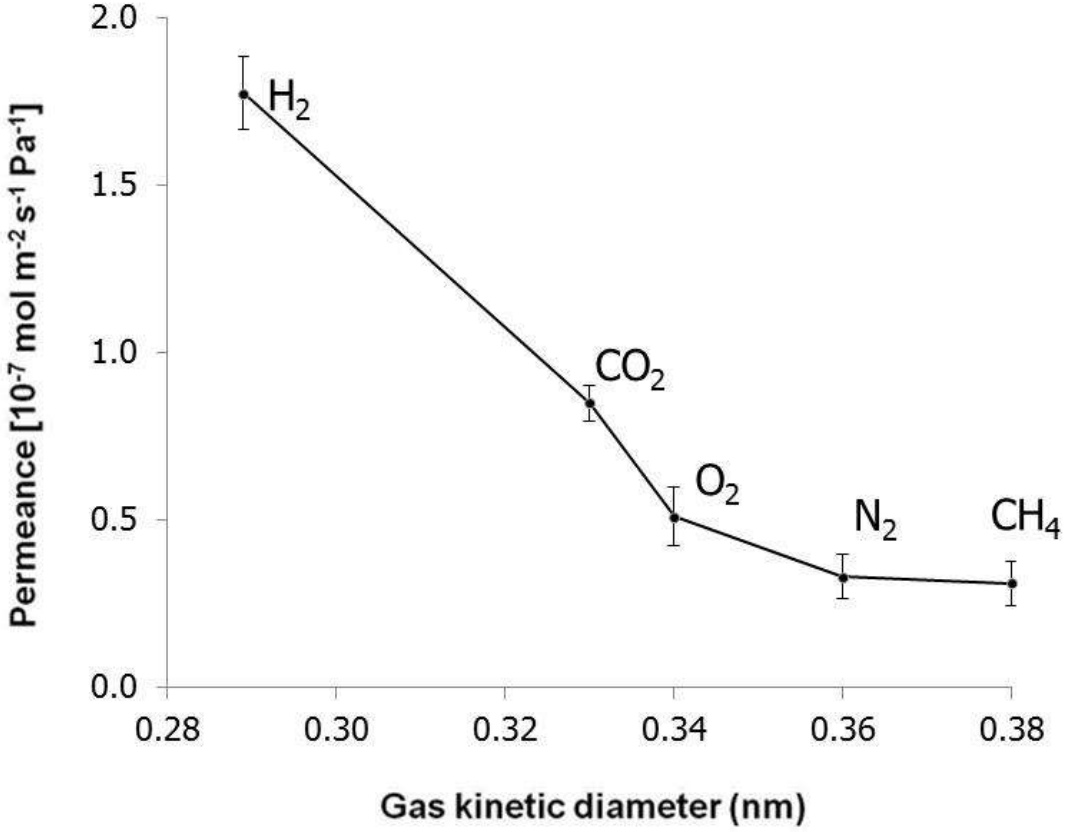

Figure A3 Single gas permeance results for well-intergrown ZIF-7 membranes (repeated 3 times on 3 different samples)

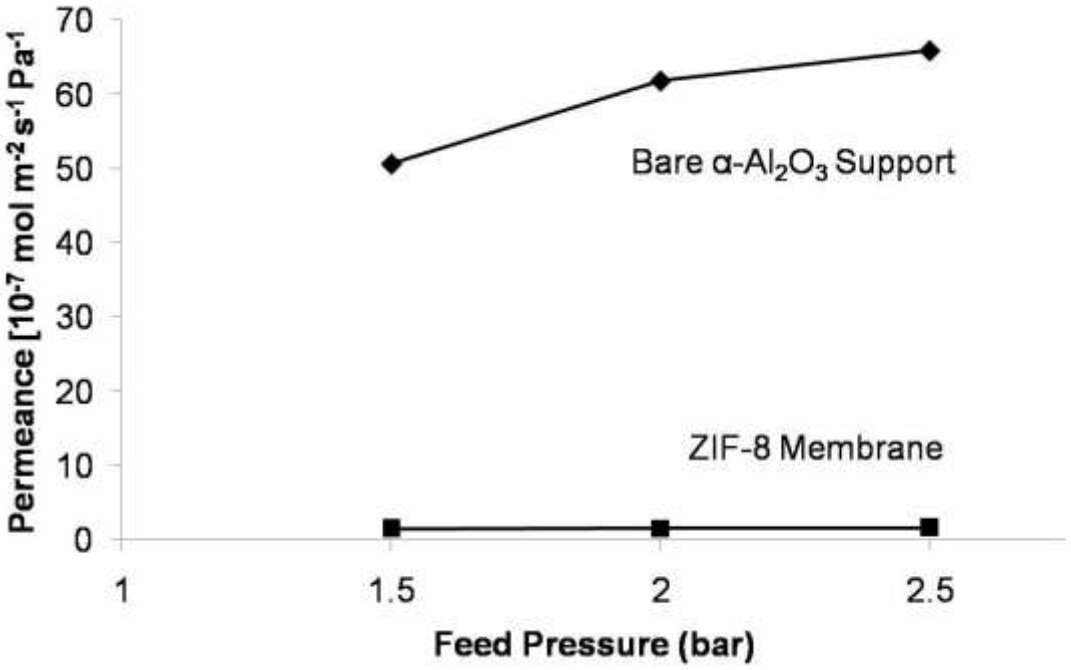

Figure A4 Hydrogen permeance measured at different feed pressures and room temperature. The upper curve is the bare support, indicating viscous flow (permeance depends on pressure). The lower curve is a well-intergrown ZIF-8 membrane, indicating a lack of macroscopic cracks of defects

Table A1. ZIF-8 membrane single gas permeation results measured at 1 bar feed pressure and different temperatures compared with previously reported data (Bux et al.[1] J. Am. Chem. Soc. 2009, 131, 16000-16001). The first column is data from three different ZIF-8 membranes tested three times each at 25 ^{o}C. The next two columns are data from one ZIF-8 membrane measured at 90 ^{o}C and 170 ^{o}C

Gas	Permeance [10^{-7} mol/(m^2 s Pa)]			
	McCarthy et al., 25 °C	*McCarthy et al., 90 °C	*McCarthy et al., 170 °C	Bux et al., 25 °C
H_2	1.732 ± 0.37	0.965	0.823	0.604
CO_2	0.445 ± .078	-	-	0.133
O_2	0.522 ± .084	0.204	0.127	0.104
N_2	0.149 ± .036	0.088	0.069	0.052
CH_4	0.133 ± .028	0.085	0.063	0.048

* Preliminary results (one membrane).

VITA

Name: Victor Varela Guerrero

Address: Universidad Autonoma del Estado de Mexico,
Instituto Literario S/N
Toluca, Mex, C.P 50000

Email Address: vvgvic@hotmail.com

Education: B.A., Chemical Engineering, Universidad Autonoma del Estado de Mexico, 1997
M.S., Chemical Engineering, Iberoamerican University, 2003
Ph.D., Materials Science and Engineering,
Texas A&M University, 2011